# MASTERARBEIT | MASTER'S THESIS

Titel | Title

Set-up of In Vitro and In Vivo Models to Study the Impact of HDAC Inhibition

verfasst von | submitted by

Adrian Arnel Lauber BSc

angestrebter akademischer Grad | in partial fulfilment of the requirements for the degree of

Master of Science (MSc)

Wien | Vienna, 2024

| | |
|---|---|
| Studienkennzahl lt. Studienblatt \| Degree programme code as it appears on the student record sheet: | UA 066 830 |
| Studienrichtung lt. Studienblatt \| Degree programme as it appears on the student record sheet: | Masterstudium Molecular Microbiology, Microbial Ecology and Immunobiology |
| Betreut von \| Supervisor: | ao. Univ.-Prof. Dr. Christian Seiser |

# Acknowledgments

First, I want to say a big Thank you to Professor Christian Seiser for giving me the opportunity to do my master's thesis practical in his lab. I've always appreciated his guidance and constructive feedback. A special thank goes to my Supervisor Lena Hess who took her time to guide me through the lab work with great patience and motivation. In addition, I want to acknowledge both for the many suggestions and corrections of my thesis. Further, I want to thank the lab members who were there at that time and who I could always count on for help. Here, Terka and Stephan offered great help for the cloning and transfection process. Also, I want to thank Jelena for all the service she provided to keep the Seiser lab in the CACB running.

A thank goes also to Sophie from the Dagmar Stoiber-Sakaguchi lab for her help with the *in vivo* model. Many thanks also to Robert from the pharmacology animal facility for taking care of our mice.

Then, I want to mention Renato Paro and his group at ETH Zurich who aroused my interest in epigenetics research during a practical course for my Matura many years ago.

Many thanks apply also to my parents who made studying possible for me and to my aunt who stood always on my side to find the best education. Thanks also to the gratuitous support of the Institut St. Ursula over the years of my studies.

Thanks as well to all my friends and colleagues who kept me motivated to finish this thesis.

And of course, I would like to thank my better half for her endless support during all of this journey.

## Abstract

Broad spectrum Histone deacetylase inhibitors are already in use for cancer treatment and have proven to be useful primarily in non-solid tumours. Since these drugs are not specific to subsets of the existing 11 members of the classic Histone deacetylase (HDAC) family and have considerable side effects, more specific inhibitors might be beneficial. Therefore, the characterization of individual members of the HDAC family in tumour cells is required. The class I HDACs are widely expressed in different human tissues and are thought to strongly contribute to the total deacetylase activity in mammalian cells.

We aimed to investigate catalytic and non-catalytic functions of class I HDACs as well as of their corepressor complexes in human tumour cells. To this end, our lab has generated an *in vitro* model in the nearly haploid human tumour cell line HAP1 to mimic and explore isoform-specific targeting. Consistent to previous in-vivo studies by Hagelkruys et al. results *in vitro* show that catalytically inactive HDAC1 & HDAC2 have a significantly higher negative impact in the deacetylation activity of corepressor complexes compared to knockouts.

Bioinformatical processing of RNA- and ChIP-seq data to further analyse the changes in gene expression profiles resulting from distinct expression (KOs) of class I isoforms and the effects of reintroduction of HDAC transgenes into KO cells or wildtype HAP1 cells was done. Comparison to cells treated with class I HDAC inhibitors MS275 (Entinostat) and the recently developed JQ12 show that the expression of catalytically inactive HDAC1 & HDAC2, and surprisingly also HDAC8, have a more similar effect to drug treatment than the knockout of the respective gene.

An attempt to establish a novel in-vivo system for investigation of HDAC inactivation in acute myeloid leukemia (AML) in fetal liver cells was accompanied by unexpeceted impediments such as the spontaneous activation of the transgene. Nevertheless, it could be readopted with a different recombination system for future studies.

# Zusammenfassung

Histon-Deazetylase-Inhibitoren werden bereits in der Klinik für die Krebsbehandlung angewendet und haben sich vor allem bei nicht-soliden Tumoren als nützlich erwiesen. Da diese Medikamente nicht spezifisch sind für Untergruppen der bestehenden 11 Mitglieder der klassischen Familie der Histon-Deazetylasen (HDAC) und nicht unerhebliche Nebenwirkungen haben, wären spezifischere Inhibitoren von Vorteil. Aus diesem Grund sollte die Charakterisierung einzelner Mitglieder der HDAC-Familie in Tumorzellen vorangetrieben werden. Die Klasse I HDACs werden in verschiedenen menschlichen Geweben exprimiert, wo sie vermutlich stark zur gesamten Deacetylaseaktivität in Säugetierzellen beitragen.

Die katalytischen und nicht-katalytischen Funktionen von HDACs der Klasse I sowie ihrer Corepressor Komplexe in menschlichen Tumorzellen sollten untersucht werden. Zu diesem Zweck hat unser Labor ein in vitro Modell in der beinahe haploiden menschlichen Tumorzelllinie HAP1 erstellt, um isoformspezifisches Targeting nachzuahmen und zu untersuchen. In Übereinstimmung mit früheren in vivo Studien von Hagelkruys et al. konnte so in vitro gezeigt werden, dass katalytisch inaktives HDAC1 & HDAC2 einen deutlich größeren negativen Einfluss auf die Deazetylierungsaktivität von Corepressor Komplexen haben als Knockouts (KO) derselben.

RNA- und ChIP-seq-Daten wurden bioinformatisch verarbeitet, um sich mit Hilfe von KO die Änderungen in den Genexpressionsprofilen anzuschauen, die sich aus der unterschiedlichen Expression von Klasse-I-Isoformen ergeben. Des Weiteren wurden die Auswirkungen der Wiedereinführung von transgenen HDACs in KO-Zellen gegenüber Wildtyp-HAP1-Zellen analysiert. Ein Vergleich mit Zellen, die mit dem Klasse I HDAC Inhibitor MS275 (Entinostat) und dem kürzlich entwickelten JQ12 behandelt wurden, zeigt, dass die Expression von katalytisch inaktivem HDAC1 & HDAC2, und überraschenderweise auch von katalytisch inaktivem HDAC8, der medikamentösen Behandlung ähnlicher sieht als der KO des jeweiligen Gens, was die Wirkung betrifft.

Ein Versuch, ein neuartiges in vivo System zur Untersuchung der HDAC-Inaktivierung bei akuter myeloischer Leukämie (AML) in fetalen Leberzellen zu etablieren, war von unerwarteten Hindernissen begleitet, wie z. B. der spontanen Aktivierung des Transgens. Dennoch könnte das System für zukünftige Studien in Betracht gezogen werden insofern ein anderes Rekombinationssystem verwendet wird.

# Table of Contents

# 1. Introduction

## 1.1. Definition of epigenetics

In 1942, Conrad Hal Waddington proposed the term “epigenetics” [1]. The discovery that genes as units of genetic information are encoded by bases of deoxyribonucleic acid would still take more than 10 years at this time [2], [3].

In fact, Waddington suggested already 1940 the idea of an “epigenetic landscape” as representation of the dynamic interplay between genes and the environment in developmental biology and defined the term “epigenetics” later as “the branch of biology which studies the causal interaction between genes and their products, which bring the phenotype into being“ [4]. In the book “The Strategy of the Genes”, which was published in 1957 by Waddington, the epigenetic landscape (**Fig. 1**) is further described as valleys and hills, which are modelled from top to bottom [5]. A ball (illustrating the cell), rolling down this landscape, reaches a “determined” phenotype at the bottom. The ball can readily change its path at branch points or by a small change in the landscape or even an external push [5]. The longer the ball rolls down the landscape, the deeper the valleys get and changes are less likely to happen and harder to initiate [5]. Although Waddington focused on developmental biology, he defined epigenetics as a method of explaining how cellular phenotypic changes are inherited independently of changes in the genetic code during the development of cells [6]. While the “epigenetic landscape” was a qualitative metaphor for a simple downhill process, as described above, the mechanisms contributing to “decisions” towards a specific cell fate have recently been quantified in the probabilistic landscape and in this context further mechanisms, which lead to differentiation and dedifferentiation, were defined [7].

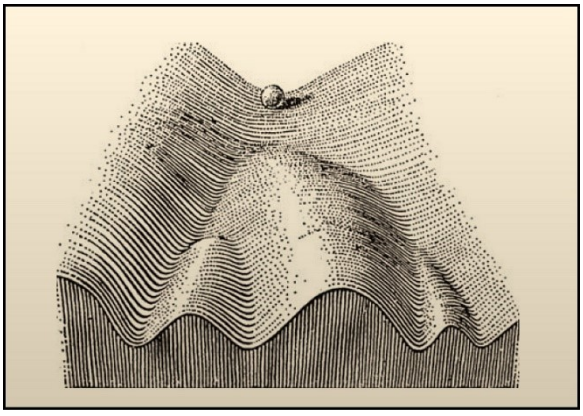

***Fig. 1: Waddington’s illustration of the epigenetic landscape from 1957.*** *Reprinted from* Cell, Vol. 128, Aaron D. Goldberg,C. David Allis, Emily Bernstein, Epigenetics: A Landscape Takes Shape, p. 635-638, Copyright © 2007 with permission from Elsevier Inc. Published by Elsevier Inc.

Nowadays, epigenetics is defined more broadly: A definition proposed by Berger SL. et al. implies: “An epigenetic trait is a stably heritable phenotype resulting from changes in a chromosome without alterations in the DNA sequence.” In order to reach and keep the epigenetic state, three main mechanisms are crucial (**Fig. 2**): 1) The “Epigenator“ is

defined as the signal which arises from changes in the cellular environment or in the cell itself. The “Epigenator signal” leads to an intracellular signalling pathway which is activated for an amount of time, long enough so that epigenetic mechanisms can take place. 2) The “Epigenetic Initiator“ translates the upstream signal and integrates it at sites on the chromatin in the nucleus (discussed in **chapter 1.2**). Through mediation of the upstream signal it predefines the location on the chromatin, where epigenetic manifestation is going to take place. 3) The Epigenetic Maintainer keeps the epigenetic state of the chromatin by epigenetic modifications which will be discussed in **chapter 1.3**. The Maintainer is not sufficient to create a changed chromatin state, it is usually dependent on the Initiator. [8].

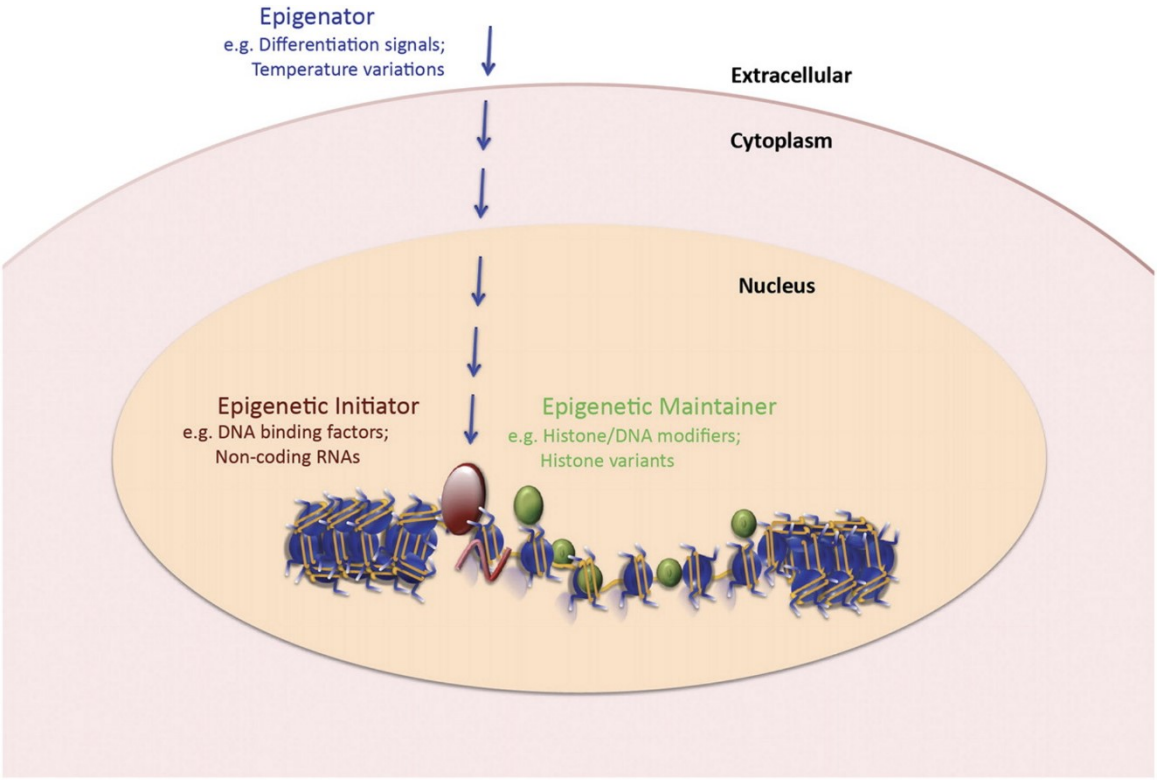


***Fig. 2: The three main mechanisms involved in epigenetic signalling to reach a stable epigenetic state.*** *The Epigenator collects signals from the environment of the cell or from the cell’s interior to signal downstream to the Epigenetic Initiator (in red). While the Initiator defines the location on the chromatin for the epigenetic signal, the Epigenetic Maintainer (in green) marks and sustains the chromatin state.* Picture adapted from Shelley L. Berger et al. Genes Dev. 2009;23:781-783. Copyright © 2009 with permission by Cold Spring Harbor Laboratory Press.

## 1.2. Chromatin in eukaryotes

Chromatin, which is found in the nucleus of eukaryotic cells, was first observed in the 19th century. It can be seen using a basic light microscope when cells divide and the chromatin condenses [9], [10]. During this process, the chromatin is arranged in a way that allows

individual chromosomes to be distinguished. In humans, the chromatin in the nucleus is organized into 23 pairs of chromosomes [11]. Each set of 23 chromosomes is inherited from a parent. For 22 chromosomes there are always two copies present in the cell, one copy is inherited maternally, and the other copy is inherited paternally. They pair up as autosomal chromosomes. The 23rd pair is different in females (they carry 2 X-chromosomes) and males (carrying one Y-chromosome and one X-chromosome) [12], [13]. Understanding the structure and function of chromatin is essential for comprehending the mechanisms involved in epigenetic regulation.

### 1.2.1. The composition of chromatin

Under the electron microscope, chromatin looks like “beads on a string”. This structure is determined by repeating units, which are called nucleosomes [14]–[17]. Nucleosomes generally consist of a histone octamer and a portion of DNA which is wrapped around it. The octamer contains each of the following histone variants twice: H2A, H2B, H3 and H4 [18]–[21]. DNA with a length of 147 base pairs is wrapped around each histone octamer in approximately 2 left-handed turns, which is facilitated through the positively charged histones (by basic amino acids) that attract the negative charged DNA. The part containing the histone octamer together with the 147 base pairs DNA is also called the nucleosome core particle. Histones H3-H4 dimers form a stable tetramer whereas the histones H2A-H2B appear as separate dimers. Each histone possesses a flexible N-terminal “histone tail” which can be subject to histone modifications. Changes to these modifications heavily influence chromatin structure, accessibility and consequently gene transcription [22], [23]. They are discussed in **chapter 1.3.2.** [24]–[27]. A linker histone H1 is localized between the nucleosome core particles and stabilizes the structure [28], [29].

The “beads-on-a-string” structure of nucleosomes in a row is around 10 nm thick [14], [25], [30] and can be further condensed into a 30 nm thick chromatin fiber (secondary structure). The position of H1 histones and histone modifications play a crucial role for the formation of these chromatin fibers [29]–[32].

### 1.2.2. Chromatin remodelling complexes

Chromatin remodelling, as a part of epigenetic mechanisms in cells, is carried out by chromatin remodelling complexes. They are member of either the SNF2H family, also called ISWI, or the SWI/SNF family. Proteins of the ISWI family are responsible for the

mobilization and repair of chromosomes. On the other hand, SWI/SNF family proteins can change the composition of nucleosomes. Complexes from both families can further have the ability to remove histones and facilitate gene transcription and replication [33], [34].

### 1.2.3. Chromatin density and accessibility

Densities of chromatin vary from region to region, depending on the temporal and spatial context. The temporal context is mainly determined by the cell cycle while the spatial context is derived from and maintained by the epigenetic state of the cell.

#### *1.2.3.1. Chromatin changes in the temporal context*

While in interphase cells the chromatin is rather "relaxed", it condenses into chromosomes during mitosis, which was observed already at the beginning of the 20th century. [10], [35]. The following phases are depicted in **Fig. 3**.

In interphase (G1-, S-, G2-phase), cells transit from G1- to S-phase upon CyclinE/Cdk2 activity, which initiates expression of histone assembly genes through phosphorylation of nuclear protein ataxia-telangiectasia locus (NPAT), while gene replication is being started. The nuclear envelope enwraps the content of the nucleus. It is disrupted by embedded nuclear pore complexes (NPC). The nuclear lamina which spans across the nucleus also stabilizes the envelope. Both the NPCs as well as the lamina has the chromatin anchored to the envelope at lamina-associated domains while in interphase. Pre-replication complexes start to be assembled alongside of regions in the chromatin, where histone H4 is hyperacetylated (H4Ac) [36].

During the S-phase, old histones are resegregated into both the newly synthesized as well as into the parental DNA strands. New histones are then deployed beside existing ones to fill the gaps along the DNA strands with help of the histone chaperone Chromatin assembly factor 1 (CAF1).Histones are recycled this way and it makes inheritance of histone marks possible, since epigenetic information is preserved on both strands [37], [38]. Histone modifications are set post-translationally (see **chapter 1.3.2**.) [39]. HP1 and the protein complex PRC2 carry out the task of post-translational modifications (PTMs) to inherit epigenetic modifications associated with gene silencing. In contrast, members of Trithorax-group proteins (TrxG) have the task to maintain an active state of genes that is inherited to the next cell generation. HP1, PRC2 and TrxG proteins are some of the recruited factors alongside with CAF-1 which allows the DNA replication to continue [36].

At the end of S-phase CyclinA/Cdk1 starts phosphorylating histone gene-specific epigenetic repressor in late S-phase (HERS) protein. SU(VAR)3-9 is recruited to the sites of histone genes and HP1 silences these genes. Starting at G2-phase and maintained during mitosis, histone H3 tails are phosphorylated by Aurora B and condensin proteins are attracted to sites all over the chromosomes, which enable condensation. [36].

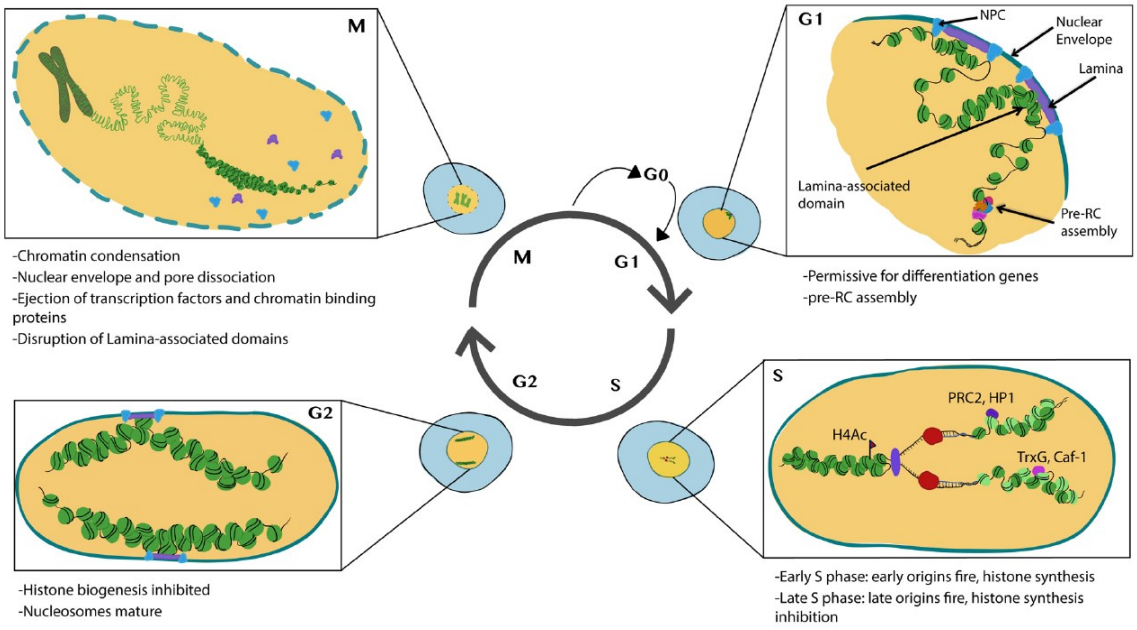


***Fig. 3: Chromatin changes during the cell cycle.*** *The interphase consists of the G1-, S- & G2-phase, where DNA replication takes place and new histones are synthesized. Histone resegregation at a replication fork in S-phase is depicted with recycled (dark green) and new (light green) nucleosomes. In mitosis (M-phase) chromatin is condensing and chromosomes are prepared to be distributed to both daughter cells which eventually transit into G1- or G0-phase. Resting cells are in G0-phase.* Figure taken from: Ma Y, Kanakousaki K and Buttitta L (2015) How the cell cycle impacts chromatin architecture and influences cell fate. Front. Genet. 6:19. under the CC BY 4.0 license

### *1.2.3.2. Chromatin differences in the spatial context*

Chromatin can be spatially subdivided into heterochromatin and euchromatin.

Euchromatin is less condensed than heterochromatin and accessible for transcription [40]. In these regions the alternative histones H3.3 (derived from H3) and H2A.Z (derived from H2A) are deployed [41]. H2A.Z also protects the open regions from the silencing heterochromatic state [42]. Euchromatin is also characterised by hypersensitivity to DNAse I [43], [44]. While genes in the euchromatin are accessible for transcription factors (TFs), the histones must be still (re-)moved to enable the replication fork to slide over the DNA. This task is done by chromatin remodeling complexes, such as SWI/SNF or NURF by ATP hydrolysis [45], [46]. TF binding can be facilitated by multiple epigenetic factors such as histone acetylation [47].

Heterochromatin is condensed and most sections are inaccessible to TFs, thus kept in an inactive (silent) state [48]. Heterochromatin can be further divided into facultative and constitutive heterochromatin.

Constitutive heterochromatin is defined to be generally condensed and poor in genes in all cell types. Although a low number of genes can be also found in heterochromatic regions [49]. Facultative heterochromatin is silenced but has the potential to change from the heterochromatic condensed state to an open (euchromatic) state to allow transcription [50].

Constitutive heterochromatin contains repetitive elements and noncoding sequences [51]. Heterochromatin is present at the centromeres, which are determined by the H3 histone variant CENP-A. Centromeres serve as attachment points for spindle fibers during cell division. [52], [53]. Another crucial heterochromatic structure are telomeres, which act as protective caps at the ends of chromosomes. [54]. These elements play a vital role in maintaining chromosome stability. [55]. Formation of constitutive heterochromatin can be propagated by the heterochromatic reader protein HP1 [56].

Facultative heterochromatin is silenced but has the potential to change from the heterochromatic condensed state to an open (euchromatic) state to allow transcription. Whether gene expression is active depends on either the temporal, spatial or heritable context [50]. A prominent example for facultative heterochromatin are the X-chromosomes in female somatic cells, from which one is always silenced [57]. Silencing of one of the X-chromosomes is called X-chromosome inactivation. It is is initiated by the XIST non-coding RNA [13], [58].

## 1.3. Epigenetic modifications

The effects of alternative histones as chromatin modification that regulate gene expression have been discussed above (**chapter 1.2.2**). In this chapter, the most important epigenetic modifications will be presented.

### 1.3.1. The concept of writers, readers and erasers

The concept of the epigenetic initiator and maintainer mentioned in **chapter 1.1** can be translated into the widely distributed terms of writers and readers. Additionally, there are also erasers [59]. Often, specific protein reading domains are shared in all three categories

of histone modifiers [60]. These terms are depicted in the following sections with examples for the most known epigenetic modifications.

### 1.3.2. Posttranslational modification of histones

#### *1.3.2.1. The histone code*

Each histone possesses a variety of amino acids in the N-terminal “histone tail” which can be modified. For easier understanding, each mark on the histone’s tail has a specific code which states on which histone to find the modification, the position of the amino acid seen from the N terminus and which modification is added. For example, H3K9me means, that the 9. amino acid, which is a lysine, on the histone tail of H3 is methylated. Tri-methylation of the same site would be written as H3K9me3. The “histone code” hypothesis predicts that specific combinations of these modifications can impact gene expression and other cellular processes. This “histone code” is still subject to investigations and many findings were made in recent years [61]–[63].

#### *1.3.2.2. Histone Acetylation*

Acetylation of histones co-occurs with active gene promoters [64], [65]. In general, lysine residues of histone tails can be acetylated. By doing so, the affinity of histones to DNA is lowered by neutralization of positive charges on the histone tails [66], [67]. Additionally, alteration of lysines through acetylation facilitates binding of regulatory proteins to DNA and improves flexibility for nucleosome sliding. Furthermore, the interaction with other neighbouring nucleosomes can be changed [68].

Histone acetyltransferases (HATs) are the writers of histone lysine acetylation. HAT1 was the first one identified [69], [70]. HATs transfer the acetyl group through a mechanism which is dependent on the general metabolite acetyl-CoA [71], [72]. Many complexes which are recruited by transcriptional activators possess HAT activity [73]. The majority of HATs can be categorized into 5 families which are HAT1, MYST, p300/CBP, Gcn5/PCAF and Rtt109 [74].

Reading of acetylated histone lysins happens mainly through bromodomain containing proteins such as bromodomain-containing protein 2 (BRD2), which is able to recognize H3K12ac with its first bromodomain and H4K5ac/H4K8ac with its second bromodomain [75]. One important function of BRD2 is the recruiting of TATA-binding protein (TBP) to

E2F1 transcription factors to promote cell cycle genes [76]. There are 8 families of bromodomain containing proteins [74]. Another group of readers are proteins which contain the YEATS domain. [77].

Erasers of acetylation are the histone deacetylases (HDACs) which will be described in **chapter 1.4** as the main topic of this thesis.

#### *1.3.2.3. Histone Acylation*

The addition of an acetyl group to lysine residues of histone tails is, albeit the most common, in fact just one of many histone acylation modifications [78].

Regarding acylation the formyl group (COH) is the shortest chemical modification added to lysine residues followed by the acetyl group ($CH_3CO$) as the next longer one. Many other acyl groups exist with longer chains such as propionyl, butyryl and crotonyl [79].

p300 was shown to possess HAT activity as well as histone crotonylation transferase (HCT) activity [80]. Recent experiments have shown that altered p300 proteins, which carry a HAT deficiency mutation, are still able to facilitate gene expression *via* their HCT activity, although in a less efficient manner [81].

The YEATS domain was shown to read preferentially crotonylated lysine sites, besides of recognizing acetylation [77].

Class I HDACs seem to be at the same time also the major histone decrotonylases (HDCRs) [82].

#### *1.3.2.4. Histone Methylation*

Lysine residues of histone tails are also targets of methylation [83]. Methylation of arginine residues is also often observed [84]. In both cases, besides of monomethylation, also di- and trimethylation is possible [85].

Histone lysine methyltransferases (KMTs) and protein arginine methyltransferases (PRMTs) act as writers. KMTs can mark lysine residues on H3 and H4. It has been shown that H3K9me1 (Histone 3 lysine 9 monomethylation), H3K27me1 or H3K36me3 are associated with upregulation of genes. Activation of transcription can be initiated by methylation of H4R3 by PRMTs (H4R3me2) [86]. On the other hand, H3K9me2,3 or H4K20me3 are associated with silencing and can be found in heterochromatin [87]. EZH2

as part of the polycomb repressive complex 2 (PRC2) has an H3K27 di- and tri-methyltransferase activity as example of a KMT that leads to gene silencing [60]. PRC2 itself plays a role in cancer development in a double-edged manner, depending on the cell identity [88].

Recognition of histone lysine methylation is done by proteins possessing a chromodomain, plant homeodomain (PHD) or Tudor domain, among others. HP1 and polycomb proteins have a chromodomain, which can recognize H3K9me3 and H3K27me3 [89]. The KMT Suv39h leaves a methylation mark on H3K9 that can be recognized by heterochromatin protein 1 (HP1), a reader of histone methylation, which reads and binds specifically this mark with its chromodomain [63]. After binding, it promotes the silencing of genes nearby [90].

The lysine specific demethylases (LSD) proteins and the Jumonji C domain containing (JmjC) proteins belong to histone demethylases (HKDMs). LSD1 is an eraser of H3K4 and thus a histone lysine demethylase [91]. It was later classified as KDM1A [92]. As part of the Mi-2/nucleosome remodelling and deacetylase complex (NuRD), LSD1 brings together histone acetylation and demethylation in the same protein complex and plays a role in the inhibition of breast cancer [93].

#### *1.3.2.5. Other well-known histone modifications*

Beside of acetylation and methylation there are many other modifications that influence the chromatin and gene transcription. Phosphorylation is important for chromosome condensation, gene regulation and repair mechanisms of DNA [94]. Another important modification which regulates DNA damage repair is ubiquitination [95]. In recent years an additional group of histone tail modifiers gained attention which also plays an important role in DNA repair pathways. They are called Small ubiquitin-like modifiers (SUMOs) and are transferred to histone tails through sumoylation. [96].

### 1.3.3. DNA methylation

Modification can not only take place on histones but also on the DNA double strand itself. Cytosine can be modified to 5-methylcytosine by adding a methyl group [97]. This modification appears usually at CpG dinucleotides and leads to silencing of surrounding genes [98], [99].

DNA methyltransferases Dnmt3a and Dnmt3b were found to play a crucial role in the establishment of *de novo* methylation in mammalian development, which has to be taken place since paternal methylation patterns are being erased genome wide in the very early development stage of embryos [100], [101]. Dnmt1 is in contrast essential for maintenance of methylated sites after DNA replication and thus often called maintenance DNA methyltransferase [102]–[104].

Two mechanisms contribute to gene silencing: Methylation of DNA interrupts binding of transcription factors to DNA which often bind in GC-rich regions [105]. Furthermore, there are proteins which repress gene expression upon binding to methylated CpG sites, such as MeCP1 and MeCP2 which both contain a methyl-CpG binding domain (MBD). These MBD proteins recruit histone deacetylases as has been shown for instance for MeCP2, which recruits the Sin3 complex [106]. Histone deacetylation has a repressing effect on accessibility and transcription which is discussed in **chapter 1.4**.

Strikingly, many actively expressed genes possess an enriched site of CpG dinucleotides which is situated at the 5' end, called CpG island, where DNA is hypomethylated [107].

## 1.4. Histone deacetylases

### 1.4.1. HDAC families

Histone deacetylases (HDACs) are crucial regulators of gene transcription. By removing acetyl marks on histone tails, they allow condensation of chromatin and thus restrict access of transcription factors to DNA [47], [108].

Beside of histones, HDACs are also known to target many other proteins and influence their stability, activity and protein-protein interaction [109].

In mammals there are in total 18 HDACs which are subdivided into 4 classes, based on sequence homology with yeast Hda1, Rpd3 and Sir2: Class I HDACs are homologs to yeast Rpd3. Harboring HDAC1, HDAC2, HDAC3 and HDAC8, this class is responsible for most of the histone deacetylation activity in the cell. Class IIa (HDAC4, HDAC5, HDAC7, HDAC9) and Class IIb (HDAC6 & HDAC10) are homologs to yeast Hda1. HDAC11 is the only member of class IV HDACs and has similarities to both Hda1 and Rpd3. While class I, IIa, IIb and Class IV belong to the family of classical (Zn2+ dependent) HDACs, the class III HDACS belongs to the family of nicotinamide adenine dinucleotide (NAD) dependent HDACs and harbors SIRT1-7, whose homolog in yeast is Sir2 [110], [111].

### 1.4.2. Structure and mode of action of class I HDACs

All Class I HDACs possess a nuclear localization signal sequence (NLS). While HDAC1 & HDAC2 are primarily found in the nucleus, HDAC3 & HDAC8 can localize to the nucleus as well as to the cytosol [112]

HDAC1 and HDAC2 are 482 amino acids (aa) and 488 aa in length, respectively. HDAC3 is shorter with 434 aa. As shortest class I member HDAC8 owns only 377 aa. The molecular weight has been observed to be between 40-60 kDa for class I HDACs. In all 4 HDACs the catalytic domain is located at the N-terminal part and makes up the largest part of the sequence [113]. HDAC1 and HDAC2 possess a HDAC association domain (HAD) at the N-terminus which facilitates homo- and heterodimerization with HDAC1 or HDAC2, respectively [114]. Also, with 86% sequence similarity, they are the most related among class I HDACs [112].

HDAC3 has the ability to build homodimers as well. Further, it has been shown that it can interact directly with class II HDACs [115].

First hints about the mechanism of histone deacetylation were found after resolving the structure of the bacterial HDAC homologue Histone Deacetylase-Like Protein (HDLP) in *Aquifex aeolicus* and later translated to mammalian HDACs following the discovery of the HDAC8 structure [116], [117].

Two aspartic acid amino acid residues and one histidine residue coordinate a $Zn^{2+}$ ion as cofactor in the catalytic center (**Fig. 4**).

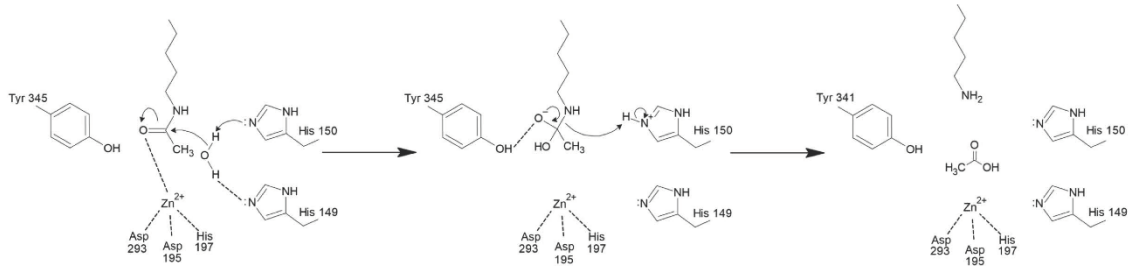


***Fig. 4: Mechanism of histone deacetylation on a lysine residue.*** Figure taken and modified from Milazzo G, Mercatelli D, Di Muzio G, Triboli L, De Rosa P, Perini G, Giorgi FM. Histone Deacetylases (HDACs): Evolution, Specificity, Role in Transcriptional Complexes, and Pharmacological Actionability. Genes. 2020; 11(5):556. under the CC BY 4.0 license

Two histidine residues recruit a water molecule and activate it by dissociation of the proton. $Zn^{2+}$ helps to polarize the C-O bond of the acetyl group and catalyse the nucleophilic attack

which originates from the activated water. The transfer of the proton onto the acetyl group and subsequent removal from lysine is stabilized by a tyrosine residue [113].

A particular role of stabilization and sustainment of class I HDAC activity is incumbent on inositol phosphates [118].

### 1.4.3. Co-repressor complexes

If purified, HDAC1, HDAC2 and HDAC3 are found to be inactive. Deacetylation activity requires their incorporation into co-repressor complexes. To date HDAC1/2 have been shown to be part of different co-repressor complexes, including the Sin3-, NuRD,- CoREST- and MiDac-complex (**Fig. 5**). HDAC3 is associated with the NCoR/SMRT complex [119].

The composition of co-repressor complexes determines their direction to particular histones [120].

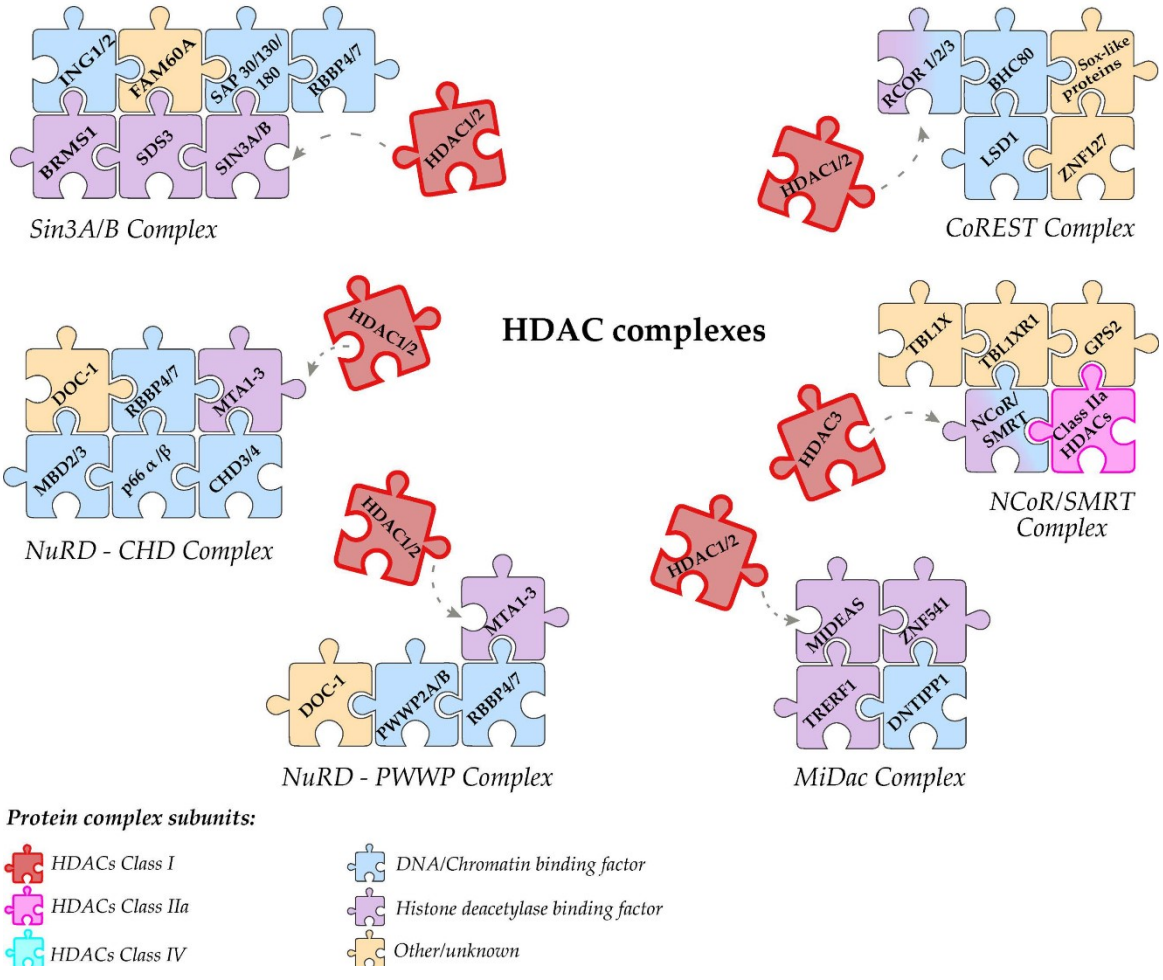

***Fig. 5: Co-repressor complexes of HDAC1, HDAC2 and HDAC3.*** Figure taken and modified from Milazzo G, Mercatelli D, Di Muzio G, Triboli L, De Rosa P, Perini G, Giorgi FM. Histone Deacetylases (HDACs): Evolution, Specificity, Role in Transcriptional Complexes, and Pharmacological Actionability. Genes. 2020; 11(5):556. under the CC BY 4.0 license

#### *1.4.3.1. Sin3 complex*

The Sin3 complex either comprises Sin3a or Sin3b, which have been found in a variety of cell types [121]. Both, Sin3a and Sin3b have HDAC-interacting domains, which recruit HDAC1/2 as well as direct interfaces to other cofactors [122].

Sin3 as prototypical Co-repressor complexes are involved in almost all nuclear processes. HDAC1 incorporated in the Sin3a complex controls cell cycle progression with cofactors like Rb and Mxd1. Class I HDAC inhibitors SAHA and MS275 have been shown to downregulate Sin3a activity and inhibit cell proliferation [121]. In endoderm cells total inhibition of Sin3a lead to a stop of the cell cycle in G1/S-phase through upregulation of p16 and p21 [123].

#### *1.4.3.2. CoRest complex*

The rather specialized chromatin-modifying co-repressor complex CoRest, harboring HDAC1 and HDAC2, regulates transcription and differentiation in neuronal (stem) cells [124]. CoREST can bind to Sin3a *via* the REST protein, which is part of the CoREST complex and thus both complexes can be found together at specific REST binding sites on chromatin [125].

LSD1 as part of CoREST enables the complex to carry histone demethylase activity, specifically H3K4 mono- and dimethylation [126]. LSD1 in CoREST plays a role in development of hematopoietic stem cells. The transcription factors GFI1/1B recruit CoREST *via* LSD1 to chromatin in myeloid cells and ultimately repress gene expression at specific sites, leading to a halt of dedifferentiation of myeloid cells [127].

#### *1.4.3.3. NuRD complex*

Another co-repressor complex which contains HDAC1 and HDAC2 is the nucleosome remodeling and deacetylase complex (NuRD). It possesses ATP-dependent remodelling activity as well as histone deacetylation activity, which are usually two independent activities regulating the chromatin. [128].

The NuRD complex has either PWWP2A/B or CHD3/4 integrated beside of the other components. The presence of MBD2/3 rules out the binding of PWWP2A/B and CHD3/4 can only be found in complexes, where MBD2/3 is bound [113].

Binding partners such as MBD2/3 and PWWP2A/B specify the recruitment of the NuRD complex to methylated or hemi-methylated DNA through a methyl-CpG-binding domain, which regulates differentiation of cells [129]. It has been shown for MBD3/NuRD that their activity inhibits expression of pluripotency genes, thus it is useful to downregulate NuRD to reprogram cells into induced pluripotent stem cells (iPSC) [130].

On the other hand, inhibition of NuRD leads to higher infiltration rates of $CD8^+$ and dendritic cells in hepatocellular carcinoma (HCC) [131].

#### *1.4.3.4. MiDac complex*

Mitotic deacetylase complex (MiDac) is the latest co-repressor complex found that activates HDAC1 and HDAC2. It participates in regulation of chromosome alignment throughout mitosis and is regulating neural differentiation in embryonic development [132].

#### *1.4.3.5. NCoR/SMRT complex*

Two proteins are name-giving for this HDAC3 containing complex, in which either one of them is incorporated: First, the silencing mediator for retinoid and thyroid hormone receptors (SMRT or also NCoR2), or second, the nuclear receptor corepressor 1 (NCoR1) [133], [134]. NCoR/SMRT was shown to be significant for preservation of cellular identity. Strikingly it was shown that the NCoR complex is an antagonist of OSKM (OCT4, SOX2, KLF4, c-MYC) reprogramming for pluripotency, thus pan-HDAC inhibitors are being used to increase reprogramming efficiency [135]. Further, NCoR/SMRT complexes together with HDAC3 are observed to be upregulated in many tumours and HDAC3 RNA expression shows a positive correlation with poor prognosis [136]. The activity of the HDAC3 NCoR/SMRT complexes is dependent on the presence of inositol trisphosphate (IP3) [137].

## 1.5. HDAC inhibitors

HDAC inhibitors (HDACi) can either target the whole range of HDACs (pan HDAC inhibitors) or inhibit only a specific subset (specific HDAC inhibitors). The latter ones target rather a specific class of HDACs and isoform specific HDACi are rarely available yet [113].

The need of specific HDACi is given since HDACs are involved in many different processes through regulation of histones, targeting of themselves with broad range inhibitors can lead to many side-effects and even be counterproductive. It has been shown that lowering of HDAC1/2 levels in T-cells causes lymphoma formation in mice [138]. The effect was dose-dependent and further investigation led to the insight that critical HDAC activity levels are required for tumour cell viability, suggesting that cells with a low base level of HDAC activity are more prone targets for HDAC inhibitors [139].

The inhibitors can be classified into one of the following four groups, regardless of their synthetic or natural origin.

*Hydroxamic acids (hydroxamates)*

The broadly known and clinically available pan HDAC inhibitors Trichostatin A (TSA), Vorinostat (SAHA) and Panobinostat (LBH589) belong to this group. They chelate $Zn^{2+}$ in the active center of classical HDACs and hereby block the catalysis of deacetylation. Many of these inhibitors block transition of cells from G1 to S-phase or G2 to M-phase, respectively. This is caused to a big extent by upregulation of p53 activity through hyperacetylation. Vorinostat has been approved by the FDA for cutaneous T cell lymphoma (CTCL) treatment. Panobinostat, which has been approved as well for multiple myeloma was shown to be effective in treatment of acute lymphoblastic leukemia (ALL) caused by mixed lineage leukemia (MLL) rearrangement [140], [141].

*Short chain fatty (aliphatic) acids*

The naturally available sodium butyrate and valproic acid (VPA) belong to this group. VPA is a specific class I HDACi and is tested in phase I-III studies against a broad range of solid tumor cancers [113].

*Benzamides*

The benzamide Entinostat (MS275), which has a preference to class I HDACs, is currently under investigation in various phase I-II studies against solid tumors as well as against non-solid tumors (leukemia and lymphoma). The combination therapy along with PD-L1 antibodies seems promising and is subject to clinical trials [113], [142].

*Cyclic tetrapeptides*

The last group of HDACi's promises a more specific targeting of HDAC isoforms since compound structures are more complex. Romidepsin is the only FDA approved HDACi in this group and is used to treat Cutaneous T-cell lymphoma (CTCL) [113].

## 1.6. Acute myeloid leukemia

### 1.6.1. General emergence and treatment

In Acute myeloid leukemia (AML) hematopoietic stem cells become cancerous and lose the ability to properly develop into mature blood cells. Consequently, immature myeloid cells proliferate and accumulate, with a blast-like morphology and thus called blasts [143]. That leads to severe infections, anaemia, and haemorrhage [144].

With a portion of 1.3% of all new cancer cases in the USA, AML is the most frequent tape of acute leukemia in adults. The median age of diagnosis is 68 years which categorizes it as disease arising preferably in higher age [144].

Genomic analysis of patient derived samples with the goal to find driver mutations revealed that 96% of the patients with newly developed AML have at least 1 driver mutation and 86% of the patients have at least 2 driver mutations. [145].

Along with common driver mutations that enable leukemia disease classification, great diversity exists between derived subclones, complicating targeted treatment [146].

Several driver mutations identified in AML are of epigenetic nature, including DNA methylation or histone acetylation. Subsequently, a series of treatments were developed and approves that inhibit DNA methylation such as azacitidine and decitabine. [147].

Since the effects of these drugs are somewhat limited, combination treatments of hypomethylating agents with HDAC inhibitors, among others, are currently tested in the clinic, with yet modest results. More successful but still unsatisfactory results were achieved in combination with isocitrate dehydrogenase inhibitors catalyzing the conversion of isocitrate to α-ketoglutarate in the Krebs cycle [147].

In many patients, gene rearrangements (e.g. translocation, inversion, deletions) are observed [148]. Abnormal karyotypes are seen in 55% of adults. In children, though AML is rare, abnormal karyotypes can be seen in up to 80% of patients of whom around 25% suffer from mixed lineage leukemia (MLL) rearranged abnormality [149].

### 1.6.2. MLL-AF9

MLL with more than 50 fusion partners is the most frequent form of translocation seen in AML and is often associated with poor prognosis. The normally occurring MLL gene

product acts as a histone methyltransferase specifically for H3K4 residues and positively regulates Hox gene expression important for development and growth [150].

The MLL-AF9 fusion gene (t(9;11)(p22;q23)) is a prominent MLL fusion product, which activates cell self-renewal associated pathways by targeting and activating homeobox A9 (HOXA9) and Meis homeobox 1 (MEIS1) genes. While the presence of MLL-AF9 is sufficient to induce AML in mice the maintenance of leukemia is dependent on these so called leukemia stem cells (LSC) [151], [152].

It has been stated that LSCs, which are fueled by inappropriate activation of pathways, become dependent on a small subset of oncogenes such as Myb, which could be used as target for treatment [153]. In principle, inactivation of particular oncogenes should lead to senescence and cell death or differentiation, also called oncogene addiction [154]. While targeting of cancer specific oncogenes is often effective at the start of treatment, it becomes apparent, that plasticity leads to circumventing dependence and cells with new mutations arise, which shows the need for combinatorial treatments [155].

## 1.7. Mouse models

### 1.7.1. Mouse models for class I HDAC characterization

Targeted inhibition of both HDAC1 alleles in mouse embryos result in death before E10.5. While HDAC1 deficiency in embryonic stem cells (ESCs) showed reduced proliferation and was lethal, HDAC2 expression was upregulated but couldn't compensate for the full loss of HDAC1 in co-repressor complexes [156]. Investigations in a mouse teratoma tumor model showed an increase in apoptosis as seen before, but different than in ESCs the proliferation was also upregulated which led to no significant change of teratoma volume in HDAC1 deficient mice compared to wildtype mice [157].

Like HDAC1 depleted mouse embryos, the deletion of HDAC2 can lead to death, albeit shortly after birth with signs of cardiac abnormalities [158]. In another study newborn mice were viable but harboured a thickened ventricular wall in the first two months after birth [159]. These studies show the importance of HDAC1/2 in development.

Opposite to full deletion, conditional deletion of HDAC1 or HDAC2 in various tissues shows little or no effect, which could be due to the ability of HDAC1 and HDAC2 to compensate for each other to a certain degree in co-repressor complexes [112]. An example is the deletion of HDAC1 or HDAC2, respectively, in epidermis cells, where a severe phenotype is only observed after the deletion of one HDAC2 allele simultaneously with deletion of

both HDAC1 alleles [160]. In contrary, the same experiment in cells of the nervous system in mouse embryos shows that one single HDAC2 allele is sufficient for normal brain development [161].

### 1.7.2. Mouse models to investigate MLL-AF9 caused leukemia

A variety of mouse models exist in the field to study MLL-AF9. Most widely used are irradiated mice where MLL-AF9 transduced BM is reconstituted. While these mouse models can depict the disease to a high degree, they are time and cost consuming [162].

From the many used mouse models MLL fusion genes are among the most powerful, which allows disease onset with 1 genetic alteration. Many discoveries were made with the most frequent used MLL-AF9 model, where the rearrangement is introduced retrovirally in bone-marrow (BM) cells. Therefore, the BM has to be irradiated and is then reconstituted with the transduced population. The usage of the murine stem cell virus (MSCV) facilitated the transduction process significantly. Drawbacks of this method are the irreversible damage of the BM microenvironment and species barriers for patient-derived xenotransplants. Further, the model does not account for the fact, that the cancer emerges from a single cell that acquired mutations and rather a big number of cells from an expanded cell colony is transplanted [162].

Another problem is the varying transduction efficacy by virus integration and the rather excessive overexpression of the MLL fusion transgene. A series of conditional models were developed to face these problems. Widely used is the regulation *via* a doxycycline inducible construct [163].

## 1.8. Previous results

### 1.8.1. Dominant negative effect of HDACs

The analysis of HDAC1 & HDAC2 knockout mice gave interesting insights into the biological dependency to these HDACs [156], [164], [165]. HDAC1 & HDAC2 can compensate each other in co-repressor complexes [112], [160]. This led to the hypothesis that an HDAC knockout would not be the same as an inactivation of an HDAC. Our lab initiated studies in mouse models to investigate the impact of introducing catalytically inactive HDAC1 or HDAC2, as no previous studies had addressed this question. Surprisingly, the introduction of catalytically inactive HDAC2 (HDAC2 CI) into mice leads

to a more severe phenotype than the HDAC2 knockout in a mouse. Mice with a copy of HDAC2 CI are not viable. Thus, this was called dominant negative effect. In HDAC2 knock out mice, HDAC1 can compensate for the loss [166].

### 1.8.2. Toolbox for class I HDAC analysis

To further explore the differences between knockout and inactivation of class I HDACs, our lab established a genetic toolbox in HAP1 cells, which confirmed that HDACi treatment can be mimicked better with cells which express catalytically inactive HDAC1 or HDAC2 [167].

HAP1 cells are derived from the near haploid leukemia cell line KBM7. Through CRISPR/Cas9 targeted “deletion” of the remaining diploid genes, the HAP1 cell line was created which is almost perfectly haploid [168]. Thus, further engineering, to create knockdown, knockout or knock-in cell lines is relatively straightforward and was done in collaboration with the company Horizon Genomics (now Horizon Discovery).

HDAC knockout cell lines were generated by CRISPR/Cas9 targeting of respective sequences and introduction of an indel [167].

Catalytically inactive HDACs were introduced into both wildtype HAP1 cell lines as well as into the respective HDAC knockout cell lines. Therefore, using CRISPR/Cas9 technology and subsequent homologous recombination (**Fig. 6A**), the AAVS1 locus was targeted to introduce the coding sequences of class I HDACs which carry a point mutation in the catalytic center (HDAC1 H141A, HDAC2 H142A, HDAC3 H135A, HDAC8 H143A). Additionally, to the inactivation, a FLAG-tag was added C-terminally to allow for comparable detection and enrichment by Western blot and immunoprecipitation (**Fig. 6B**). The ability of inactive and FLAG-tagged HDACs to be still incorporated into co-repressor complexes was checked and confirmed [166], [167].

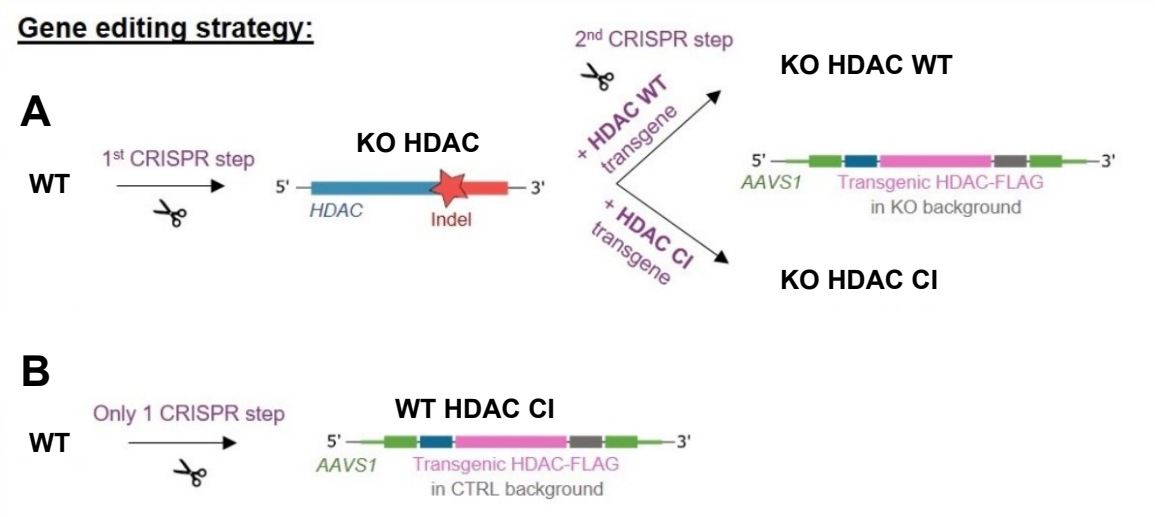


***Fig. 6: Gene editing strategy taken from Lena Hess' PhD thesis**. **(A)** HAP1 cells were subject to indel introduction through CRISPR/Cas9 targeting to generate HDAC KO cells for HDAC1-8. In a 2nd gene editing step either the catalytically inactive (CI) transgene was introduced or the wildtype (WT) transgene was reintroduced. Subsequently, homologous recombination into the AAVS1 locus was accomplished **(B)** To generate cell lines which express the CI HDAC transgene beside of the WT HDAC transgene, the CI transgene was integrated directly into the AAVS1 locus in only 1 CRISPR/Cas9 step.* Figure adapted from Hess L, Moos V, Lauber AA, Reiter W, Schuster M, Hartl N, et al. (2022) A toolbox for class I HDACs reveals isoform specific roles in gene regulation and protein acetylation. PLoS Genet 18(8): e1010376 under the CC BY 4.0 license

This model allows a systematic study of all class I HDACs, which increases reliability since comparison of results from different studies can be challenging especially when models differ.

## 1.9. Aims of this thesis

### 1.9.1. Optimization and data analysis for HAP1 paper

By utilizing the previously generated HAP1 cell lines, it was possible to characterize HDAC1, HDAC2, HDAC3 and HDAC8. Different approaches were tested in this thesis to optimize immunoprecipitations and activity measurements for class I HDACs, focusing on HDAC3 and HDAC8, which contributed to the paper. Further, data from RNAseq and CHIPseq experiments was analysed to gain an insight of changes in the transcriptome upon isoform specific targeting of class I HDACs.

### 1.9.2. Establishment of an *in vivo* model for AML

The second focus of this thesis was the establishment of an MLL-AF9 mouse model to characterize catalytic functions of HDAC1/2 in AML. Our lab already developed a MX1-cre inducible HDAC1 and HDAC2 transgene model [169]–[171]. Dagmar Stoiber's lab

(Medical University of Vienna and Karl Landsteiner University Krems) has developed an AML model system that involves the transformation of fetal liver cells by the MLL-AF9 oncogene (Iida et al, 1993; Corral et al, 1996). This model is suitable for *in vitro* investigation of the transformed cells and can be further applied to subsequent *in vivo* studies.

Since HDAC inhibitors have shown promising results in the clinics but still some questions as for instance HDACi resistance remain, the investigation of isoform-specific inactivation of HDAC1 & HDAC2 could reveal interesting insights by utilizing this AML model [127], [172].

In this thesis, I outline the modification of the model from the Stoiber lab to be made compatible with the existing HDAC mouse model that is being used in our lab. The MLL-AF9 transformation vector carries the VENUS detection tag which is on the same channel as our EGPF detection tag which is expressed downstream of the HDAC transgenes. Therefore, the modification of the vector through cloning was necessary.

# 2. Material and Methods

## 2.1. Cell culture

### 2.1.1. Cultivation and harvesting of HAP1 cells

HAP1 cells were obtained and modified previously by Horizon Genomics. The following cell lines were used and characterized to a certain extend in this thesis.

| name | background | transgene |
|---|---|---|
| **WT** | wt | - |
| **WT HDAC1 CI** | wt | HDAC1 CI |
| **WT HDAC2 CI** | wt | HDAC2 CI |
| **WT HDAC3 CI** | wt | HDAC3 CI |
| **WT HDAC8 CI** | wt | HDAC8 CI |
| **KO HDAC1** | HDAC1 KO | - |
| **KO HDAC2** | HDAC2 KO | - |
| **KO HDAC3** | HDAC3 KO | - |
| **KO HDAC8** | HDAC8 KO | - |
| **KO HDAC1 WT** | HDAC1 KO | HDAC1 WT |
| **KO HDAC2 WT** | HDAC2 KO | HDAC2 WT |
| **KO HDAC3 WT** | HDAC3 KO | HDAC3 WT |
| **KO HDAC8 WT** | HDAC8 KO | HDAC8 WT |
| **KO HDAC1 CI** | HDAC1 KO | HDAC1 CI |

| | | |
|---|---|---|
| **KO HDAC2 Cl** | HDAC2 KO | HDAC2 Cl |
| **KO HDAC3 Cl** | HDAC3 KO | HDAC3 Cl |
| **KO HDAC8 Cl** | HDAC8 KO | HDAC8 Cl |

*Table 1: cell lines used in this thesis*

#### *2.1.1.1. Thawing*

Frozen vials were quickly thawed in a 37° C water bath until almost everything was thawed, and the cells were taken up in 5ml IMDM medium in a Falcon tube while shaking gently. To remove the toxic DMSO from the cells, they were harvested by centrifugation at 1200 rpm for 5 minutes at RT. The supernatant was discarded, the pellet was resuspended with an appropriate amount of medium and the cells were seeded in a dish of the appropriate size in the desired dilution. The cells were grown in IMDM medium at 37° C, 5% $CO_2$.

#### *2.1.1.2. Splitting*

When 80-90% confluent, the cells were split in 1:5 – 1:30 ratio. Therefore, the medium was aspirated, the cells were washed with sterile 1x PBS and subsequently trypsinized with 1 - 1.5 ml trypsin (depending if a 100 mm or a 150 mm plate was used, respectively). The plate was incubated at 37° C until the cells had completely detached from the plate surface (3 minutes). Afterwards, the cells were resuspended in 9 ml of IMDM medium and seeded at the desired density. In case there were many death cells, a centrifugation at 1200 rpm for 5 minutes was done, to discard the death cells.

#### *2.1.1.3. Freezing*

The HAP1 cells were trypsinized and pelleted as described above and resuspended in 500 µl of freezing medium 1 (FM1). Afterwards, the cells were added into a 1.5 ml cryovial which contained already 500 µl of freezing Medium 2 (FM2) and put on ice for approximately 10 minutes. The cells were put on -80° C for further usage, when required and subsequently stored in liquid nitrogen for long time storage.

#### *2.1.1.4. Harvesting*

Before further processing the cells (e.g. protein extraction), HAP1 cells were scraped off the plates with a cell scraper (Biologix #70-1180) and collected in a Falcon tube. Therefore, the plates were washed twice with 10 ml of a 1x PBS (from 150 mm dish). Cells were scraped off in 1 ml 1x PBS and transferred into a 2 ml Eppendorf tube. 1 ml 1x PBS was used to rinse off the rest of the cells and also transferred into the Eppendorf tube. The cells were washed by centrifugation at 1200 rpm for 5 minutes at 4° C, the supernatant was discarded. The pellet was resuspended in 1200 µl PBS and were pelleted as described

above (5 min, 1200 rpm, 4° C) and the supernatant discarded. The pellet was put on ice for 5 minutes before it was frozen in -80° C until further usage.

IMDM medium
GIBCO IMDM (*Thermo Fisher Scientific Cat. No. 12440061*)
10% FBS
1x penicillin/streptomycin
1x glutamine

Trypsin/ EDTA
Trypsin-EDTA phenol red (*Sigma Aldrich Cat. No. T2601*)

Freezing Medium 1 (FM1)
GIBCO IMDM (*Thermo Fisher Scientific Cat. No. 12440061*)
20% FBS

Freezing Medium 1 (FM1)
GIBCO IMDM (*Thermo Fisher Scientific Cat. No. 12440061*)
20% FBS
20% DMSO

10x PBS
8% sodium chloride
0.2% potassium chloride
0.2% monopotassium phosphate
1.11% disodium hydrogen phosphate
Diluted in dH2O and pH adjusted to 7.4 with NaOH

### 2.1.2. Retroviral infection of fetal liver cells

Plat-E cells were obtained from Stefan Schuckert. They were split with a confluency of 80% were 1:2 in a 100 mm dish in DMEM -FBS -P/S and incubated for 5 h. After the cells were attached, calcium-phosphate transfection was done by adding 25 µg of plasmid DNA in 400 µl $dH_2O$ and 62.5 µl of 2M ice cold $CaCl_2$ buffer. 500 µl 2x HBS buffer was bubbled while adding the plasmid-$CaCl_2$ mix dropwise into a FACS tube. After 15 min incubation on RT the suspension was added dropwise to the Plat-E cells. The next morning, medium

was changed to DMEM 20% FBS. In the afternoon the FL cells were thawed in BCM, spun down 1200 rpm for 5 min on 4° C, and resuspended in 2 ml BCM with supplements in a 6-well plate. Each vial of FL cells was distributed onto 2 wells. Also, the Medium of Plat-E cells was changed to BCM w/o cytokines. On day 2, the supernatant of Plat-E cells was harvested and filtered through a 0.45 µm filter and supplements added to the BCM. Additionally, polybrene (1 µl/ml of 1000x) was put into the medium. 3 ml of viral supernatant was added to fetal liver (FL) cells into each well. Integration of the virus into the cells was aided by centrifugation 1000g for 90 min at 37° C. Fresh BCM was added to the Plat-E cells. The same procedure was repeated after 5 h by adding additional viral supernatant (3 ml) onto the FL cells. On day 3, the medium of the FL cells was aspirated and again, the same procedure as on day 2 was repeated once and after 5 h, 1.5 ml of fresh BCM with supplements was added to the FL cells.

BCM Medium
DMEM/ IMDM 1:1
10% FBS
1% PenStrep
2% L-Glutamine
1.7 µl β-Mercaptoethanol

2x HBS
NaCl 280 mM
HEPES ([4-(2-hydroxyethyl)piperazin-1-yl]ethanesulfonic acid ) 50 mM
$Na_2HPO_4 \cdot 7H_2O$ 1.42 mM
Diluted in $dH_2O$ and pH adjusted to 7.05 with 10M NaOH

Cytokines
mSCF (*Miltenyi Biotec Cat. No. 130101698*) 100 ng/ml final
mIL-6 (*Miltenyi Biotec Cat. No. 130096685*) 10 ng/ml final
mIL-3 (*Miltenyi Biotec Cat. No. 130099510*) 10 ng/ml final

### 2.1.3. Flow cytometry

On day 4 after viral transduction, an aliquot of infected FLs was analyzed by flow cytometry to assess the efficacy of the transduction. The efficacy was measured by detecting the mCherry fluorophore which is co-expressed on the cells infected with the MAIM plasmid

and was expected to range between 8-12% of the total cell population. Following the first analysis, each week an aliquot was taken to monitor the homogeneity of the FL cell population. Therefore, 200 µl were taken from each sample and transferred into a V-bottom 96-well plate. The cells were washed twice in 200 µl FACS buffer (centrifugation 400g, 3 min, 4° C) and afterwards resuspended in 160 µl FACS buffer. The analysis was done on Cytoflex (Beckman Coulter) with the Channels FITC for GFP and PE for mCherry. Death cells and singlets were excluded by size and/or complexity (forward scatter area vs. side scatter area and forward scatter area vs. side scatter height). Gates were positioned for FITC and PE according to intensities of the signal from positive controls (to include positive signals) while excluding the signal from negative control (**Fig. 7**).

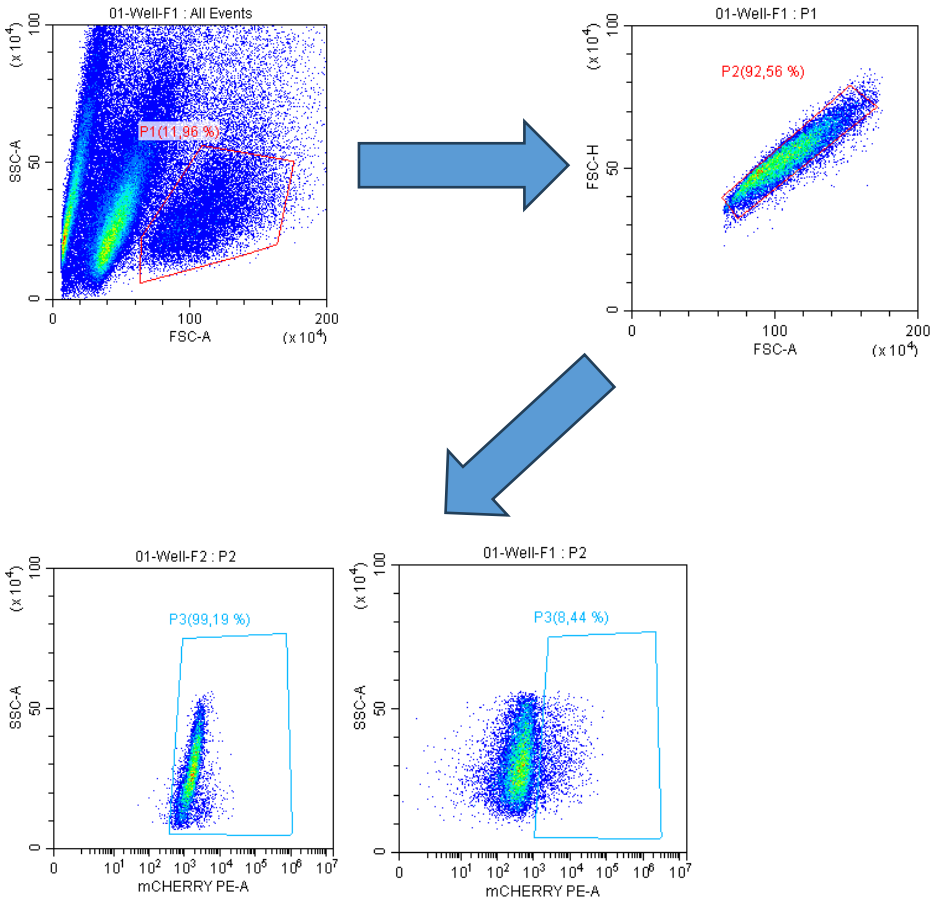


*Fig. 7:* ***Gating strategy for determining the populations to be positive for the mCHERRY reporter on the PE channel.***

FACS Buffer

1x PBS

1 mM EDTA

0,01% sodium azide

1% FBS

## 2.2. Bacterial culture

Chemically competent *Escherichia coli (E. coli)* DH5α-F' strains, which have been used before in our lab by Susanna Leiter in her Master thesis [173], were used for the amplification of the desired plasmids. For liquid cultures, competent cells were grown in 2-4 ml lysogeny broth (LB) medium supplemented with ampicillin and incubated at 37° C on a shaker with 180 rpm overnight or plated on LB-ampicillin agar plates and grown at 37° C overnight in an incubator. The final concentration of ampicillin for liquid LB medium and agar plates was 50 µg/ml.

LB medium and LB agar (pH 7.5, autoclaved)
10 g/l Bacto tryptone
5 g/l Bacto-yeast extract
5 g/l Sodium chloride
Diluted in dH2O and adjusted to pH 7.5 with 10M NaOH
15 g Bacto agar (only for agar plates)
Stored at 4° C

Ampicillin stock (100 mg/ml)
1 mg Ampicillin sodium (*Sigma Aldrich Cat. No. A9518-5G*)
dH2O to 10 ml
sterile filtered (0.2 µm filter) and stored at -20° C

### 2.2.1. Transformation of DH5α-F' E.coli

200 µl of chemically competent DH5α-F' E.coli bacteria were thawed on ice for each transformation. 10 µl (1/2 of the Ligation) of the plasmid DNA from the Ligation were added into a vial of competent cells, mixed gently, and incubated for 30 minutes on ice. Same was done with the positive control. Afterwards, the cells were heat-shocked for 45 seconds at 42° C without shaking. The vial was removed from the thermoshaker and incubated for 2 minutes on ice. 150 µl of prewarmed SOC medium were added to the transformed bacteria. The vial was capped tightly and shaken horizontally on a heat block at 37° C 350 rpm for 1 hour. During this time the LB-AMP plates were also preheated in the incubator, slightly opened to dry them, upside down. After the incubation step, the transformed

bacteria were plated on pre-warmed selective LB agar plates and incubated at 37° C overnight (Upside down). The next day, the plates were stored at 4° C.

SOC medium (500 ml)

10 g Yeast Extract (0.5% final)
2.5 g Tryptone (2% final)
0.25 g NaCl (10 mM final)
0.9 g KCl (2.5 mM final)
2.5 ml $MgCl_2$ (10 mM final from 2M stock)
2.5 ml $MgSO_4$ (10 mM final from 2M $MgSO_4 \cdot 7H_2O$)
Add 5 ml Glucose (20 mM final from 2M stock) after autoclaving
sterile filtered (0.2 µm filter) and stored at RT

### 2.2.2. Colony PCR

Bacterial colonies that grew on plates can be quickly analyzed by Colony PCR reactions, which enable the amplification of inserts present in plasmids from the bacteria, without specifically isolating DNA from these cells. With this time-saving technique a single colony can be used instead of isolated template DNA in the reaction mix. All other components are mostly the same as in a conventional PCR. In this way, the screening can identify cells with the desired insert very quickly. The colony PCR was performed with the 2x OneTaq 2X Master Mix with Standard Buffer (*NEB*) on a Thermocycler PCR machine (T100, Biorad). The OneTaq 2x MMX with standard buffer is a combination of two different polymerases - the Taq polymerase and the Deep Vent polymerase. The Deep Vent DNA polymerase from Pyroccocus species GB-D is a recombinant, high-fidelity enzyme with extreme thermostability and 3'→5' exonuclease activity that increases the fidelity of the Taq polymerase. It is a ready-to-use blend that can be used for routine PCR applications using purified DNA, cDNA or bacterial colonies. Besides the two polymerases this master mix already contains dNTPs, $MgCl_2$ and all necessary components of the reaction buffer. Additionally, there are two loading dyes present for running DNA gels. Used primers and their combinations are listed in **2.4.2.**

Colony PCR reaction mix
12.5 µl Green MM (2X)

8.75 µl $dH_2O$
0.5 µl forward primer (10 µM)
0.5 µl reverse primer (10 µM)
0.75 µl DMSO
2 µl colony water

To prepare the colony water, 50 µl of $dH_2O$ were filled into clean 0.2 ml PCR tubes and single colonies were picked up from the plates using a pipette tip. The colonies were then placed together with the tip in the PCR tubes. By shaking the tubes, the colonies were mixed with the water. 2 µl of this colony water was used in the reaction mix to provide the template DNA. As a positive control an already confirmed plasmid with known product size was used. The negative control only contained the master mix without any DNA. The success of the amplification was tested by loading an aliquot of the PCR reaction onto an agarose gel. The percentage of the gel was depending on the size of the expected fragment.

### 2.2.3. Inoculation of bacterial clones and preparation of glycerol stocks

Grown colonies picked with a pipette tip or 10-30 µl of the prepared colony water were inoculated in 4 ml LB medium supplemented with ampicillin for the preparation of liquid cultures. They were incubated overnight at 37° C on a shaking platform with 180 rpm for about 16 hours. Next day 500 µl of the culture were mixed in a 1:1 ratio with 500 µl of a 50% (v/v) glycerol solution for the preparation of glycerol stocks. They allow a long-term storage of bacterial clones that carry desired plasmids. Glycerol stocks were stored at -80° C.The rest of the liquid culture was used to isolate plasmid DNA from the bacteria.

### 2.2.4. Plasmid Minipreps

To isolate small amounts of plasmid DNA, overnight cultures were processed using the PureYield Plasmid Miniprep System (Promega). With this protocol up to 3 ml of overnight cultures could be processed. 1.5 ml of overnight culture were added to a 1.5 ml Eppendorf tube and centrifuged for 30 seconds at maximum speed in a tabletop centrifuge. The supernatant was discarded, and the step was repeated with another 1.5 ml of bacterial culture. Afterwards 600 µl $dH_2O$ were added and the pellet was resuspended completely. 100 µl Cell Lysis Buffer were added and the solution was mixed by inverting the tube 6 times. Then 350 µl of cold Neutralization Solution were added and the tube was inverted

again several times until the sample turned to yellow to signalize that the neutralization was completed. After centrifugation for 3 minutes at maximum speed, the supernatant was carefully transferred to a PureYield minicolumn assembled into a Collection tube, without disturbing the cell debris pellet. The tube holding the minicolumn was centrifuged at maximum speed for 30 seconds and the flowthrough was removed. Then two washing steps were performed: first, 200 µl Endotoxin Removal Wash were added to the minicolumn and centrifuged for 30 seconds. Next, 400 µl Column Wash Solution were added and centrifuged again for 3 minutes. To remove the residual wash solutions, the minicolumn was recentrifuged one minute at maximum speed with opened lid in a clean 2 ml Eppendorf tube, the minicolumn was turned 180° around its rotary axis and the centrifugation step was repeated. Afterwards the column was transferred to a clean 1.5 ml Eppendorf tube, 30 µl nuclease-free water were added to the minicolumn matrix and incubated for 1 minute at RT. After a final centrifugation step at maximum speed for 30 seconds, the minicolumn was removed and the DNA concentration was measured by NanoDrop. The DNA was then stored at -20° C.

### 2.2.5. Plasmid Midiprep

A Midiprep is the medium size preparation of plasmid DNA from bacterial cultures to gain higher amounts of isolated DNA. It was done using the centrifugation protocol of the QIAGEN® Plasmid Midi Kit. To prepare the overnight culture, a bacterial clone or small amount of a bacterial glycerol stock was inoculated in 2 ml LB medium supplemented with ampicillin and incubated for 4-6 hours at 37° C and 180 rpm. Then the whole culture was poured into 100ml of the corresponding LB medium and incubated overnight at 37° C shaking at 180 rpm. Next day the culture was transferred into each 2x 50 ml tubes and centrifuged at 5100 rpm for 30 minutes at 4° C. The supernatant was removed, and the pellet was resuspended completely in 4 ml Resuspension Solution (Buffer P1). Then 4 ml Cell Lysis Solution (Buffer P2) were added and the tube was mixed thoroughly by vigorously inverting 4-6 times. After 5 minutes incubation at RT 4 ml Neutralization Solution (Buffer P3) were added, the tube was mixed thoroughly by vigorously inverting 4-6 times and incubated for 15 minutes on ice. The lysate was centrifuged at 5100 rpm at 4° C for 90 minutes. A QIAGEN-tip 100 column was placed into a 50 ml plastic tube and equilibrated with 4 ml Buffer QBT. The lysate was poured into the column and allowed to flow through. The column was then washed 2x with 10 ml of Buffer QC. The flowthrough was discarded, and the Binding Column was placed into a new 50 ml plastic tube. The DNA was eluted by adding 5 ml buffer QF onto the column and precipitated with 3.5 ml

isopropanol on RT. The eluted DNA was mixed thoroughly with the isopropanol and subsequently centrifuged at 5100 rpm for 1 h at 4° C. The supernatant was discarded, and the pellet washed with 2 ml 70% ethanol. The DNA was centrifuged once again at 5100 rpm for 30 min, the supernatant was discarded, and the pellet air-dried for at least 10 min to get rid of residual ethanol and the pellet got transparent. 100 µl-300 µl of nuclease-free water were used to redissolve the DNA. The eluted DNA was finally transferred to a clean 1.5 ml Eppendorf tube. DNA concentrations were measured by NanoDrop. The purified DNA was stored at -20° C.

## 2.3. Animal studies

Mice were bred and kept under pathogen-free conditions at the Institute of Pharmacology, Medical University of Vienna. All animal experiments were approved by the Animal Ethics Committee of the Medical University of Vienna and granted by the Austrian Federal Ministry of Education, Science and Research and were performed by or under supervision of Lena Hess according to the guidelines of FELASA.

### 2.3.1. Breeding

Black 6 mice (C57BL/6) with the catalytic inactive *Hdac1* transgene were provided by my supervisor Lena Hess. The *Hdac1 CI* gene was introduced into the safe harbor locus *Rosa26*. A STOP cassette upstream of the HDAC1 transgene prevents its expression in absence of the Cre recombinase. An IRES-GFP reporter downstream of the HDAC1 transgene allows confirmation of its expression.

IFN-β-inducible *Mx1-Cre* black 6 mice were a gift from Sophie Edtmayer from the Stoiber-Sakaguchi lab [174]. *Rosa26 Hdac1 CI* and *Rosa26 Hdac2 CI* mice were crossed with *Mx1-Cre* mice. *Mx1-Cre* recombinase was expressed in a heterozygous manner throughout all experiments.

For timed breedings, which were performed to isolate fetal liver cells, mouse pairs were separated after 2 nights, and female mice were monitored during the next days for weight gain to assess pregnancy. For experiments, mice were sacrificed using isoflurane and cervical dislocation.

### 2.3.2. Isolation of murine fetal liver cells

In order to obtain fetal livers, mouse pairs were separated after 2 nights and monitored for up to two weeks to assess pregnancy by examining weight gain. On embryonic day 13.5

(E13.5) pregnant mice were sacrificed by applying 400 µl isoflurane in a closed vessel, the uteri isolated (kept in PBS on ice) and the embryos one by one separated from the yolk sac under sterile conditions. After removing all maternal tissue, samples of each embryo were taken for DNA isolation and subsequent genotyping where they were screened for *Hdac1* and *Mx1-Cre*. Fetal livers were dissected from each embryo using sterile forceps, and gently pressed through a pre-rinsed 70 µM cell strainer by using the flat end of a plunger of a 5 mL syringe to produce a single-cell suspension. The cell strainer was rinsed with PBS and the fetal liver cells (FLs) were centrifuged at 1200 rpm (Eppendorf tabletop centrifuge Centrifuge 5430R) for 5 min at RT. The pellet was resuspended in freezing medium and kept at -80° C for further usage.

Freezing Medium (FM)
FBS
20% DMSO

## 2.4. Work with DNA

### 2.4.1. Lysis of mouse tissue

Mouse toe tips were digested with 100 µl tail lysis buffer, containing 4 µl proteinase K (20 mg/ml) shortly added before incubation. After shaking at 55° C overnight, proteinase K was deactivated by incubating the samples at 95° C for 5 minutes. Then, 400 µl $H_2O$ were added and the samples were stored at 4° C.

Tail lysis buffer
100 mM Tris-HCl, pH 8.0
5 mM EDTA
200 mM sodium chloride
0.1% SDS

### 2.4.2. Polymerase chain reaction

The genomic regions of interest were amplified during a PCR reaction. In case of mouse tissue lysates, the samples were centrifuged at 14000 rpm for 10 minutes at 4° C

(Eppendorf tabletop centrifuge Centrifuge 5430R) and 1 µl of the supernatant was used as DNA template. For the PCRs, an appropriate positive control and a negative control without DNA was included. Primers were designed using the SnapGene software (5.0) and the appropriate annealing temperature of the primer pairs was determined with a gradient thermocycler. 2x OneTaq 2X Master Mix with Standard Buffer (NEB) was used (genotyping, restriction enzyme fragment analysis and colony PCR). If the PCR products were potentially required for further sequencing or during the cloning process, the Q5 polymerase from NEB was used.

Gradient PCRs were run with and without DMSO, which was added to the reactions to an end concentration of 3%, to test the inhibiting effect of secondary structure formation. The elongation time was adjusted according to the size of the expected fragment, given that the Taq polymerase is able to amplify 1 kb of DNA within 1 minute. The reactions were performed in a Thermocycler PCR machine (T100, Biorad) and the PCR products were separated on an agarose gel.

Forward primers for Cloning were designed to either include the restriction enzyme cutting sites (forward primers) or to anneal them to the resulting PCR products (reverse primers). Primers and PCR conditions are listed in the tables below in this section.

Taq polymerase PCR

1 µl DNA template
0.5 µl forward primer (10 µM)
0.5 µl reverse primer (10 µM)
12.5 µl 2x OneTaq 2X Master Mix with Standard Buffer (*NEB*)
Nuclease free $dH_2O$ ad 25 µl

PCR conditions

*Target: Cre*

| Temperature | Time | Cycles |
|---|---|---|
| **94° C** | 3 min | 1 |
| **94° C** | 45 sec | 40 |
| **58° C** | 60 sec | 40 |
| **72° C** | 90 sec | 40 |
| **72° C** | 3 min | 1 |

| | | |
|---|---|---|
| **12° C** | Hold | - |

*Target: HDAC1 Screen1*

| Temperature | Time | Cycles |
|---|---|---|
| **95° C** | 5 min | 1 |
| **95° C** | 30 sec | 35 |
| **56° C** | 30 sec | 35 |
| **72° C** | 120 sec | 35 |
| **72° C** | 5 min | 1 |
| **12° C** | Hold | - |

*Target: Stat3b*

| Temperature | Time | Cycles |
|---|---|---|
| **95° C** | 5 min | 1 |
| **95° C** | 30 sec | 40 |
| **56° C** | 60 sec | 40 |
| **72° C** | 45 sec | 40 |
| **72° C** | 5 min | 1 |
| **12° C** | Hold | - |

Q5 High-fidelity PCR

1 µl DNA template

0.5 µl dNTPs (10 mM)

1.25 µl forward primer (10 µM)

1.25 µl reverse primer (10 µM)

5 µl 5x Q5 reaction buffer

0.25 µl Q5 High-Fidelity DNA Polymerase (NEB)

Nuclease free $dH_2O$ ad 25 µl

*Target: Rosa26_IRES_mCherry*

| Temperature | Time | Cycles |
|---|---|---|
| **98° C** | 30 sec | 1 |
| **98° C** | 10 sec | 30 |

| | | |
|---|---|---|
| **65° C** | 30 sec | 30 |
| **72° C** | 30 sec | 30 |
| **72° C** | 120 sec | 1 |
| **12° C** | Hold | - |

Gradient PCR conditions

| Temperature | Time | Cycles |
|---|---|---|
| **98° C** | 30 sec | 1 |
| **98° C** | 10 sec | 40 |
| **52° C-65° C*** | 30 sec | 40 |
| **72° C** | 30 sec | 40 |
| **72° C** | 2 min | 1 |

*Primers were tested at 52° C, 54.5° C, 62.4° C and 65° C and a template free ctrl at 52° C for all 4 primer combinations.

*Primers*

| *PCR* | *Primer* | *Sequence* | *Product size* | *AT* | *ET* | *Cycles* |
|---|---|---|---|---|---|---|
| ***Cre*** | *Cre_F* | TAATCGCCATCTTCCAGCAG | *Cre+ 1000 bp* | *58° C* | *90 s* | *35* |
| | *Cre_R* | CAATTTACTGACCGTACAC | | | | |
| ***Hdac1 Screen 1*** | *Hdac1_ Screen 1_F* | GCATCGCCTTCTATCGCCTTC | *Rosa26 KI+, stop cassette present 1241 bp* | *56° C* | *120 s* | *35* |
| | *Hdac1_ Screen 1_R* | CTTGGTCATCTCCTCAGCATTGG | | | | |
| ***Stat3b*** | *Stat3_11_ fwd* | GCGTCTGACTCTACAACC | *fl/fl: 480 bp* *wt: 352 bp* | *56° C* | *60 s* | *40* |
| | *Stat3_11_ rev* | AGCCTCATCCTTAGGTACT | | | | |
| | *Stat3_14_ rev* | GACTGTGATAACCTTCAGTG | | | | |
| | *mCHERRY fwd* | ATTCCACAACCATGGTGAGCAAGGGCGAG | | *65° C* | *30 s* | *40* |

| | | | | | | |
|---|---|---|---|---|---|---|
| ***Rosa26_ IRES_ mCherry*** | *mCHERRY rev 1* | TATCTCGAGATCGCGG CCGCTTTACTTG | *PCR Fragment 727 bp* | | | |
| ***Rosa26_ IRES_ mCherry*** | *IRES_mCHE RRY fwd* | CGGTATCGATAAGCTT GATATCGAATTCCGCC | *PCR Fragments 1353 bp* | *65° C* | *30 s* | *40* |
| | *mCHERRY rev 2* | AATACTCGAGCCGCTT TACTTGTACAGCTCGT CC | | | | |
| ***MAIM*** | *MAIVmCherry _EcoRI_XhoI_ CPCR_fwd1* | GTCAAGACCACCTACA AGGCC | *PCR Fragment 211 bp* | *65° C* | *30 s* | *40* |
| | MAIV_CPCR _rev1 | ATCGATAAGCTTGGCT GCAGG | | | | |
| ***MAIM*** | MAIV_CPCR _fwd2 | AGTTACCTGGAAACAT CTGGAACATCC | *PCR fragment 720 bp* | *65° C* | *30 s* | *40* |
| | MAIVmCHERR Y_EcoRI_XhoI_ CPCR_rev2 | CATGAACTCCTTGATG ATGGCC | | | | |

*Table 2: List of primers used in this thesis*

### 2.4.3. Agarose gel electrophoresis

Dependent on the size of the expected DNA fragments or products, a 0.8-2% agarose gel was prepared. Therefore, an appropriate amount of agarose was dissolved in 100 ml 1x TAE buffer by boiling and mixed with 5 µl ethidium bromide (0.5 mg/l, Sigma). This was poured into a gel tray for polymerisation and the appropriate combs were inserted. Genomic DNA was mixed with 6x Orange G DNA loading dye; PCR products amplified with OneTaq 2X Master Mix (NEB) did not require any further preparation. The DNA samples were loaded into the gel pockets next to appropriate markers (1 kb Plus DNA Ladder (NEB), GeneRuler 1 kb DNA Ladder (Fermentas)). Usually, gels were run in 1x TAE buffer at 120 V and the DNA was visualised under UV.

<u>10x TAE buffer</u>
400 mM Tris-Acetate
20 mM EDTA

### 2.4.4. DNA extraction from agarose gels

DNA bands representing linearized plasmids after restriction digests were gel extracted using the Wizard® SV Gel and PCR Clean-Up System (Promega). Briefly, after agarose gel electrophoresis the bands were visualized under UV light and the desired bands were excised from the gel with a scalpel and transferred into a clean 1.5 ml Eppendorf tube. An appropriate volume (10 µl/10 µg of gel slice) was added to the gel and vortexed. Then the tube was incubated at 50-65° C on a heat block until the gel was completely dissolved. In the meantime, an SV minicolumn was inserted into a Collection tube. The dissolved gel was then transferred to the minicolumn and incubated for 1 minute at RT. Then the tube was centrifuged for 1 minute at 14,000 rpm. Also, all following centrifugation steps were performed at 14,000 rpm. The flowthrough was discarded and the minicolumn was placed back in the same collection tube. 700 µl Membrane Wash Solution were added and the tube was centrifuged again. After removing the flowthrough, the step was repeated with 500 µl Membrane Wash Solution and a centrifugation time of 5 minutes instead of 1 minute. An additional centrifugation step for 1 minute with opened lid was performed to remove any residual ethanol. Afterwards, the minicolumn was placed in a clean 1.5 ml Eppendorf tube, 40-50 µl (depending on the gel size) nuclease-free water were added carefully to the membrane and incubated for 1 minute. The tube was centrifuged again for 1 minute, the minicolumn was removed and the eluted DNA was either directly used for a subsequent ligation reaction or stored at -20° C. DNA concentrations were measured by NanoDrop (Thermo Fisher).

### 2.4.5. Restriction enzyme digests

Restriction enzymes EcoRI and XhoI were used for digestion of plasmids. Analysis of ligated plasmids was done with StuI *via* agarose gel electrophoresis. The DNA (0.5 µg) was mixed with one or two restriction enzymes and an appropriate buffer. The reaction was incubated at 37° C and 350 rpm on a heat block for at least one hour. In the case of FastDigest enzymes, the incubation took only 15 minutes. A heat inactivation of the used enzymes was performed if the DNA was further processed but not for control digests. Afterwards the whole sample (when the DNA needed to be eluted from the gel) or only an aliquot for analysis was loaded onto an agarose gel.

<u>RE reaction mix (20 µl)</u>

1 µg DNA template

1 µl restriction enzyme(s)

2 µl 10x buffer
Nuclease free $dH_2O$ ad 20 µl

| Restriction enzyme | Company | Restriction site | Incubation Temp. | Buffer | Heat inactivation |
|---|---|---|---|---|---|
| ***EcoRI-HF*** | New England Biolabs | 5'...GAATTC...3'<br>3'...CTTAAG...5' | 37° C | CutSmart™ Buffer | 65° C |
| **XhoI** | New England Biolabs | 5'...CTCGAG...3'<br>3'...GAGCTC...5' | 37° C | CutSmart™ Buffer / NEBuffer™ r3.1 | 65° C |
| **StuI** | New England Biolabs | 5'...AGGCCT...3'<br>3'...TCCGGA...5' | 37° C | CutSmart™ Buffer | No |
| **BstXI** | New England Biolabs | 5'...CCANNNNNNTGG...3'<br>3'...GGTNNNNNNACC...5' | 37° C | NEBuffer™ r3.1 | 80° C |

### 2.4.6. Ligation

Digested linearized DNA fragments were ligated with the T4 Ligase (*Thermo fisher Scientific*). The molar ratio of vector and insert was either 1:3 or 1:4 and 50 ng of vector were used per ligation reaction. Thus, the appropriate amount of the insert needed to be estimated first using the following equation:

$$\left[\frac{\text{ng vector} * \text{Kb insert}}{\text{Kb vector}}\right] * \left[\text{ratio } \frac{\text{insert}}{\text{vector}}\right] = \text{ng insert}$$

The calculated amounts of vector backbone and insert DNA were mixed with 2 µl 10x T4 Ligase buffer, 1 µl T4 Ligase and an appropriate volume of $dH_2O$ to a total volume of 20 µl. The incubation was performed at 25° C for 1 hour. If the transformation was done immediately afterwards, no heat inactivation was necessary. Otherwise Heat inactivation was done at 65° C for 10 min.

### 2.4.7. Cloning strategies

#### *2.4.7.1. Cloning strategy A) Basic cloning*

Rosa26_IRES_mCherry was amplified in PCR with the primers IRES_mCherry fwd (includes the RE site EcoRI) and mCherry rev 2 (adding the RE site sequence as adapter for XhoI). The acquired DNA sequence was purified with the Wizard® SV Gel and PCR Clean-Up System from Promega, by adding an equal volume of Membrane Binding Solution to the PCR amplification. The purified linear sequence of IRES_mCherry and MAIV were subject to restriction enzyme digestion with EcoRI and XhoI. The linearized DNA strands were gel purified by cutting the band at the expected height out of the gel after running an agarose gel chromatography and subsequent purification with the Wizard® SV Gel and PCR Clean-Up System from Promega. Both the digested and purified linear vector MAIV and IRES_mCherry gene were ligated with the T4 Ligase and the resulting vector MAIM used for transformation of competent DH5α-F' E.coli bacteria.

#### *2.4.7.2. Cloning strategy B) TA cloning*

Taq polymerase has the tendency to add a single deoxyadenosine (A) to the 3' end of PCR products. The linearized vectors supplied in the TOPO® TA Cloning® Kit (Invitrogen) have single, overhanging 3´ deoxythymidine (T) residues, which allows PCR inserts to ligate efficiently with the pCR™2.1-TOPO® vector in a TOPO® Cloning reaction.

Rosa26_IRES_mCherry was amplified as described above. The acquired DNA sequence was used in the subsequent ligation reaction without purification, but was checked in a agarose gel chromatography for correct size. The IRES_mCherry PCR product was directly used in the TOPO® Cloning reaction which was incubated for 10 min at 24° C and directly used for transformation of competent DH5α-F' E.coli bacteria. X-gal plates (1250 µg X-gal spread per plate and incubated till dry) were used to confirm the successful cloning of the TOPO® plasmid into the cells. Positive and negative colonies were picked for the colony PCR (Primers: See section **2.4.2**). Midipreps were made from 2 successfully cloned plasmids. The acquired TOPOmCherry plasmid was then, together with the MAIV plasmid digested in a ligation reaction with EcoRI and XhoI for 60 min on 37° C. The linearized plasmids were gel purified by cutting the band at the expected height out of the gel after running an agarose gel chromatography and subsequent purification with the Wizard® SV Gel and PCR Clean-Up System (Promega). Ligation with both the purified TOPOmCherry and MAIV plasmids was done with the T4 Ligase for 60 min on 24° C. Transformation of DH5α-F' E.coli bacteria was done as describe above. Insertion of

mCherry into MAIV was confirmed by colony PCR and control digest with the restriction enzyme StuI. 2 positive colonies were incubated for Midiprep and the successful generation of MAIM plasmids was checked again *via* StuI control digest.

TOPO Cloning reaction

1 µl PCR product

3 µl ddH2O (Nuclease free)

1 µl TOPO TA Cloning salt solution

1 µl TOPO plasmid

## 2.5. Work with proteins

### 2.5.1. Protein extraction of cells

#### *2.5.1.1. Freeze and thaw method*

The cells were resuspended in a suitable amount of Hunt buffer, containing protease inhibitors directly added before use. To lyse the cells, the sample was frozen in liquid nitrogen and rapidly thawed at 37° C, while shaking. Altogether this “freeze and thaw” cycle was done for three times. Following another freezing step, the sample was centrifuged at 14000 rpm for 30 minutes at 4° C and the supernatant, containing the cellular proteins, was transferred into a fresh tube. The protein concentration was determined by the Bradford protein assay.

#### *2.5.1.1. Extraction by sonication*

The cells were resuspended in a suitable amount of Karin buffer containing the protease inhibitors. Cells were lysed by sonication 2x 3 seconds for 6 cycles, while the power was kept in the range of 45-50%. The sample was centrifuged at 15000 rpm for 15 minutes at 4° C and the supernatant, containing the cellular proteins, was transferred into a fresh tube. The protein concentration was determined by the Bradford protein assay.

Hunt buffer

20 mM Tris-HCl (pH 8.0)

100 mM NaCl

1 mM EDTA

0.5% (vol/vol) NP-40

Low salt Hunt buffer
20 mM Tris-HCl (pH 8.0)
50 mM NaCl
1 mM EDTA
0.5% (vol/vol) NP-40

Karin lysis buffer
20 mM Tris-HCl (pH 8.0)
138 mM NaCl
10 mM EDTA
100 mM NaF
1% (vol/vol) NP-40
10% (vol/vol) glycerol

Inhibitors
1x complete protease inhibitor cocktail (Roche)
100 µM PMSF
10 mM sodium fluoride
10 mM β-glycerophosphate
10 µM sodium molybdate
100 µM orthovanadate (activated 5 minutes at 95° C)

### 2.5.2. Bradford protein assay

The “Bradford protein dye reagent concentrate” (BioRad) was diluted 1:5 with dH2O and 1 ml of this solution was mixed with 1µl of the protein extract. The absorbance at 595 nm was measured with a photometer and the concentration was calculated as follows: absorbance*10 = µg/µl). If the absorbance was below 0.150 or higher than 0.5, the measurement was repeated and the 1 ml Bradford reagent was either mixed with a higher or a lower amount of the protein extract, respectively. The protein concentration was always determined in triplicates and the average concentration was calculated.

### 2.5.3. SDS polyacrylamide gel electrophoresis (SDS-PAGE)

Proteins were separated according to their size by SDS-PAGE. First, the glass plates (BioRad) were assembled, the separation gel was filled between the spaces and covered with isopropanol. After polymerisation of the separation gel, the stacking gel was prepared and a comb was inserted. The protein samples were mixed with SDS loading dye and denatured for 5 minutes at 95° C. In case of multiple gel runs (e.g. 7% and 12%) for the same sample, double amount of protein samples were prepared and mixed to ensure homogenous denaturized lysates to be loaded. Next to the samples, 5 µl Precision Plus Protein all Blue ruler (BioRad) was loaded (**Fig. 8**). The gels were run up to 120 V, in an electrophoresis chamber (BioRad) filled with 1x Western running buffer.

<u>10% SDS separation gel (2 gels)</u>
3.45 ml 30% acrylamide
3.9 ml 1M TRIS, pH 8.8
3.06 ml $dH_2O$
52.5 µl 20% SDS
112 µl 20% APS
7.5 µl TEMED

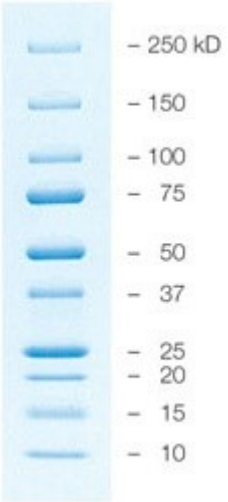

*Fig. 8: Precision Plus Protein all Blue ruler*

<u>5% stacking gel (2 gels)</u>
510 µl 30% acrylamide
375 µl 1M TRIS, pH 6.8
2.1 ml $dH_2O$
15 µl 20% SDS
28 µl 20% APS
7.5 µl TEMED

<u>Ammonium persulfate (APS)</u>
20% APS
Diluted in $dH_2O$

<u>SDS loading dye</u>
100 mM Tris-HCl, pH 6.8

20% glycerol
0.01% bromophenol blue
10% β-mercaptoethanol
5% SDS

10x Western running buffer
14.4% glycine
3% Tris/HCl
1% SDS

### 2.5.4. Western blotting (wet transfer)

After separation by SDS-PAGE gel electrophoresis, proteins were blotted on a nitrocellulose membrane. The support pads, 3MM filter paper (Whatman) and the nitrocellulose membrane (Amersham Protran, GE Healthcare) were moisturized with wet transfer buffer and the sandwich was assembled as following on a transfer cassette:

*Support pad*
*3MM filter paper (2 sheets)*
*Nitrocellulose membrane*
*SDS-PAGE gel*
*3MM filter paper (2 sheets)*
*Support pad*

The cassette with the sandwich was correctly positioned in the electrotransfer unit (Hoefer) which was subsequently filled with wet transfer buffer. The transfer of the proteins from the gel onto the membrane was performed at 4° C for 2 hours at 250 mA or alternatively at 40 mA overnight. Then, the membrane was shortly stained with Ponceau S and destained with dH2O.

Wet transfer buffer
25 mM Tris-HCl
190 mM glycine
20% methanol

10x Ponceau S

2% Ponceaus S

30% trichloracetic acid

30% sulfosalicylic acid

To prevent non-specific interactions, the membrane was incubated in blocking solution for 30 minutes, while shaking at RT.

Blocking solution, pH 7.4

1x PBS

1% polyvinylpyrrolidone

1% non-fat dried milk

0.1% Tween-20

0.01% sodium azide

### 2.5.5. Immunodetection of Western blots

Primary antibodies were diluted in 5 ml blocking solution according to the information in the Table below. After blocking, the Western blot membrane was incubated with the primary antibody overnight at 4° C while rotating. The next day, the blot was washed for three times in 1x PBS containing 0.1% Tween-20 for 15 minutes at RT. Then, the blot was incubated with the secondary antibody, diluted 1:10000 (In case where light chain secondary antibody was used it was diluted 1:5000), for 1 hour at RT on a shaker. After another three washing steps, the blot was prepared for detection using the chemiluminescent ECL Western Blotting Detection Reagent (GE Healthcare). 1 ml Detection Reagent 1 was mixed with 1 ml Detection Reagent 2 and pipetted onto the membrane. After short incubation, the blot was inserted into the chemiluminescence detection system Fusion-FX7-Spectra (Vilber) for imaging. Exposure time and image quality were adjusted according to the visibility of the bands due to the different antibodies.

### 2.5.6. Co-Immunoprecipitation

Whole cell extracts of HAP1 cells of which protein concentrations have been measured were investigated using co-immunoprecipitation assay (co-IP) in order to pull down the

proteins of interest. Therefore 80-1000 µg of proteins were diluted in Hunt buffer supplemented with inhibitors in a total volume of 300 µl. Then, 4 µg of a specific antibody (or 30-60 µl of antibodies from the Lab Seiser/Lab Ogris collaboration self-made stock) were added to the extracts and, if not stated differently, the vials were incubated for at least 1 hour on a rotor at 4° C and 25 rpm. A control sample for unspecific binding was included with IgG mouse and/or IgG rabbit, which was eventually used as background control. Meanwhile, the used magnetic beads, either protein A- (rabbit) or G- (mouse) beads (Dynabeads) from Invitrogen, were blocked with BSA (Bovine serum albumin). For this purpose, 30 µl beads or 60 µl beads, respectively, per sample were transferred to a 1.5 ml Eppendorf tube. The tube was then placed in a magnetic rack and the supernatant was removed. The beads were washed 3 times with 500 µl Hunt buffer with inhibitors each. After removing the supernatant, 90 µl Hunt buffer with inhibitors and 10 µl BSA (10 mg/ml) per sample were added to the beads. Then the vials were incubated on a rotor for at least 30 minutes at 4° C for blocking of the beads. As soon as the incubation time was over, the beads were taken from the rotor, spun down quickly and then aliquoted into 100 µl per co-IP. The tubes were placed again on the magnetic rack and the supernatant was discarded. Then, the whole volume of the incubated protein-antibody-mixture was added. The co-IP took place overnight at 4° C on the rotor if nothing else is stated. Next day, the samples were taken from the rotor and put on the magnetic rack to remove the supernatant. The beads - that were now coupled to the appropriate target protein and its complex partners - were washed 3 times with 500 µl Hunt buffer with inhibitors. After removing the supernatant 300 µl Hunt buffer with inhibitors were added to each sample and mixed well. Then, the samples were separated into two parts: 2/3 (200 µl) were used for Western blotting and (1/3) 2x 50 µl (distributed among two technical replicates) were used to perform HDAC activity assay. The samples used for Western blotting were mixed with 30 µl SDS loading buffer without DTT and denatured for 5 minutes at 60° C on a heat block. Then, the samples were placed back to the magnetic rack and 15 µl of the supernatant (without beads) were transferred to a new tube where 5 µl SDS loading buffer with DTT were added and denatured for 5 minutes at 95° C. 15 µl of the denatured proteins were loaded on the prepared SDS gel.

For NCOR IP 1 mg of cell lysate in Hunt buffer was used as INPUT. Cells where lysed with the freeze and thaw method. The IP was done with 3 µl of the primary antibody NCOR1 ab24552 per IP. 30 µl of A-beads (Dynabeads®) were used as secondary antibody. 20 µg of INPUT WCL and 1/3rd of the IP eluate was applied on a western blot. Secondary AB detection on blots was done with a light chain antibody.

### 2.5.7. FLAG-Immunoprecipitation

30 µl of FLAG M2 Magnetic Beads (M8823, Sigma-Aldrich) were used per sample. The beads were washed three times in 1x TBS (Tris-buffered saline) and blocked for 30 min in 1 mg/ml BSA in 1x TBS. The blocking reagent was removed, and the beads were incubated overnight with 400-800 µg of protein extract in Hunt buffer containing protease inhibitors, rotating at 4° C. The next morning, the beads were washed 3x with 1x TBS. After the last washing step, the beads were resuspended in 300 µl Hunt buffer. 1/3 of the beads were used for the histone deacetylase assay and were further distributed into technical duplicates (2x 50 µl) and 2/3 of the beads were used for Western blotting. For elution of IP (immunoprecipitation) samples from the beads, the Hunt buffer was removed. Per sample, 30 µl SDS loading dye without dithiothreitol (DTT) were mixed with the beads and incubated at 55° C for 5 min, 500 rpm in an Eppendorf Thermomixer. Finally, the eluate was separated from the beads, and further processed for Western blotting.

1x TBS
50 mM Tris-HCl
150 mM NaCl
in dH2O and adjusted to pH 7.4

### 2.5.8. Histone deacetylase activity assay (HDAC activity assay)

Input samples containing 20 µg of proteins were mixed with Hunt buffer with inhibitors in a total volume of 20 µl. The supernatant of 2x 50 µl eluate from IP samples (as technical replicates) was discarded and the beads containing precipitated HDAC brought into 20 µl of Hunt buffer. Samples were then supplemented with 2 µl [$^3$H]-acetate-labeled chicken erythrocyte histones (1.5-2 mg/ml). The samples were incubated for 4-6 hours at 30° C and 300 rpm on a heat block. Also, a BLANK sample was prepared that contained 20 µl Hunt buffer with inhibitors and 2 µl $^3$H-Histones. Afterwards, 35 µl Histone Stop Solution and 800 µl ethyl acetate were added to the samples for phase separation. In between they were inverted 4 times. They were vortexed for at least 15 seconds and then centrifuged for 4 minutes at 10,000 rpm at RT using a swing out bucket. 600 µl of the upper, organic, phase that should contain released radiolabelled acetyl groups were transferred to scintillation bottles containing 3 ml of a Scintillation Solution. The vials were inverted in order the solution to be mixed and finally placed in a Liquid Scintillation Analyzer (Packard) that measured the detected ionization events per minute (counts per minute, CPM). **Fig. 9** illustrates the principle of the HDAC activity assay.

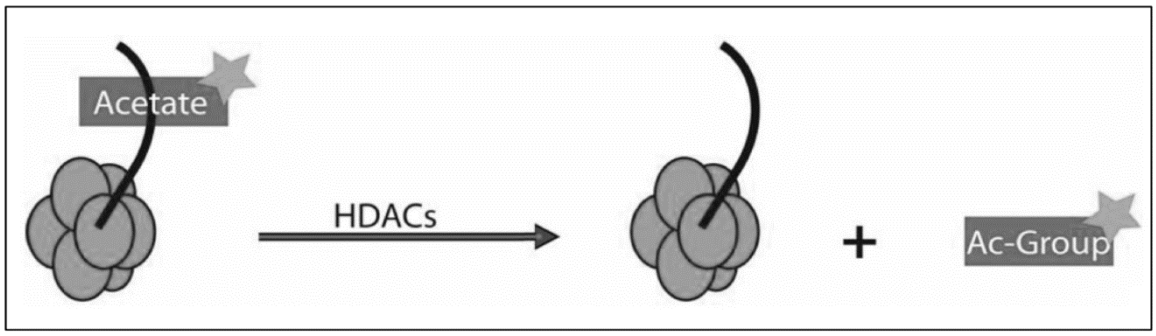


***Fig. 9: Principle of HDAC activity assay (illustration made by A. Leopoldi).*** *Protein extracts are incubated with histone proteins that contain $^{3}$H-labelled acetyl groups. If active deacetylases are present, they should be able to remove the acetyl-groups that can be extracted using the organic solvent ethyl acetate. Released acetyl-groups migrate into the upper organic phase and are transferred into a scintillation solution, containing two scintillators (PPO & POPOP) that are excited by the radioactivity and emit light that is detected.*

Histone Stop Solution

1 M HCl

0.4 M Sodium acetate

Scintillation Solution

5 g/l PPO (2,5-Diphenyloxazole)

0.5 g/l POPOP (1,4-Bis-(5-phenyl-2-oxazolyl)-benzol)

Filled up with toluene

### 2.5.9. HDAC activity assay with HDAC3 and HDAC8 kits

Both the HDAC3 (Cat. #EPI004) and HDAC8 (Cat. #EPI006) kits from Sigma are based on the feature of AFC covalently bound a short target peptide containing acetylated lysine ([R-H-K-K(Ac)-AFC] in case of the HDAC3 kit, [R-H-K(Ac)-K(Ac)-AFC] in case of the HDAC8 kit). Deacetylation activity of HDACs leads to cleavage and release of the quenched fluorescent group, AFC. AFC can be detected at 500nm fluorescence ($\lambda_{ex}$=380 nm). Further, samples can be prepared and measured in a 96-well format.

#### *2.5.9.1. HDAC3 Activity Assay kit*

Samples were prepared and measured according to the suggested manufacturers procedure in black flat-bottom 96-well plates with clear bottom (Thermo Scientific). Briefly,

input samples which were taken the day before and contain 20 µg of proteins were mixed with HDAC3 assay buffer a total volume of 60 µl and 25 µl distributed into two wells as duplicates. The supernatant of 100 µl (2x 50 µl) eluate from IP samples (as technical replicates) was discarded and the beads containing precipitated HDAC resuspended in 60 µl HDAC3 assay buffer. 25 µl of each duplicate was distributed per well. A mix of 25 µl total volume HDAC3 assay buffer containing 2 µl of HDAC3 substrate was added to a well and, after shaking, incubated 30 min at 37° C. To complete the cleavage reaction, 10 µl developer and 40 µl HDAC3 assay buffer were added, mixed well and incubated again at 37° C for 5 min. Plates were measured in the Enspire 2300 multilabel reader (Perkin Elmer).

#### *2.5.9.2. HDAC8 Activity Assay kit*

Samples were prepared and measured according to the procedure suggested by the manufacturer in black flat-bottom 96-well plates with clear bottom (Thermo Scientific). Briefly, input samples containing 20 µg of proteins were mixed with Hunt buffer with inhibitors in a total volume of 20 µl. The supernatant of 2x 50 µl eluate from IP samples (as technical replicates) was discarded and the bead fraction containing the precipitated HDAC transferred into 20 µl of Hunt buffer and 30 µl HDAC8 assay buffer were added. A mix of 38 µl total volume HDAC8 assay buffer containing 2 µl of HDAC8 substrate was added to a well and, after shaking, incubated 60 min at 37° C. To complete the cleavage reaction, 10 µl developer were added, mixed well and incubated again at 37° C for 5 min. Plates were measured in the Enspire 2300 multilabel reader (Perkin Elmer).

### 2.5.10. Antibody list

#### *2.5.10.1. Primary Antibodies*

| Name | Antigen | Cat. Number / clone | Species | Company | Dilution |
|---|---|---|---|---|---|
| **M2 FLAG** | M2 FLAG | F1804 | mouse | Sigma | 1:1000 |
| **HD1 SAT 208** | HDAC1 | SAT208 | rabbit | Seiser lab | 1:10000 |
| **HD2 ab7029** | HDAC2 | ab7029 | rabbit | Abcam | 1:5000 |
| **HD2 3F3** | HDAC2 | 3F3 | mouse | Seiser/Ogris labs | 1:1000 |
| **HD3 ab7030** | HDAC3 | ab7030 | rabbit | Abcam | 1:5000 |
| **HD8 ab187139** | HDAC8 | ab187139 | rabbit | Abcam | 1:10000 |
| **DYKDDDDK (M2 FLAG)** | M2 FLAG | 2368S | rabbit | Cell Signaling | 1:1000 |

| | | | | | |
|---|---|---|---|---|---|
| **B-Actin ab8226** | B-Actin | ab8226 | mouse | Abcam | 1:1000 |
| **B-Actin ab8227** | B-Actin | ab8227 | rabbit | Abcam | 1:1000* |
| **B-Actin ab8227** | B-Actin | ab8227 | rabbit | Abcam | 1:10000 |
| **B-Actin A5316** | B-Actin | A5316 AC74 | mouse | Sigma | 1:5000 |
| **sin3a AK-11** | sin3a | sc767 | rabbit | Santa Cruz | 1:500 |
| **Sin3a ab3479** | Sin3a | ab3479 | rabbit | Abcam | 1:1000 |
| **MTA-2** | MTA2-276 | sigma276 M7569 | mouse | Sigma | 1:1000 |
| **sin3a G-11** | sin3a | G-11 | mouse | Santa Cruz | 1:200 |
| **NCoR1** | NCoR | ab24552 | rabbit | Abcam | 1:1000 |
| **NCoR2** | SMRT | ab24551 | rabbit | Abcam | 1:1000 |
| **p53 DO-7** | p53 | DO-7 | mouse | Santa Cruz | 1:20 |
| **HD3 3G6** | HDAC3 | 3G6 | mouse | Seiser/Ogris labs | 1:25 |
| **HD8 ab187139** | HDAC8 | sc11405 | rabbit | Santa Cruz | 1:500 |
| **NCoR1** | NCor | ab3482 | rabbit | Abcam | 1:700 |
| **NCoR1** | NCor | ab3482 | rabbit | Abcam | 1:500* |
| **NCoR2** | SMRT | ab5802 | rabbit | Abcam | 1:250 |
| **Vinculin** | Vinculin | sc25336 | mouse | Santa Cruz | 1:500* |
| **Vinculin** | Vinculin | sc25336 | mouse | Santa Cruz | 1:250 |
| **HDAC8 sc11405** | HDAC8 | sc11405 | rabbit | Santa Cruz | 1:500 |
| **CoREST** | CoREST | 07-455 | rabbit | Sigma | 1:1000 |

*Table 3: List of primary antibodies used in this thesis for WB and (Co-)IP. *main dilution is marked.*

#### *2.5.10.2. Secondary antibodies*

| Name | Antigen | Cat. Number / clone | Species | Company | Dilution |
|---|---|---|---|---|---|
| **Mouse HRP** | mouse | | mouse | | 1:10000 |
| **Rabbit HRP** | rabbit | | rabbit | | 1:10000 |
| **Mouse HRP LC (light chain)** | mouse | 115-035-174/142604 | mouse | Jackson ImmunoResearch | 1:5000 |
| **Rabbit HRP LC (light chain)** | rabbit | 211-032-171/142605 | rabbit | Jackson ImmunoResearch | 1:2500 |

*Table 4: List of secondary antibodies used in this thesis for WB.*

## 2.6. Data analysis and statistics

### 2.6.1. HDAC activity assays

Graphical visualization and statistical analysis were done by GraphPad Prism version 5.00 for Windows (GraphPad Software, San Diego, California, USA). Statistical analysis of two samples with at least 3 replicates per sample was performed using the Welch's t-test.

### 2.6.2. RNA-seq/ChIP-seq and Heatmap

RNA samples for RNA-seq were isolated by Verena Moos [167]. Sequencing for RNA-seq and ChIP-seq was done at CEMM. Reads were aligned with STAR (as reference served genome hg38 (December 2013) and transcriptome hg38_e100 (April 2020) and raw gene count data was provided by Michael Schuster from CEMM. The analysis of differentially expressed genes was performed with DEseq2 (*1.30.0)* in R (version *4.0.4)*. DEseq2 was run with default parameters with the design formula = *~ group*, Rows with a raw data count below 1 were dropped. Beside of the wt ctrl samples (n=6) only the samples of interest (each samples n=3) shown in the heatmaps are considered as factor in *group* for the design formula. After running DEseq2, genes with an adjusted p-value below 0.1 were kept and subgroups were created which are depending on the log2-Fold change of the respective gene between the wt condition and the condition of interest (Above 1, between -1 and 1, below -1). The RNA-seq data has been deposited to the NCBI Gene Expression Omnibus (GEO) under GSE193885 (**https://www.ncbi.nlm.nih.gov/geo/query/acc.cgi?acc=GSE193885**)

RNA-seq gene set similarity was subsequently estimated with GeneOverlap (*1.32.0*) in R.

To compare data from RNA-seq to ChIP-seq data, significant genes from RNA-seq samples analyzed by DEseq2 ($p < 0.1$, log2Fold < 1) were compared to significant genes from ChIP-seq samples analyzed by Diffbind (run by Michael Schuster, CEMM) (FDR < 0.05, log2Fold < 0). Peaks from -500 basepairs to +1000 basepairs around the Transcription Start Site (TSS) were taken.

Heatmaps were created in pheatmap (*1.0.12)* with genes only fulfilling the demanded classifications. For Heatmaps in KO background genes were further classified by behaviour between the wt cell and additional different conditions as stated in the figures.

The R package tidyverse (*1.3.2*) supported table adaptions to create input and export data in the workflow.

Selected clusters of differentially expressed genes which grouped together after the DEseq2 run were analysed through ENRICHR [175], [176] for enrichment of genes for ontologies in GO 2023 [177].

### 2.6.3. Code (R scripts) availability

The source code of the R scripts which have been written and used are available in the folder under the following link in the Github repository:

**https://github.com/laubera14/HDAC_HAP_RNAseq/tree/main**

# 3. Results

## 3.1. Activity of endogenous class I HDACs in HAP1 cells

To systematically study the catalytic functions of class I HDACs we compared their activity in HAP1 cells against acetylated histones using antibody-based approaches. In previous experiments our lab precipitated either HDAC1, HDAC2, HDAC3 or HDAC8, using specific antibodies (Immunoprecipitation – IP), and measured their activity with help of [$^3$H]-acetate-labelled chicken erythrocyte histones as substrate (HDAC activity assay). These experiments were established in our lab before with HAP1 cells (Horizon genomics, near-haploid, fibroblast-like cells derived from the human male chronic myelogenous leukemia (CML) cell line KBM-7). HAP1 HDAC knockout cell lines were produced by Verena Moos and her Master student Susanna Leiter in collaboration with Horizon Genomics.The initial characterisation of the generated cell lines by HDAC activity assays and Western blot analysis was done by Verena Moos, Susanna Leiter, Anna Riegler, Brigitte Gundacker and Petra Vician [167].

Preliminary experiments with newly thawed cell batches from the generated cell lines were performed by me and my supervisor Lena Hess for measurement of HDAC activity with the HDAC activity assay. HDAC1, 2, 3 & 8 were immunoprecipitated from HAP1 WT and the individual knockout cell extracts and the deacetylase activity was measured. The HDAC activity assay worked well for HDAC1 and HDAC2, albeit the measured activity at around 850 CPM (counts per minute) left room for improvement (see **supplemental 5.1**). In contrast, HDAC3 had very low deacetylase activity and HDAC8 showed only background activity (**supplemental 5.1**).

Therefore, different approaches were tested in this thesis to optimize immunoprecipitations and activity measurements for HDAC1, HDAC2 and HDAC3.

### 3.1.1. Optimization of HDAC1/2 immunoprecipitation

HDAC1 and HDAC2 are both interacting with the same co-repressor complexes such as Sin3, CoREST and NuRD, and were subsequently analysed together.

In order to improve immunoprecipitations of HDAC1/2, new monoclonal antibody aliquots, which were produced in collaboration with the Ogris lab and targeting endogenous HDAC1 and HDAC2 (10E2 and 3F3, respectively), were obtained and tested for IP.

Protein extracts from wildtype HAP1 cells, as well as from KO HDAC1 cells and KO HDAC2 cells, which were used as background controls, were used for IP.

As shown in **Fig. 10 A & B** wildtype HAP1 cells showed deacetylase activities for HDAC1 and HDAC2 that were approximately 40% higher compared to the previous experiment (intro of **section 3.1**), which suggests that the new antibody aliquots work better than the old ones.

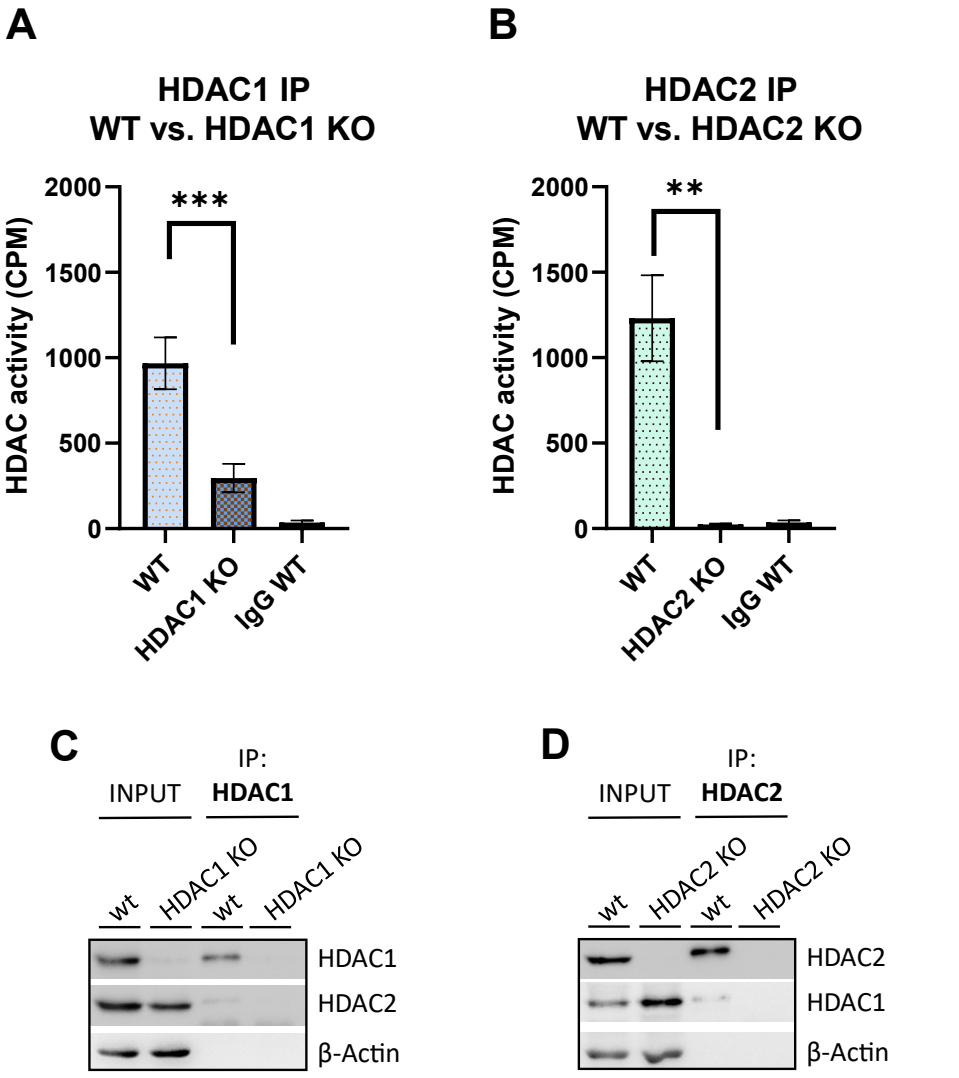


***Fig. 10: Determination of histone deacetylase activity of endogenous HDAC1 and HDAC2.*** *Endogenous HDAC1 or HDAC2 enzymes were precipitated from wildtype HAP1 cells using monoclonal antibodies specific for HDAC1 or HDAC2. HDAC1 and HDAC2 KO cell lines were included in the experiment as background controls. As additional negative control sample, a mouse IgG antibody was used for IP, together with wildtype HAP1 cellular extract. 700 µg of each whole cell lysate were used for each IP.* ***(A & B)*** *Bar charts showing absolute deacetylase activity of precipitated HDAC1 and HDAC2 towards histones in CPM (counts per minute). Statistical significance was calculated by Welch's t-test. **p < 0.01, ***p< 0.001.* ***(C & D)*** *Western blot analysis of corresponding precipitates. 20 µg of INPUT extract (cellular extract taken before IP) and 1/3rd of the IP-eluate was applied on a Western blot.* n=4

While almost no HDAC activity was observed for the HDAC2 IP in the HDAC2 KO, the HDAC1 IP in the HDAC1 KO still yielded a relatively high background activity. In detail, HDAC1 KO cells show a 3-fold lower activity in HDAC1 precipitates compared to the wildtype cells. For HDAC2 KO cells the activity drops 50-fold in comparison to wildtype cells.

Western blot analysis of input and IP samples (**Fig. 10 C & D)** confirmed the knockout of HDAC1 and HDAC2 in the respective cell lines. In input samples of HDAC2 KO cells, the HDAC1 band was more prominent compared to input samples of wildtype cells, while β-Actin shows equal amount of loaded protein lysate. It was previously shown, that HDAC1 and HDAC2 can compensate for the loss of the paralogue in co-repressor complexes [160], [161], [178]. HDAC1 and HDAC2 can coexist in the same co-repressor complex, which can harbor two or more HDACs (beside of CoREST where only either of them is recruited) [179]. Further, HDAC1 and HDAC2 have the ability to heterodimerize [114]. For these reasons, they co-immunoprecipitate, which can be also seen well on the blots above. All in all, it was confirmed that endogenous HDAC1 and HDAC2 display a robust deacetylase activity in activity assays with radioactive labelled acetylated histones. Additionally, the new antibody batches work significantly better (2-fold higher CPM values) compared to previously used aliquots.

### 3.1.2. Optimization of HDAC3 immunoprecipitation

Measurement of endogenous HDAC3 in HAP1 cells has been challenging since activity values obtained in HDAC activity assays are relatively low and just slightly above the

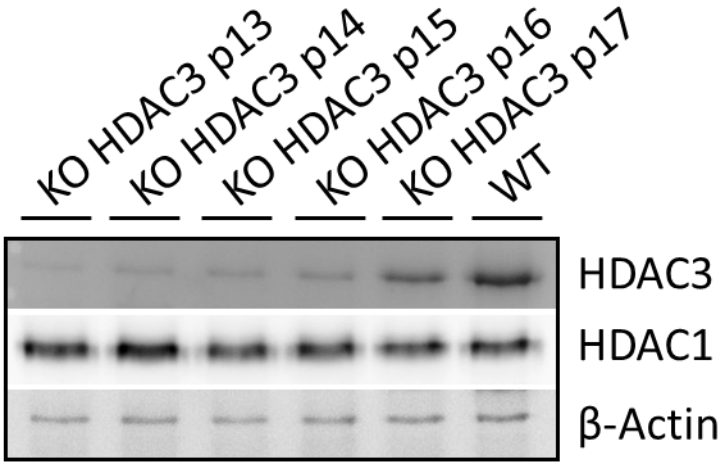


***Fig. 11: Western blot analysis of different passages of HDAC3 KO cells.***
*HDAC3 KO cell lysates from passage 13 to 17 were loaded on a Western blot. WT cells were used as control.*

background levels as seen in preliminary experiments (intro **section 3.1**). This has been repeatedly shown in this thesis with both the HDAC activity assay (e.g. **section 3.1.2.1**) as well as with a commercially available kit (**section 3.1.2.2**).

Furthermore, the HDAC3 enzyme in HDAC3 KO cells is recurrent in higher passages and the expression levels correlate with passage number (**Fig. 11**). While this circumstance is taken into consideration in the description of the results from the following experiments, this correlation was not fully understood until before the final experiment of the optimizations (**section 3.1.2.5**) was performed.

In this section, the optimization of the protocol from lysis of HAP1 cells to performance of HDAC activity assay is shown.

#### *3.1.2.1. HDAC3 immunoprecipitation using the "standard" protocol*

HDAC3 IP was initially performed by using standard conditions (Hunt buffer, 30 µl antibody, 600 µg protein lysate). Protein extracts from wildtype HAP1 cells and HDAC3 KO cells were used for IP. The precipitated proteins were analysed on Western blots and the activity was measured with the HDAC activity assay.

The activity of precipitated HDAC3 is relatively low compared to HDAC1 or HDAC2, respectively (see **section 3.1.1**) but clearly above background activity from the IgG ctrl IP. However, the measured activity of precipitates from HDAC3 KO cells is similar to precipitates of WT cells (**Fig. 12 A**). The activity associated with HDAC3 IPs in the KO cells increase depends on the passage number of the cells, which was here 132CPM for p13, 167 for p15 and 190CPM for p16. Western blot analysis shows a faint HDAC3 band in input and IP-samples from the HDAC3 KO cells, while the loading control β-Actin shows equal amounts of loaded lysates in the INPUT (**Fig. 12 B**).

It is also obvious that background bands were visible in the precipitated HDAC3 KO sample. HDAC3 is part of the NCoR/SMRT complex, thus we probed against NCoR2, which is also called SMRT [133]. The NCOR2 band is faint and cannot be seen in the samples beside of HDAC3 KO. Summarized, it can be said that the activity measurement does not show any difference between HDAC3 KO cells and WT cells. The experiments which were performed subsequently had the goal to tackle this problem by investigating the reasons for this rather unexpected outcome and optimizing the method.

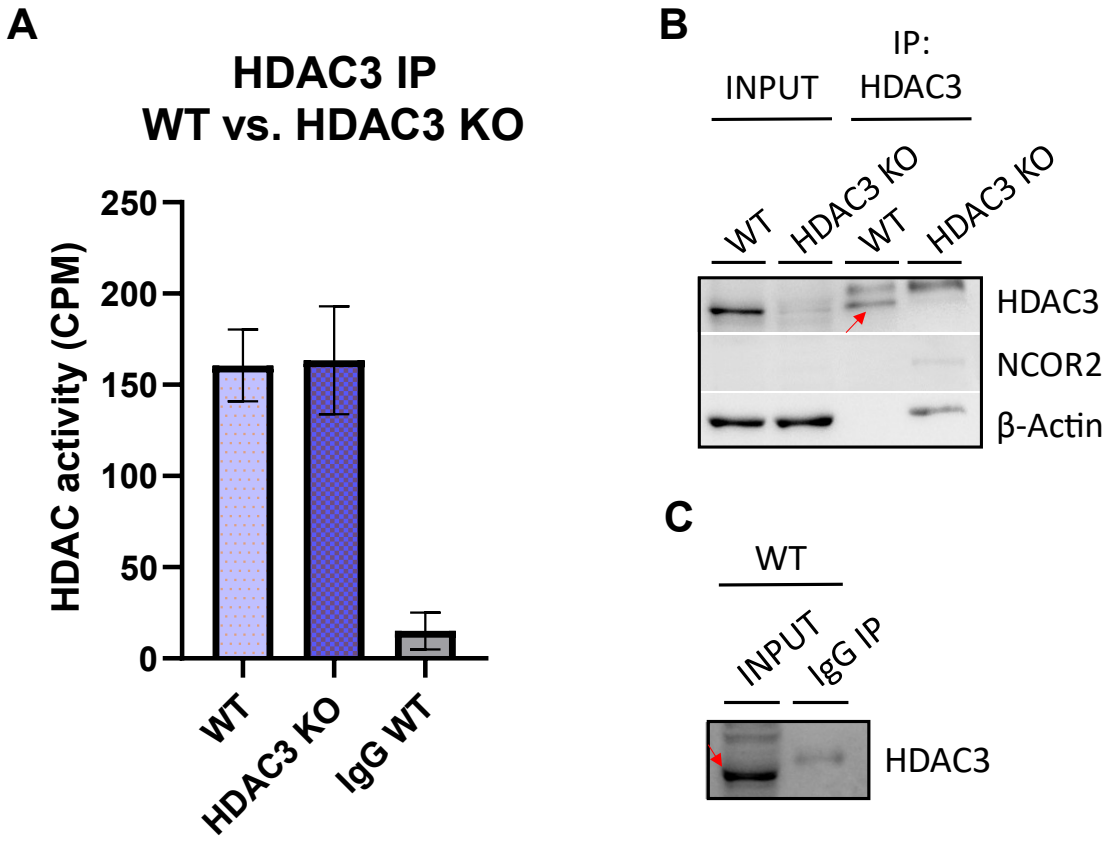


***Fig. 12: Activities of precipitated endogenous HDAC3 under standard conditions**. 600 µg of whole cell lysate was incubated with 30 µl of HDAC3 3G6 monoclonal antibody for immunoprecipitation. As additional negative control sample, a mouse IgG antibody was used for IP, together with wildtype HAP1 cellular extract. **A)** Bar chart showing absolute deacetylase activity of precipitated HDAC3 towards histones in CPM (counts per minute). Statistical significance was calculated by Welch's t-test. **B)** Western blot analysis of corresponding precipitates. 20 µg of INPUT extract (cellular extract taken before IP) and 1/3rd of the IP-eluate was applied on a Western blot. **C)** Western blot analysis of WT lysate in INPUT (before IP) and after IP with IgG. Red arrows indicate the band of HDAC3.* N=3

### *3.1.2.2. HDAC3 immunoprecipitation with higher amounts of proteins and antibody*

Since the previous HDAC3 IP experiment (**section 3.1.2.1**) showed similar HDAC activity between WT and HDAC3 KO cells, which was unexpected, various optimizations were tested for the IP. The amount of protein lysate that was used for the IP was increased to 1 mg and simultaneously it was tested whether a double amount of the HDAC3 3G6 monoclonal antibody leads to precipitation of a higher amount of HDAC3 with acceptable

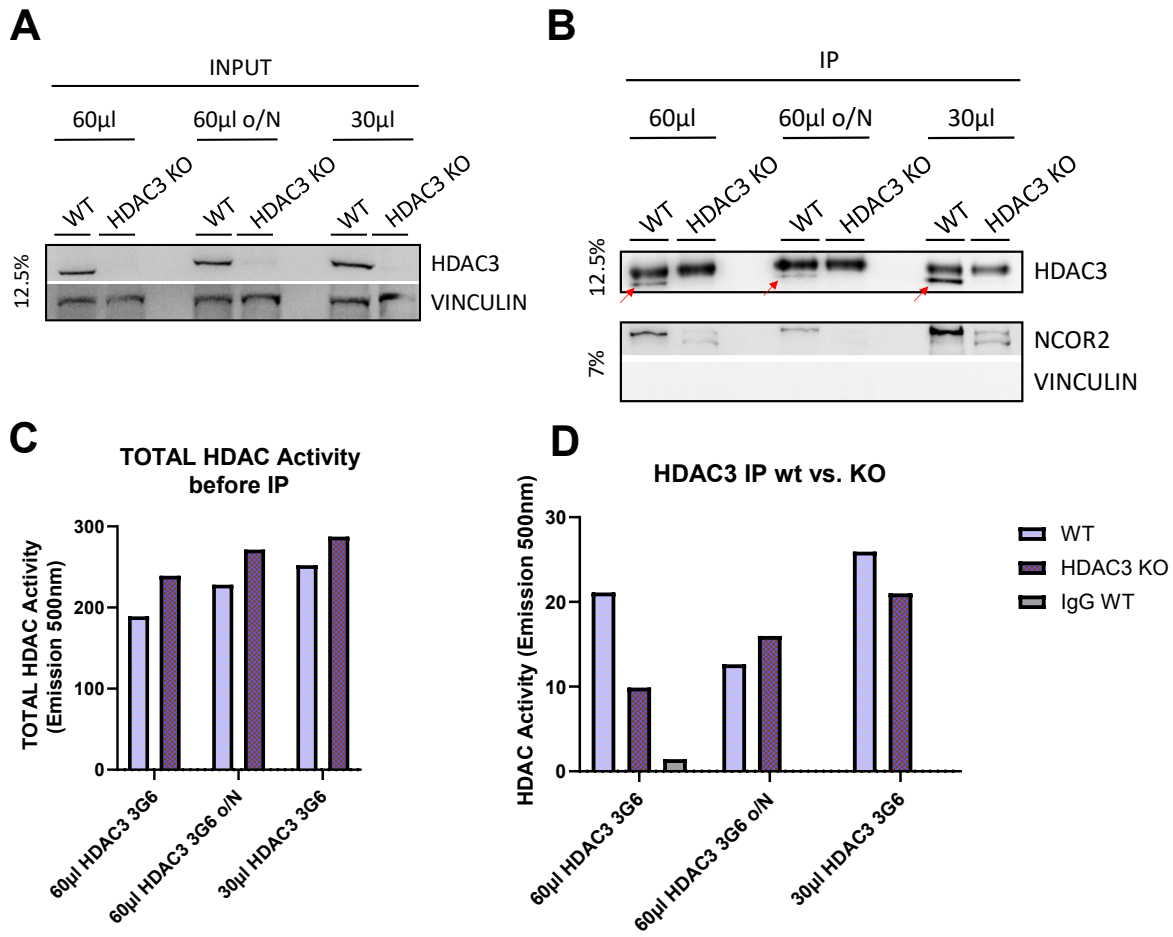


***Fig. 13: Activities of precipitated endogenous HDAC3 with different antibody amounts and incubation times used for IP****. 1 mg of whole cell lysate was precipitated with HDAC3 3G6 monoclonal antibody, either for 1h or over night. As additional negative control sample, a mouse IgG antibody was used for IP, together with wildtype HAP1 cellular extract. Deacetylation activity was measured by using the commercially available HDAC3 kit from SIGMA. HDAC3 KO cells hat passage number 14.* ***A)*** *Western blot analysis of respective INPUT samples which were subsequently used in the IP. 20 µg of cell lysate were loaded per lane.* ***B)*** *Western blot analysis of precipitated cell lysates. 1/3rd of eluate was applied per lane. Detection was done with HDAC3 antibody on a 12.5% gel and with NCOR1 and VINCULIN antibody on a 7% gel. Red arrows indicate the bands of precipitated HDAC3.* ***C)*** *bar chart showing total HDAC activity in 20 µg of WT or HDAC3 KO cell lysates prior to HDAC3 3G6 IP.* ***D)*** *bar chart showing HDAC activity of precipitates after HDAC3 IP.*

background. Additionally, we wanted to account for the possibility of HDAC3 to prefer non-histone targets and thus used a commercially available HDAC3 activity kit (with an acetylated peptide as substrate) instead of the previously used [$^3$H]-acetate-labelled chicken erythrocyte histone deacetylation activity assay (HDAC activity assay).

Protein extracts from WT cells and HDAC3 KO cells were used in 3 different IP approaches: 1) Incubation with the primary antibody for 1 hour and over night incubation with protein G beads, as in the standard method, but with 60 µl 3G6 HDAC3 antibody. 2) One replicate was incubated overnight (o/n) in primary antibody with subsequent 2-hour incubation with protein G beads on the next day. 3) Incubation of 1 mg lysate, as in 1) and 2), but with the standard 30 µl 3G6 HDAC3 antibody.

Concerning the Western blot analysis of lysates before they were used for IP (**Fig. 13 A**), the loading control VINCULIN shows nearly identical amounts in WT and HDAC3 KO samples, which were deployed before IP. On closer inspection, HDAC3 KO samples display a faint HDAC3 band. This is in line with the observation that higher passages of HDAC3 KO cell lysates are not able to maintain the full HDAC3 KO status. The passage number of HDAC3 KO cells used in this experiment was p14. Nevertheless, the HDAC3 bands in the WT samples are suggesting that HDAC3 enzyme is clearly more abundant in WT than in HDAC3 KO samples.

On the Western blot with the samples which were precipitated for HDAC3 (**Fig. 13 b**) the following can be seen: From the 3 different IPs, the IP with 30 µl 3G6 HDAC3 antibody shows the strongest band for HDAC3 in the WT cells while no HDAC3 can be seen in the HDAC3 KO. Here, NCOR2 seems to be co-immunoprecipitated the most. In the IPs with 60 µl 3G6, both, HDAC3 and NCOR2 could be precipitated, but the IP with the longer incubation time in primary antibody (HDAC3 3G6 o/n) did not work as good as the IPs with 1 hour incubation time with HDAC3 3G6. Strikingly, the bands for NCOR2 are visible as double bands after the IP of the HDAC3 KO cells.

As for the total HDAC activity of the lysates measured with the HDAC3 kit prior to HDAC3 3G6 IP, all samples show an activity of around 200 (**Fig. 13 C**).

In regard of HDAC3 activity measurement of HDAC3 precipitates (**Fig. 13 D**), the samples which were incubated with 60 µl HDAC3 3G6 antibody for 1 hour (standard incubation time) showed a considerable difference between WT and HDAC3 KO, with a two-fold higher activity for precipitated HDAC3 in WT compared to HDAC3 KO cells. The samples which were incubated with 30 µl HDAC3 3G6 antibody for 1 hour showed only a slightly lower HDAC activity in HDAC3 KO lysates. Interestingly, the deacetylation activity in WT and HDAC3 KO precipitates are higher than in the IPs where incubation was done with 60 µl HDAC3 3G6 antibody. This result could be explained with higher deacetylation activity which was measured already in the respective samples prior to IP (compare **Fig. 13 C**). The WT cell lysate precipitate which was incubated over night in 60 µl primary antibody (HDAC3 3G6), showed the lowest HDAC activity, compared to the ones from the other

IPs. Furthermore, with the o/n incubation in primary antibody, the measurable HDAC activity in HDAC3 KO cell lysate precipitates is even higher than in WT precipitates.

This experiment showed that the increase of cell lysate material for precipitation and the double amount of HDAC3 3G6 monoclonal antibody (60 µl HDAC3 3G6, 1h incubation) improves the IP in regard of the difference in measurable deacetylation activity between precipitated WT and HDAC3 KO cell lysates, compared to the standard IP (**section 3.1.2.1**). Since the measured values are still very low (10x lower than total HDAC activity before IP) the results should be taken with caution. Further, it should be kept in mind that the experiment was performed with only 1 replicate. In conclusion the IP could be improved but the use of the HDAC3 kit did not give any improvement, since the values are still near to background values, and thus, in the remaining experiments where endogenous HDAC3 was precipitated the deacetylation activity was measured by using [$^3$H]-acetate-labeled chicken erythrocyte histones (HDAC activity assay).

#### *3.1.2.3. Lysis in Karin buffer and short incubation time in secondary antibody in HDAC3 IP*

To further improve the results for the HDAC3 activity assay, another protocol was tested with the following modifications: Instead of using Hunt buffer for cell lysis, Karin buffer (higher salt concentration, as well as higher concentration of chelating agents and addition of glycerol for better protein stabilization) was used and lysis was performed by sonication. Furthermore the incubation time in the secondary antibody IgG (mouse) was reduced to 2 hours instead of over night incubation, since the HDAC3 active complexes NCOR1 and NCOR2, respectively, have shown in previous studies to be unstable [180].

Briefly, protein extracts from WT cells and HDAC3 KO cells (passages 14-16) were used for IP. For activity measurements, we used the HDAC activity assay which uses $H^3$-acetylated histones as substrate, since we could not observe any improvement by using

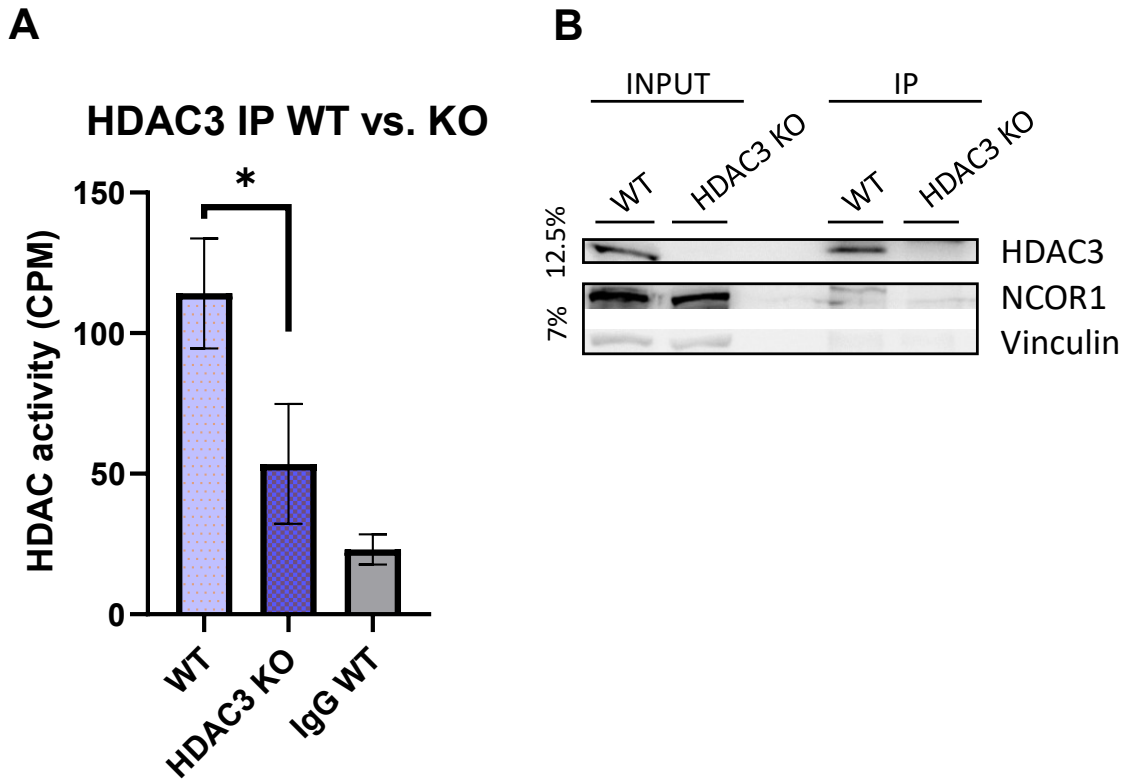


***Fig. 14: Activity of precipitated endogenous HDAC3 after short IP (3 hours)**. 1 mg of whole cell lysate was precipitated with 60 µl HDAC3 3G6 monoclonal antibody. As additional negative control sample, a mouse IgG antibody was used for IP together with wildtype HAP1 cellular extract. **A)** bar chart showing HDAC activity of precipitates after HDAC3 IP. Statistical significance was calculated by Welch's t-test. **p < 0.01, ***p< 0.001. **B)** Western blot analysis of cell lysates prior and after IP. Detection was done with HDAC3 polyclonal antibody on a blot from a 12.5% gel. NCOR1 polyclonal antibody was used for detection on a blot from a 7% gel. VINCULIN was used as loading control.* n=3

the HDAC3 kit (section 3.1.2.2). The lysates were incubated 1 hour in the primary antibody HDAC3 3G6 and 2 hours with mouse protein G-beads.

Looking at the HDAC activity (**Fig. 14 A**), HDAC3 precipitates from WT cells had a CPM of 114 while precipitates from HDAC3 KO cells had a CPM of 53. These values are low, but still considerably exceed the IgG ctrl background measurement (23 CPM). Relatively seen, the difference of deacetylation activity between HDAC3 KO and WT cells is similar to one of the IPs in Hunt buffer which was performed in section 3.1.2.2, more specifically the one which had the incubation step in secondary antibody (mouse G-beads) over night. The background activity which was measured in the IgG ctrl precipitates from WT cells with 23 CPM is also relatively higher than in this IP which was performed before in **section 3.1.2.2**. Beside of the higher background in the IgG ctrl, also the blank with a value of 47 CPM is considerably high.

Regarding the analysis of the Western blot (**Fig. 14 B**), precipitation of HDAC3 protein can be clearly seen for WT cell lysates after IP with HDAC3 antibody. It should be noted, that NCOR1 was detectable in the precipitated samples on the blot from a 7% gel. So far, in previous experiments we had difficulties to detect NCOR1.

Summarized, the short IP with only 3 hours total incubation time in primary and secondary antibody confirmed the usage of 60 µl of HDAC3 3G6 antibody. The lysis buffer change from Hunt to Karin and the different lysis method by sonication instead of freeze-thaw yielded in comparable HDAC activities in HDAC3 precipitates in WT as in the experiments with Hunt buffer (**sections 3.1.2.1 & 3.1.2.2**). The advancement of the new protocol is clearly that the differences of HDAC activity between WT and HDAC3 KO samples could be shown here with significance in triplicates, while it was difficult to show this in previous experiments.

#### *3.1.2.4. HDAC3 immunoprecipitation in low salt buffer and/or addition of IP3(1,4,5)*

IP3(1,4,5) – Inositol 1,4,5-trisphosphate – seems to have a stabilizing effect on HDAC complexes [137], [180]. For this reason, in an additional experiment the effect of IP3 was tested for potentially stabilizing the interaction between HDAC3 and NCOR1/2. Stabilizing effects have been observed also with less salt in the lysis buffer [180]. This was also tested by applying a low salt lysis buffer that contains 50 mM NaCl instead of the 100 mM NaCl which is contained in Hunt buffer. Also, the alternative lysis method through sonication instead of the freeze thaw method was assessed, since it is performed in other labs as suggested by the literature and could impact deacetylation activity [180].

Briefly, proteins were extracted from WT and HDAC3 KO cells through lysis by sonication. The lysates were incubated 1 hour in the primary antibody 3G6 and over night with mouse protein G-beads. 4 different set-ups were tested, with modifications in the lysis buffer, IP buffer and Assay buffer: 1) Lysis in low salt buffer (50 mM NaCl) and addition of IP3, 2) Lysis in low salt buffer (50 mM NaCl), 3) Lysis in Hunt buffer (100 mM NaCl) with IP3 addition and 4) control IP in Hunt buffer (100 mM NaCl) as performed previously. Each IP was with 500 µg INPUT lysate and 60 µl HDAC3 3G6 monoclonal antibody.

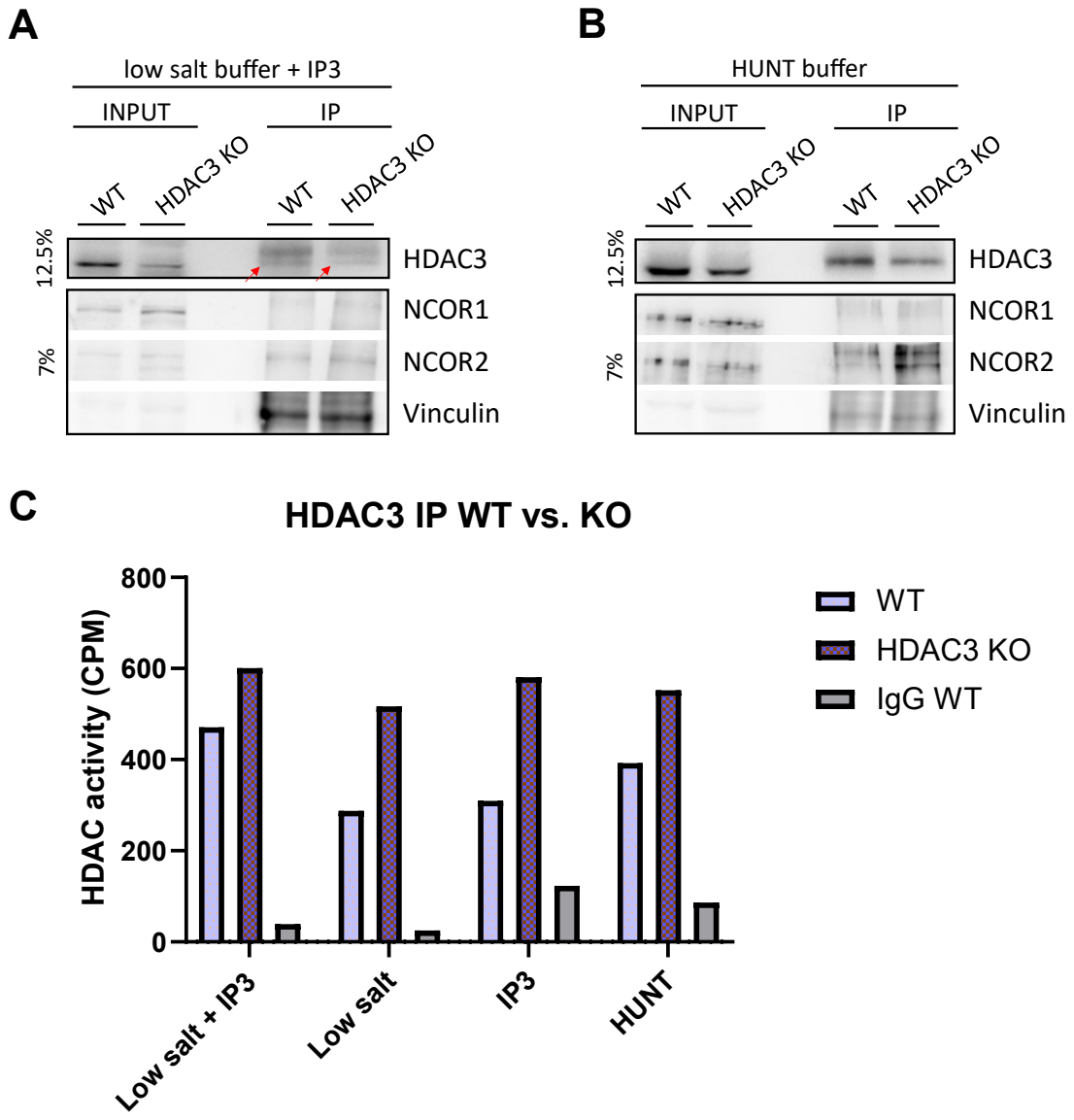


***Fig. 15: Comparison of activity of precipitated endogenous HDAC3 after IP in Hunt buffer with different salt / IP3 concentrations****. 1 mg of whole cell lysate was precipitated with 60 µl HDAC3 3G6 monoclonal antibody. As additional negative control sample, a mouse IgG antibody was used for IP together with wildtype HAP1 cellular extract.* ***A)*** *Western blot analysis of samples lysed and precipitated in low salt buffer with 50 mM NaCl prior and after IP.* ***B)*** *Western blot analysis of samples lysed and precipitated in HUNT buffer with 100 mM NaCl prior and after IP. Detection on the blot from the 12.5% gel was done with HDAC3 antibody. Detection on 7% blots was done with NCOR1 and NCOR2 polyclonal antibodies. VINCULIN was used as loading control.* ***C)*** *bar chart showing HDAC activity of precipitates after HDAC3 IP with different conditions.* n=1

The HDAC3 KO lysate in this experiment is derived from cells with passage number 16 and 17. Accordingly, the Western blot analysis shows bands for HDAC3 also in the HDAC3 KO cell lysates.

The blot with the low salt lysates with IP3 addition (**Fig. 15 A**) show weak bands of precipitated HDAC3 in both WT and HDAC3 KO samples on the blot derived from the 12% gel. The blot derived from the 7% gel for NCoR1/2 shows weak bands for NcoR1 and NcoR2 in all samples. Interestingly, the HDAC3 KO lysates prior to IP (INPUT) have double bands for both enzymes. The VINCULIN detection seemed to not have worked on the

INPUT blot, while it is clearly visible in the precipitated samples. This is not expected and is a hint for strong background.

The Western blot analysis of the samples which were lysed and precipitated in our standard Hunt buffer (**Fig. 15 B**) reveals visible bands for HDAC3 before and after IP on the blot derived from the 12% gel. In the precipitated samples only NCoR2 can be seen clearly on the blot from the 7% gel. Here, it appears as double band, opposite to the observation that the double band was visible only in the samples prior to IP (INPUT) where cells were lysed with low salt buffer + IP3. The loading control VINCULIN is weakly visible in the INPUT samples, but both the WT and HDAC3 KO sample lanes of VINCULIN look equal. Strikingly, while less HDAC3 protein is detected in the HDAC3 KO samples and amounts of NCoR1 and VINCULIN are same, NCoR2 is the most prominent band in the precipitated HDAC3 KO sample.

With all tested methods, we observed a higher deacetylase activity in HDAC3 precipitates of the HDAC3 KO cells compared to WT cells (**Fig. 15 C**). This is surprising, since the bands on the Western blots from HDAC3 KO precipitates are weaker than from WT precipitates. In general, HDAC activities across all samples are higher no matter which buffer was used.

In summary, the effect of IP3(1,4,5) and the low salt buffer individually were limited and only intensified the activity of HDAC3 KO cell lysates. Whereas the combination of both seemed to slightly increase the activity for wildtype cells and the HDAC3 KO cells. The usage of IP3(1,4,5) and low salt buffer was therefore not further pursued.

#### *3.1.2.5. HDAC3 immunoprecipitation with optimized conditions*

It was concluded, that the combination of changed conditions for cell lysis and IP which were tested in the **previous sections (3.1.2.2 - 3.1.2.4)** should be sufficient to compare the HDAC activity of HDAC3 KO cells to WT cells. Briefly, the increase of the amount of lysate used for the IP (1 mg per sample) and the higher amount of HDAC3 3G6 monoclonal antibody (60 µl) used during the IP in Karin buffer could significantly improve the relative differences of deacetylation activity between HDAC3 KO cells and WT cells.

Thus, conditions from the former IPs were combined as follows: protein extracts from WT cells and HDAC3 KO cells were used after lysis by sonication in Karin buffer. 1 mg of the lysate was used as input for IP, which was performed with 60 µl HDAC3 3G6 monoclonal

antibody. Further, it was paid attention to use passage numbers as low as possible for the experiment, which were p12-p15. The precipitated proteins were analysed in WB assay and the activity was measured using the HDAC activity assay.

In the HDAC activity assay, the WT samples which were precipitated for HDAC3 showed a deacetylation activity of 389 CPM while the HDAC3 KO precipitates showed 162 CPM, which is significantly lower, even lower than the activity of IgG WT IP (216 CPM). This might be due to unspecific binding of components in the lysate to the antibody (**Fig. 16 A**).

Western blot analysis of the 12.5% gel shows the successful precipitation of HDAC3 in the wildtype cells, while no band is visible in the KO cells. The detection was facilitated by the application of an antibody which detects only the light chain of rabbit IgG (Jackson ImmunoResearch) and thus lowers the visibility of precipitated mouse IgG which is seen

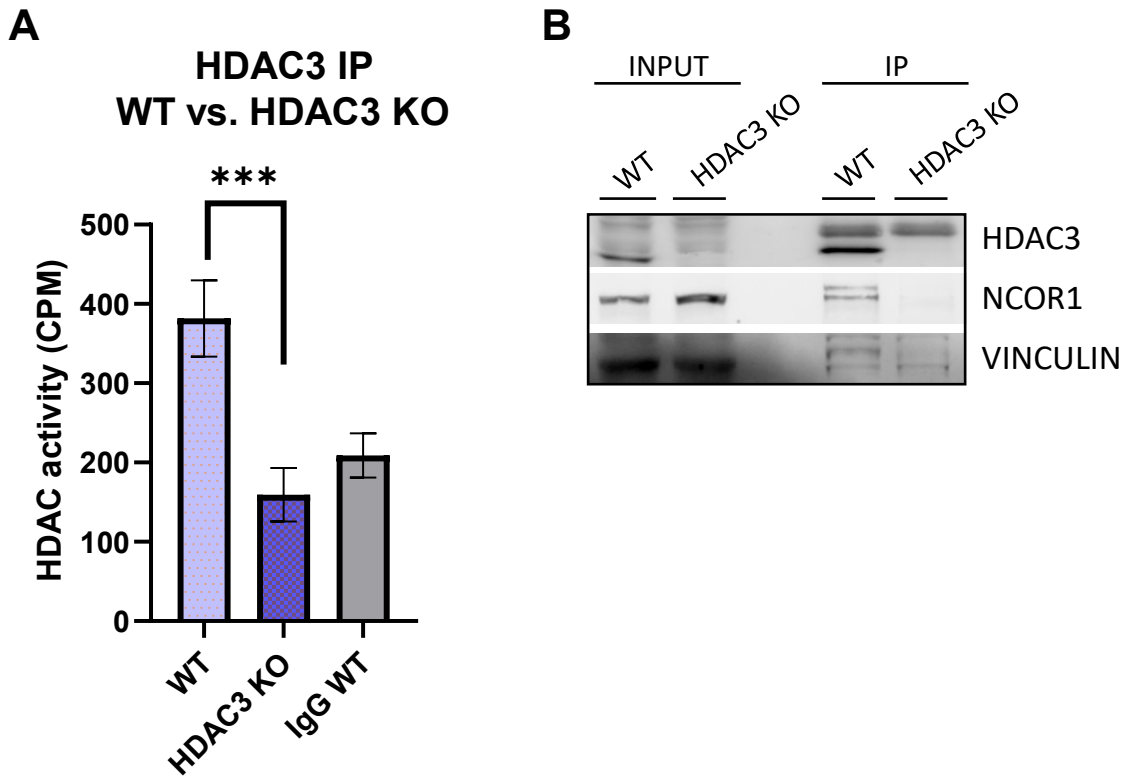


*Fig. 16:* ***Activity of precipitated endogenous HDAC3 after IP with optimized conditions****. Proteins were extracted in KARIN buffer through cell lysis through sonication. 1 mg of whole cell lysate was precipitated with 60 µl HDAC3 3G6 monoclonal antibody. As additional negative control sample, a mouse IgG antibody was used for IP together with wildtype HAP1 cellular extract****. A)*** *Bar charts showing absolute deacetylase activity of precipitated HDAC3 towards histones in CPM (counts per minute). Statistical significance was calculated by Welch's t-test. ***p< 0.001.* ***B)*** *Western blot analysis of cell lysates prior and after IP on a blot from a 12.5% gel. A light chain secondary antibody was used for detection of HDAC3 to lower the visibility of the IgG mouse heavy chain.* n=5

through cross reaction with the standard secondary anti-rabbit antibody (**Fig. 16 B**). On the same blot, NCOR1 appears as 2 bands in WT precipitates while it cannot be seen in

HDAC3 KO precipitates. VINCULIN confirms equal amounts of used lysates from each sample as INPUT that was used for the IP.

In summary, it was eventually possible to show the difference of deacetylation activity between WT and HDAC3 KO cells, which were precipitated for HDAC3. Thanks to the optimized conditions the measurable activity in the WT precipitates could be increased to almost 400 CPM. More importantly, the activity of HDAC3 KO precipitates could be kept nearly at the same levels as they were in the initial experiment (see **section 3.1.2.1**). The only drawback is the increase in background activity that is precipitated from WT cells (IgG WT).

## 3.2. Characterization of cells expressing transgenic class I HDACs in corresponding KO backgrounds

The characterization and comparison of different activities of endogenous wildtype class I HDACs is not always directly comparable between different studies: Expression levels of class I HDACs in different cell lines vary and the amount of precipitated protein differs because of reasons like different antibodies used. In order to create comparable conditions and enable a systematic analysis for class I HDACs, our lab established an *in vitro* model in HAP1 cells with the following lineages:

| name | background | transgene | CI AA modification |
|---|---|---|---|
| **WT** | wt | - | |
| **WT HDAC1 CI** | wt | HDAC1 CI | H141A |
| **WT HDAC2 CI** | wt | HDAC2 CI | H142A |
| **WT HDAC3 CI** | wt | HDAC3 CI | H135A |
| **WT HDAC8 CI** | wt | HDAC8 CI | H143A |
| **KO HDAC1** | HDAC1 KO | - | |
| **KO HDAC2** | HDAC2 KO | - | |
| **KO HDAC3** | HDAC3 KO | - | |
| **KO HDAC8** | HDAC8 KO | - | |
| **KO HDAC1 WT** | HDAC1 KO | HDAC1 WT | |
| **KO HDAC2 WT** | HDAC2 KO | HDAC2 WT | |
| **KO HDAC3 WT** | HDAC3 KO | HDAC3 WT | |
| **KO HDAC8 WT** | HDAC8 KO | HDAC8 WT | |
| **KO HDAC1 CI** | HDAC1 KO | HDAC1 CI | H141A |
| **KO HDAC2 CI** | HDAC2 KO | HDAC2 CI | H142A |
| **KO HDAC3 CI** | HDAC3 KO | HDAC3 CI | H135A |
| **KO HDAC8 CI** | HDAC8 KO | HDAC8 CI | H143A |

*Table 5: Summary of established HDAC1-8 KO and WT HAP1 cell lines with exogenically expressed either wildtype HDAC1-8 or catalytically inactive (CI) HDAC1-8.*

HDAC knockout cell lines were generated by Verena Moos and Susanna Leiter by using CRISPR/Cas9 targeting of respective gene sequences and introduction of an indel in collaboration with Horizon discovery [167].

Catalytically inactive (CI) HDACs were introduced into both wildtype (WT) HAP1 cell lines as well as into HDAC knockout (KO) cell lines (**Table 5**). Therefore, using CRISPR/Cas9 technology and subsequent homologous recombination, the AAVS1 safe harbour locus was targeted to introduce the sequences of HDAC1-8 which carry a point mutation in the catalytic center to exchange the conserved amino acid histidine to alanine (HDAC1 H141A, HDAC2 H142A, HDAC3 H135A, HDAC8 H143A). Each introduced HDAC transgene has a FLAG-tag at the C-terminal end which allows pull down of the desired

protein with streptavidin beads and subsequent analysis. The cloning of the constructs which included the template (guide RNA) for targeting the AAVS1 locus and pCas9 from *Streptococcus pyogenes* and also cloning of AAVS1 donor vector carrying the gene sequences to be inserted was accomplished by Verena Moos with help of Anna Riegler [167], [181], [182]. Previously, a number of these cell lines have been characterized already in our lab. Susanna Leiter, Anna Riegler, Brigitte Gundacker and Petra Vician contributed to further characterization of KO HDAC WT cells, the comparison of KO HDAC1-8 WT and KO HDAC1-8 CI as well as the co-repressor complexes of HDAC1. [167], [173], [181]–[183].

### 3.2.1. Comparison of deacetylase activity of transgenic FLAG tagged wildtype class I HDACs

#### *3.2.1.1. Titration of FLAG tagged wildtype class I HDACs*

To compare cells which express the FLAG tagged transgene of either wildtype HDAC1, HDAC2, HDAC3 or HDAC8 in their respective KO background, the amount of protein lysate which is necessary to precipitate similar amounts of the respective transgene must be adjusted. Therefore, cells of the different HAP1 cell lineages were lysed in Hunt buffer and different amounts of the protein lysates were analyzed by Western blotting. As background control, the same amount of WT cell lysate was loaded as was loaded from the KO HDAC3 WT cell lysate with the highest (40 µg) amount. Blots were incubated with antibodies against the FLAG tag. The resulting band intensities were compared to estimate the HDAC transgene expression ratios between the cell lineages.

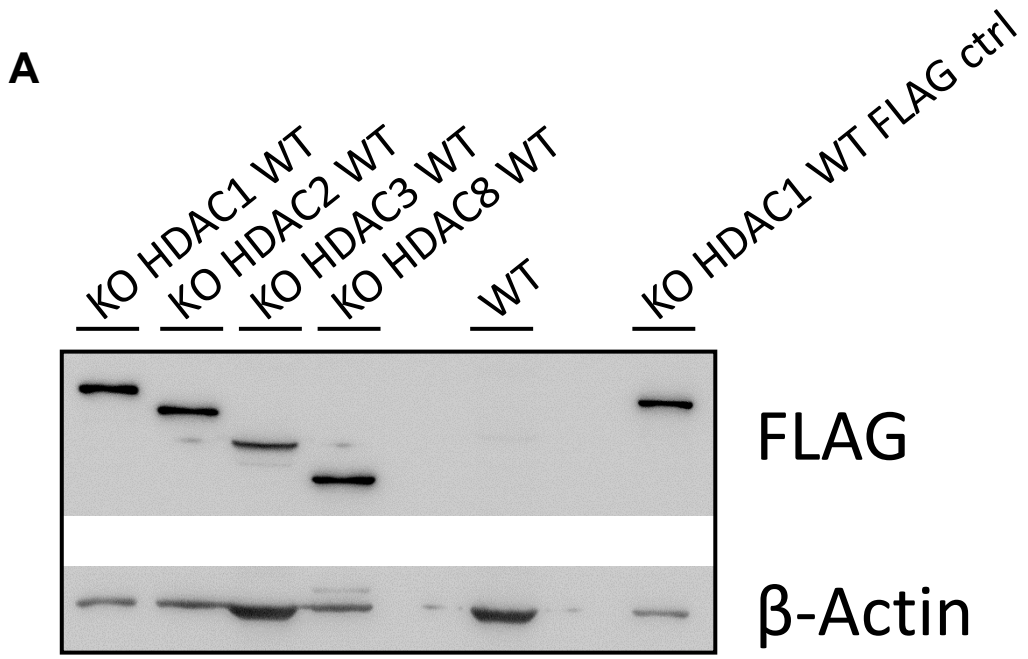


*Fig. 17:* ***Western blot analysis of HAP1 cell lysates expressing transgenic wildtype class I HDACs in respective knockout background.*** *The following amounts of whole cell lysates were analysed by immunoblotting: KO HDAC1 WT 4 µg, KO HDAC2 WT 3.2 µg, KO HDAC3 WT 40 µg, KO HDAC8 WT 4 µg. As additional negative control sample, a wildtype HAP1 cellular extract was loaded. The positive control was derived from a cell lysate previously confirmed to express transgenic FLAG-tagged HDAC1. β-Actin served as loading control.* n=1

The following ratios were determined to result in similar amounts of transgenic HDAC proteins: KO HDAC2 WT 0.8x the amount of KO HDAC1 WT, KO HDAC3 WT 10x the amount of KO HDAC1 WT, and FLAG KO HDAC8 WT 0.8x the amount as KO HDAC1 WT (**Fig. 17 A**).

#### *3.2.1.2. Precipitation and comparison of FLAG tagged wildtype class I HDACs*

In order to systematically compare the deacetylase activity of FLAG tagged wildtype class I HDACs in KO background, we performed a FLAG-IP with the above stated ratios (**section 3.2.1.1**). After determining the protein concentrations of cell lysates, the following samples were prepared for IP: 100 µg of KO HDAC1 WT, 80 µg KO HDAC2 WT, 1000 µg of KO HDAC3 WT and 80 µg of KO HDAC8 WT. In addition, we used 1000 µg of WT lysates for the IP, as negative control. Due to the absence of any transgene, it served to determine background. The precipitates were analysed using the HDAC activity assay

performed with [$^3$H]-acetate-labelled chicken erythrocyte histones (HDAC activity assay) and on a Western blot.

Western blot analysis with the FLAG antibody shows similar amounts of precipitated transgenic HDAC1-8 (**Fig. 18 A**). Concerning the activity assay analysis (**Fig. 18 B**), the absolute (CPM) value obtained from the IP of the background control (WT) was subtracted from the values that were measured for the precipitated, transgenic HDACs. Therefore, the measured background activity in the precipitated WT sample was subtracted from the KO HDAC3 WT precipitate. For the other KO HDAC precipitates the background activity of the WT sample was calculated by dividing the activity by the proportion between the 1000 µg sample and how much of an amount was used for the respective IP.

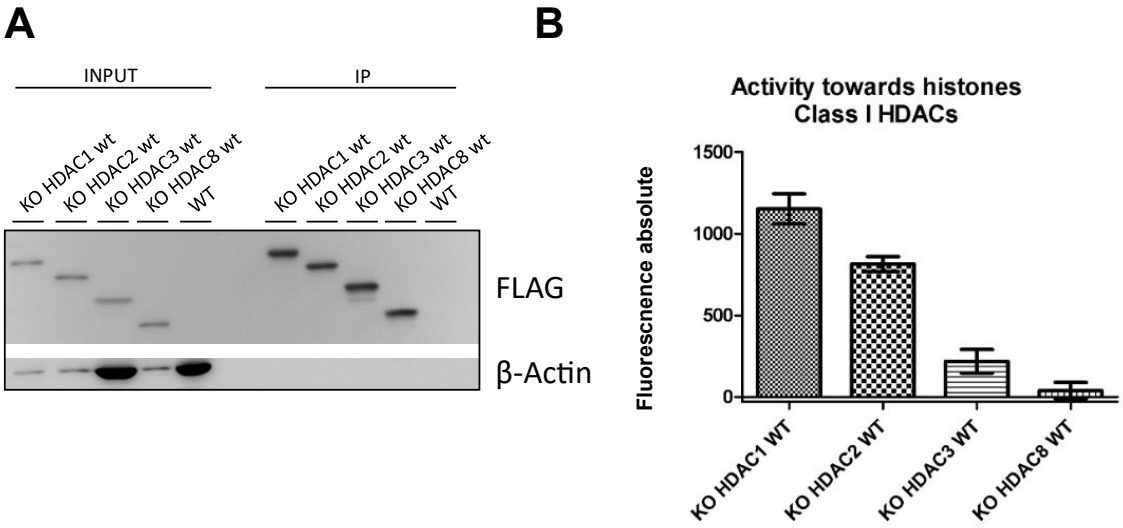


*Fig. 18:* ***Activity of precipitated transgenic class I HDACs (expressed in respective KO background)****. 80-1000 µg of cell lysate were used for IP.* ***A)*** *Western blot analysis of cell lysates prior and after IP. As additional negative control sample, 1000 µg of a wild type HAP1 cellular extract was used in IP. β-Actin was used as loading control.* ***B)*** *Bar charts showing absolute deacetylase activity of precipitated FLAG-tagged transgenic HDACs towards histones in CPM (counts per minute) obtained after IP. The background level was measured in the immunoprecipitated 1000 µg wild type HAP1 lysate and is already subtracted from measurement values* n=3

Transgenic HDAC1 and HDAC2 enzymes showed an activity of around 1000 and 800 CPM, respectively. HDAC3 had an activity around 200 CPM and HDAC8 showed almost no measurable activity.

#### *3.2.1.3. Activity levels measured with the HDAC8-kit assay*

In the previous experiment (**section 3.2.1.2**), we could not determine activity for HDAC8, using histones as substrate. for this reason, we tested another substrate. [R-H-K(Ac)-

K(Ac)-AFC] is the peptide which is provided in the HDAC8 kit. It has been shown to be a direct substrate of HDAC8 [184] The same FLAG-IP as described above was repeated and measured with the HDAC8 kit. FLAG-IP was performed with the above stated ratios. Additionally, for each amount which was used in the IP a respective amount of WT cellular extract was used in IP to subsequently have a background control that can be subtracted from each sample.

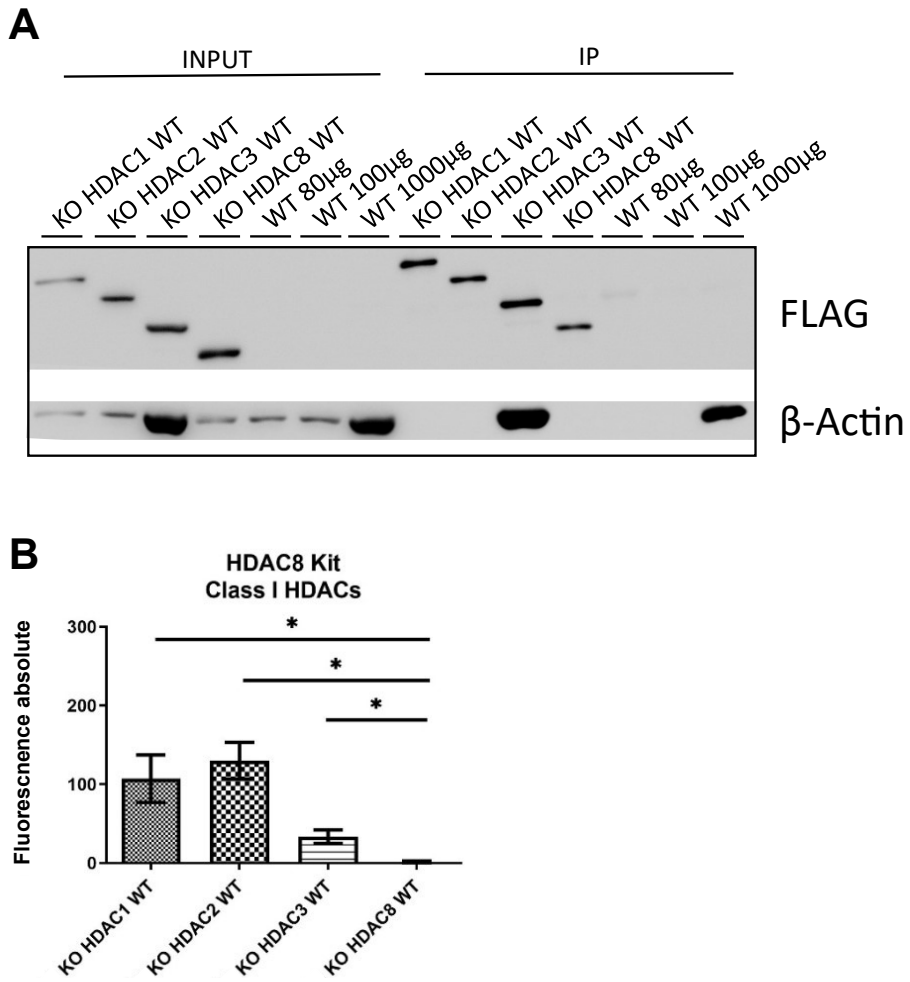


*Fig. 19:* ***Activity measurement with the HDAC8-kit of transgenic wildtype class I HDACs (expressed in respective KO backgrounds)****. 80-1000 µg of cell lysate was used for IP.* ***A)*** *Western blot analysis of cell lysates prior and after IP. Cellular extract from WT HAP1 served as negative and background control. β-Actin was used as loading control.* ***B)*** *Bar charts showing absolute deacetylase activity of precipitated FLAG-tagged transgenic HDACs towards a target peptide obtained after immunoprecipitation of respective cell lysates.* n=4

WB analysis shows similar amounts of precipitated HDACs after IP (**Fig. 19 A**). Surprisingly, HDAC1 and HDAC2 had again the highest activity measured with the HDAC8 activity kit. HDAC3 showed a much lower activity, while HDAC8 associated activity stayed

only at background levels (**Fig. 19 B**). These data suggest that the HDAC8 activity kit does not discriminate between class I HDACs.

Since neither the HDAC3 nor the HDAC8 kit gave an advantage over the HDAC activity assay with [$^3$H]-acetate-labelled chicken erythrocyte histones, the remaining experiments were always measured with the HDAC activity assay using H$^3$-acetylated histones as substrate.

### 3.2.2. Comparison of transgenic wildtype and inactive HDACs

To show that the previously generated inactive HDAC transgenes are indeed inactive, we compared FLAG precipitates from KO HDAC CI cells with FLAG precipitates from KO HDAC WT cells. The same process of titration as described above (**section 3.2.1.1**) had to be done to precipated equal amounts of HDAC transgenes. Since there are significant differences of the deacetylase activity levels of transgenes, HDAC1 and HDAC2 were grouped together in the following experiments (relative high activity measured in KO HDAC WT precipitates, around 1000 CPM) and transgenes, which were equalized on one Western blot and HDAC3 and HDAC8 were grouped together (low activity of deacetylase activity in KO HDAC WT precipitates).

#### *3.2.2.1. Comparison between transgenic wildtype and inactive HDAC1 or HDAC2 enzymes*

After titration of lysates with wildtype or inactive HDAC1 and HDAC2 transgenes, the following ratios were concluded *via* Western blot analysis: For KO HDAC1 CI, the 4x higher amount than for KO HDAC1 WT is necessary and for KO HDAC2 CI, the 7x higher amount compared to KO HDAC2 WT is required for immunoprecipitation.

FLAG-IP was performed with the stated ratios. After determining the protein concentrations of cell lysates, the following samples were prepared for FLAG-IP: 100 µg of KO HDAC1 WT, 100 µg KO HDAC2 WT, 400 µg of KO HDAC1 CI and 700 µg of KO HDAC2 CI. The precipitates were analysed using the HDAC activity assay and on Western blots.

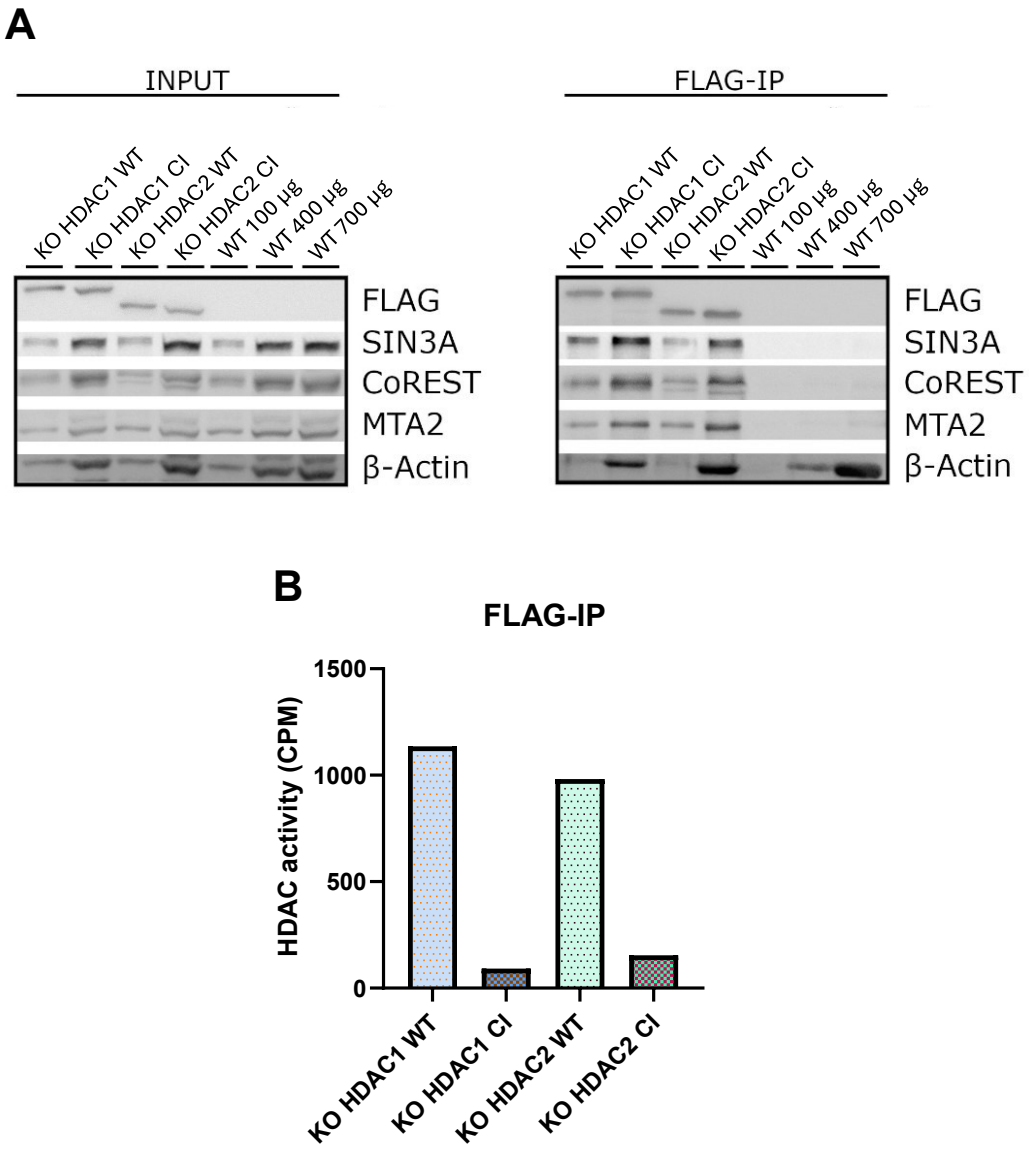


*Fig. 20:* ***Comparison of wildtype and inactive transgenic FLAG-tagged HDAC1 & HDAC2****. 100-700 µg of cell lysate was used for IP.* ***A)*** *Western blot analysis of cell lysates prior and after IP. β-Actin was used as loading control. Cellular extract from WT HAP1 served as negative and background control.* ***B)*** *Bar charts showing absolute deacetylase activity of precipitated FLAG-tagged transgenic HDACs towards histones in CPM (counts per minute) obtained after IP.* n=1

The amounts of precipitated FLAG tagged HDACs was similar for each cell line (**Fig. 20 A**). The activities which were measured for precipitates of KO HDAC1 WT and KO HDAC2 WT cell lines are definitely higher than the activity of same amounts of respective KO HDAC1 CI and KO HDAC2 CI precipitates (**Fig. 20 B**). The background activity of the WT HAP1 negative control was already considered, but there is still a residual activity that was measured for inactive HDAC1 and HDAC2. This could come from heterodimerization of the inactive proteins with wildtype HDAC1/2 enzymes.

#### *3.2.2.2. Comparison between transgenic wildtype and inactive HDAC3 or HDAC8 enzymes*

Similar as for transgenic HDAC1/2, we wanted to determine the deacetylation activity of inactive and wildtype transgenes of HDAC3/8. The titration of FLAG tagged transgenic HDAC3 and HDAC8 lysates resulted in the following ratios: From KO HDAC3 WT the 2.5x higher amount than from KO HDAC3 CI, and from KO HDAC8 WT the 8x lower amount is needed than from KO HDAC8 CI.

FLAG-IP was performed with the above stated ratios. After determining the protein lysate concentrations, the following samples were prepared for IP: 500 µg of KO HDAC3 WT, 100 µg KO HDAC8 WT, 200 µg of KO HDAC3 CI and 800 µg of KO HDAC8 CI. The precipitates were analysed using the HDAC activity assay and on Western blots.

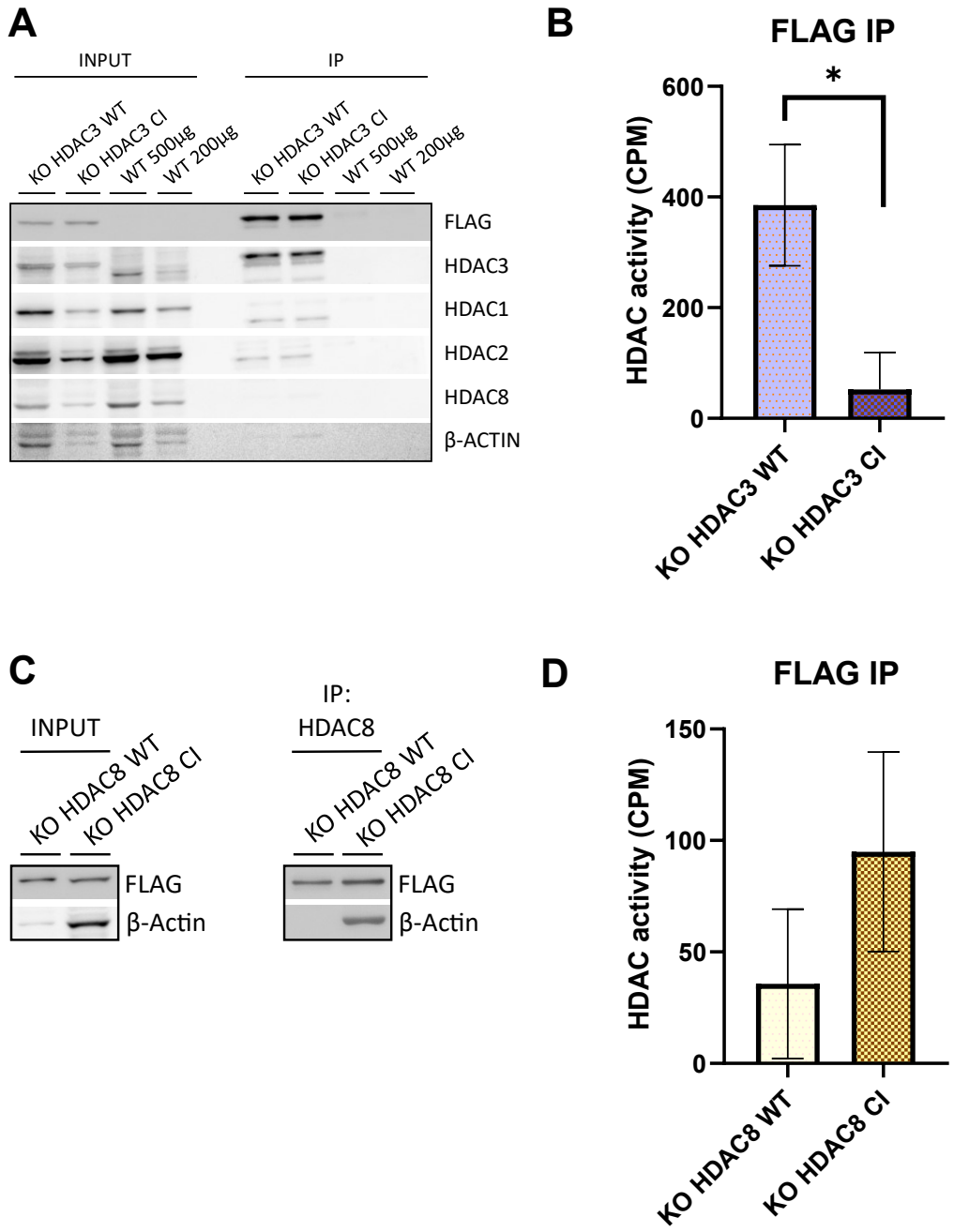


*Fig. 21:* ***Activity of precipitated transgenic HDAC3 WT/Cl & HDAC8 WT/Cl into their respective KOs****. 100-800 µg of cell lysate was used for IP.* ***A & C)*** *Western blot analysis of cell lysates prior and after IP. Cellular extract from WT HAP1 served as negative and background control. β-Actin mouse (HDAC3 IP) and β-Actin rabbit (HDAC8 IP) were used as loading control.* ***B & D)*** *Bar charts showing absolute deacetylase activity of precipitated FLAG-tagged transgenic HDACs towards histones in CPM (counts per minute) obtained after IP.* n=3

Similar amounts of precipitated HDAC transgenes can be detected on the Western blots (**Fig. 21 A & C**).

Concerning the activity assay results (**Fig. 21 B & D**), background activity is already subtracted. Precipitated HDAC3 CI shows a 7-fold decrease in deacetylation activity compared to the precipitated HDAC3 WT enzyme (385 CPM vs. 52 CPM). Although the amounts of precipitated HDAC8 transgenes are similar and clearly visible on the blot, the associated deacetylase activity was very low for both HDAC8 WT and HDAC8 CI enzymes The measured values remained in levels near to background, hence didn't allow any analysis.

### 3.2.3. Co-repressor-associated deacetylase activity upon incorporation of HDAC1 WT or HDAC1 CI enzymes

To determine the consequences of incorporation of wildtype or inactive transgenic HDAC1 into the co-repressor complexes and to compare the resulting deacetylation activities, IPs for the three complexes SIN3A, CoREST and NuRD were performed with antibodies specific for SIN3A, CoREST and MTA2.

Therefore, 700 µg of protein extracts from KO HDAC1 WT cells and KO HDAC1 CI cells were precipitated. It has been observed in our lab before that incorporation of catalytic inactive HDAC1/2 transgenes resulted in a more severe phenotype due to disruptive effects compared to the knock outs of the respective HDACs [166]. HDAC1 KO lysates were thus precipitated as well to compare the effect of loss versus inactivation of HDAC enzymes on the activity of the co-repressor complexes.

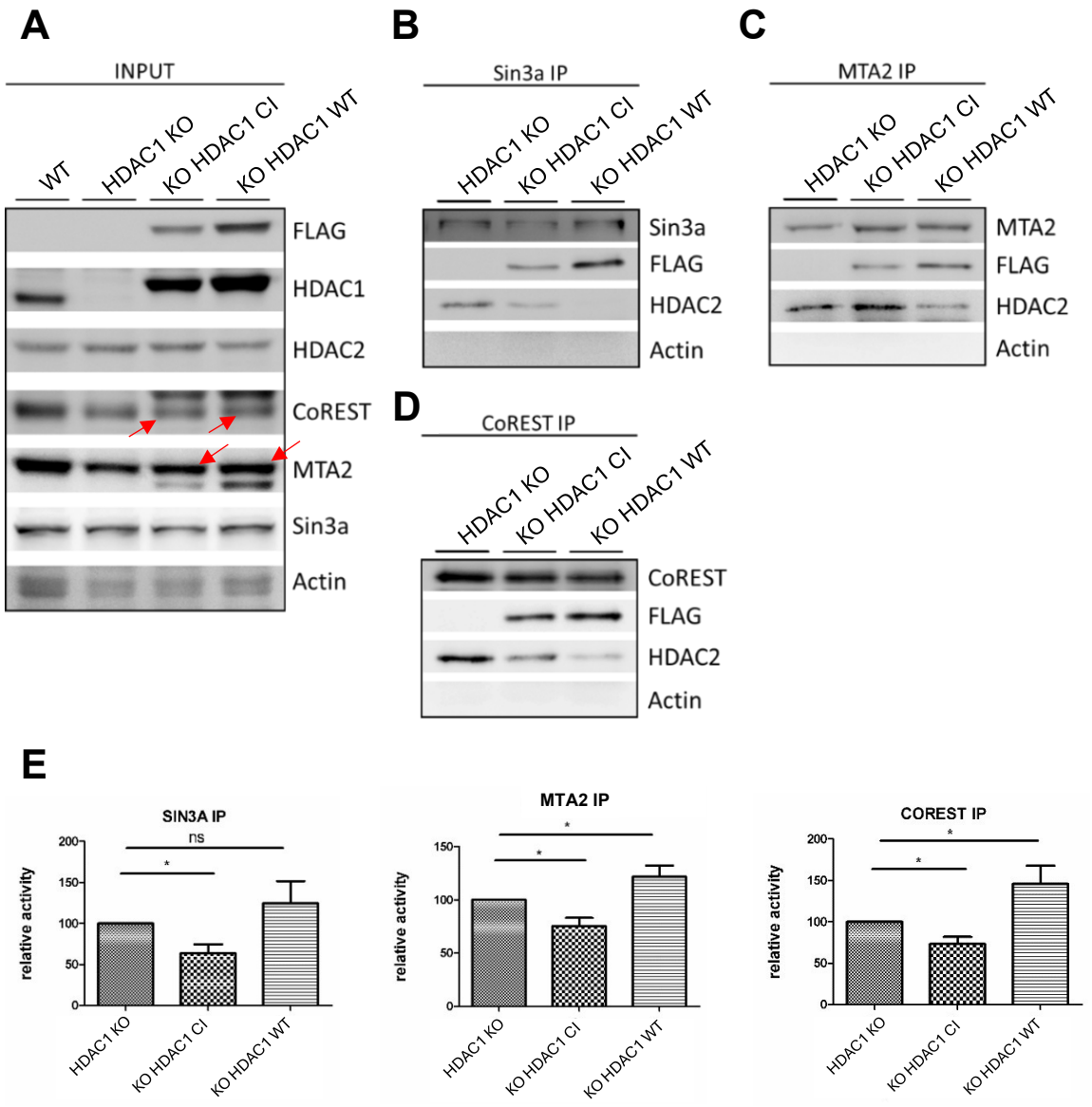


*Fig. 22:* ***Co-repressor IPs of transgenic HDAC1 (WT & Cl) expressed in HDAC1 KO background****. 700 µg of cell lysate was used for IP with either Sin3a G-11, CoREST 07-455 or MTA2 M7569 antibody.* ***A)*** *Western blot analysis of cell lysates prior and after IP. β-Actin was used as loading control.* ***B)*** *Bar charts showing absolute deacetylase activity of precipitated FLAG-tagged transgenic HDACs towards histones in CPM (counts per minute) obtained after Co-IP.* n=4

The analysis of the INPUT Western Blot (**Fig. 22 A**) shows that the expression of the wildtype HDAC1 transgene in HDAC1 KO cells is higher than the expression of inactive HDAC1 transgene, together with this observation endogenous HDAC2 seems to be slightly downregulated in cell lysates where the wildtype HDAC1 transgene is introduced. Extract of WT cell lysate was applied as positive ctrl for endogenous HDAC1; it shows a slightly higher protein concentration which is not of significance for the analysis here.

Western blot analysis of the SIN3A IPs (**Fig. 22 B**) showed, that less amount of transgenic HDAC1 protein co-precipitated in KO HDAC1 CI cells compared to the amount which precipitated in KO HDAC1 WT cells, where the band for transgenic HDAC1 is very strong. While endogenous HDAC2 is not detectable in precipitates of KO HDAC1 WT, there is still a faint band in the precipitates of KO HDAC1 CI.

In the MTA2 IP blot (**Fig. 22 C**), precipitated transgenic HDAC1 is more prominent in KO HDAC1 WT cells than in KO HDAC1 CI cells. As in the SIN3A IP it can be also observed in the MTA2 IP that less endogenous HDAC2 precipitated in lysate from KO HDAC1 WT than from KO HDAC1 CI. Strikingly, endogenous HDAC2 precipitated in higher amounts in lysates from KO HDAC1 CI cells than transgenic HDAC1.

In the Western blot analysis of the CoREST IP (**Fig. 22 D**), the FLAG signal of the transgenic wildtype HDAC1 is slightly more intense than observed for transgenic inactive HDAC1. The behaviour of HDAC2 in the CoREST IP resembles its behaviour in the SIN3A and MTA2 IP.

Concerning histone deacetylase activity **(Fig. 22 E**), our analysis suggests that the activity of precipitated complexes of HDAC1 KO cells is higher than observed for KO HDAC1 CI cells. The lowest activity in the SIN3A complex is also seen with the HDAC1 inactive transgene incorporated. In the NuRD complex as well as in the CoREST complex, significantly higher deacetylase activity was found in precipitates KO HDAC1 WT cells, compared to precipitates from HDAC1 KO cells. In summary, the complexes which have the inactive HDAC1 transgene incorporated have significantly lower activities than the complexes without HDAC1.

### 3.2.4. NCOR1 co-repressor IPs for deacetylation activity assay of incorporated transgenic active and inactive HDAC3

Analogous to the co-repressor IP, which was done above for HDAC1-associated co-repressors, we tested whether we are able to immunoprecipitate NCOR1/2 complexes,

which were found earlier to interact with HDAC3 [185]. Like the HDAC3 endogenous IP, the NCOR IPs had to be optimized. Various IP conditions were tried, amongst them different antibodies, shorter incubation times and an alternative lysis and assay buffer. It was especially tested whether these conditions could improve the enrichment of the NCOR complex together with FLAG-tagged transgenic HDAC3 (WT or CI) so that their activity become measurable. It was shown before, that the activity of HDAC3 is dependent on the incorporation into the NCOR or SMRT complex [133].

#### *3.2.4.1. NCOR1 IP with standard conditions and HDAC activity measurement with HDAC3 kit.*

In the first attempts of NCOR1 IPs the associated HDAC activity, which was measured with the HDAC activity assay, as well as the detection of HDAC3 as part of the NCOR complex stayed only vague. For this reason, the used amount for IP was increased to 1 mg per sample and the HDAC3 kit from Sigma was used for deacetylase activity measurement. Protein extracts from WT cells, KO HDAC3 WT cells and KO HDAC3 CI cells were used for NCOR1 IP with the NCOR1 ab24552 antibody. The precipitated proteins were analysed by Western blot assay and the activity was measured. The IgG background control was done with KO HDAC3 WT.

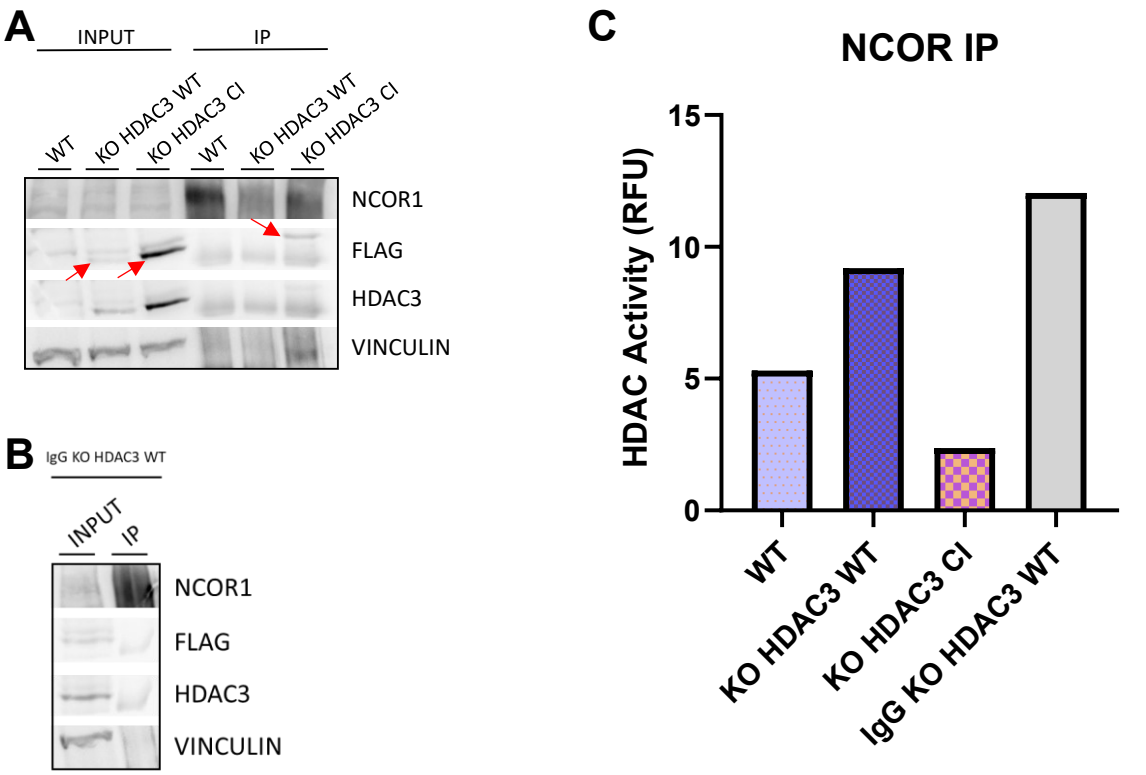


*Fig. 23:* ***NCOR1 Co-repressor Co-IP of cell expressing transgenic HDAC3 (WT & Cl) in HDAC3 KO background*** *1 mg of cell lysate in Hunt buffer was used as INPUT. Cells where lysed with the freeze and thaw method.* ***A)*** *Western blot analysis of cell lysates prior and after IP. VINCULIN was used as loading control. Secondary antibody detection on blots was done with a light chain antibody.* ***B)*** *Western blot analysis of cell lysates prior and after isotype control IP.* ***C)*** *bar chart showing HDAC activity of precipitates after NCOR1 Co-IP.* n=1

Incubation of the blot with the NCOR1 antibody ab3482 results only in a smear at around 250 kDA, where NCOR 1 would be expected, and in in the INPUT the NCOR1 bands are very faint and appear as double bands (**Fig. 23 A**). The loading control with VINCULIN confirmed that equal amounts of protein lysates were used for IP. Concerning the FLAG detection on the blot, it seems that inactive transgenic HDAC3 is clearly visible, but the wildtype transgenic HDAC3 cannot be seen in the IP samples. Indeed, in the previous section (**3.2.2.2**) it was determined that transgenic inactive HDAC3 has a 4-fold higher expression level than the wildtype transgene. Detection with the HDAC3 3G6 antibody gave no readable signal. Further, the same bands are visible as in the FLAG detection, since both antibodies were produced in mouse.

A KO HDAC3 WT sample was incubated with IgG rabbit antibody as background control (**Fig. 23 B**). The precipitates show a smear at around 250 kDa for NCOR1, as observed in the other precipitated samples. Besides of this, the samples look clear of HDAC3 or VINCULIN, which would suggest a low background.

Concerning the activities obtained for NCOR1 (**Fig. 23 C**) precipitates are around 10 RFU (relative fluorescence units, emission at 500 nm). This is very low compared to the values obtained for the INPUT samples (20 µg of whole protein extract per sample) that are around 200 RFU. The activity of NCOR1 precipitates of the KO HDAC3 WT cell line was around double as high as for NCOR1 precipitates of the WT cells. The KO HDAC3 CI cells showed around half of the activity of WT cell precipitates.

Surprisingly, the IgG ctrl, which was done with KO HDAC3 WT gives higher values than the other IP samples. This might be because of unspecific binding to the IgG antibody. However, as mentioned in the Western blot analysis, the sample looks clear beside of the smear for NCOR1.

Altogether this experiment gave a hint for the first time that our transgenic HDAC3 co-precipitates with NCOR1, although it was here only possible to detect it on the Western blot for the KO HDAC3 CI cells. However, these results can be hardly interpreted since activities are very low and the IgG background control shows similar activities as the precipitated samples for NCOR1.

#### *3.2.4.2. NCOR1 IP with optimized conditions and HDAC activity measurement with [$^3$H]-acetate-labeled histones*

Various conditions have been tested to optimize the NCOR1/2 co-IP. Finally, the best result for NCOR1/2 co-IP to visualize co-immunoprecipitation of transgenic HDAC3 with NCOR1/2, was achieved by using Karin buffer and lysis of the cells by sonication (compare **section 3.1.2.5**). 1 mg of protein extracts from HDAC3 KO cells, KO HDAC3 WT cells and KO HDAC3 CI cells was used for IP, using the NCOR1 ab24552 antibody. As background control served KO HDAC3 WT cells and WT cells, which were incubated with the IgG

antibody. The precipitated proteins were analysed by Western blot assay and the deacetylase activity was measured by HDAC activity assay.

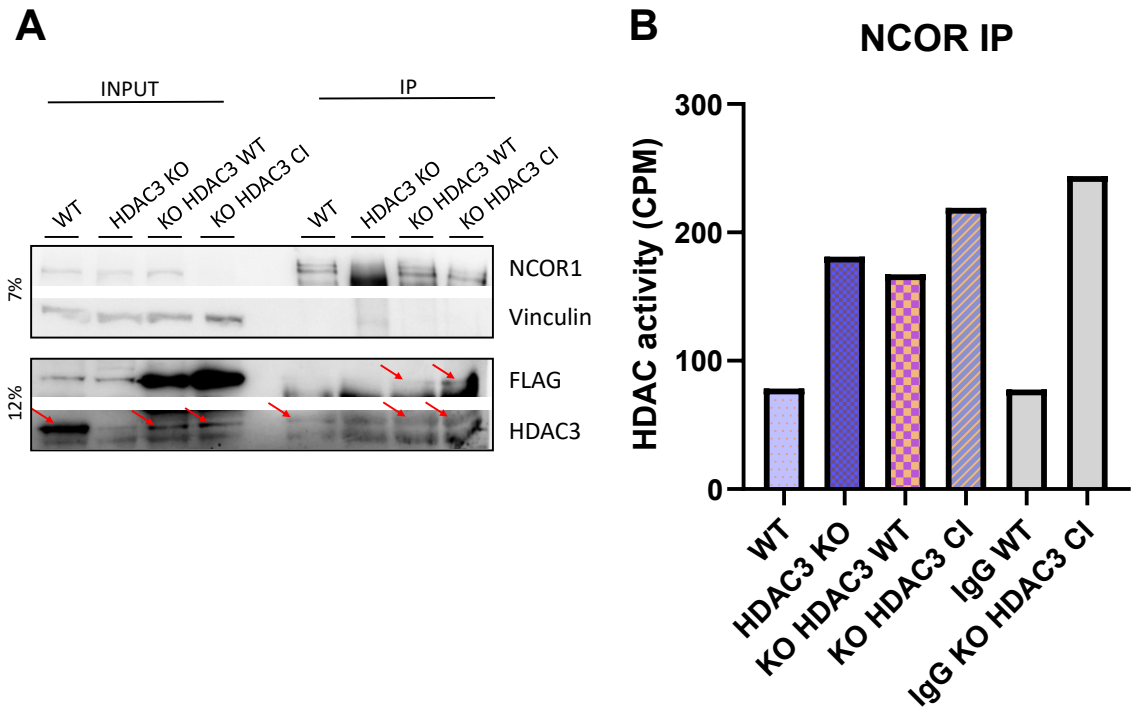


*Fig. 24:* ***Optimized NCOR1 Co-repressor Co-IP of cell expressing transgenic HDAC3 (WT & CI) in HDAC3 KO background****. 1 mg of cell lysate obtained by sonication in Karin buffer was used for IP.* ***A)*** *Western blot analysis of cell lysates prior and after IP. VINCULINwas used as loading control. Secondary antibody detection on blots was done with a light chain antibody.* ***B)*** *Bar charts showing absolute deacetylase activity of precipitated FLAG-tagged transgenic HDACs towards histones in CPM (counts per minute) obtained after Co-IP.* n=1

Incubation of the blot in rabbit secondary antibody leads to detection of the rabbit IgG, which was used as secondary antibody in the IP. To prevent detection of the IgG heavy chain, which runs approximately at 50 kDa (HDAC3 appears also at 50 kDa) on the membrane, a light chain secondary antibody was used. NCOR1 and VINCULIN were detected on a 7% gel while HDAC3 and FLAG-HDAC3 were detected on a 12% gel.

Concerning the Western blot analysis (**Fig. 24 A**), on the 7% blot NCOR1 could be detected. It seems to appear as double band again in NCOR1 precipitated samples from WT, KO HDAC3 WT and KO HDAC3 CI. In the HDAC3 KO precipitate only a smear is visible. VINCULIN detected in the INPUT lysates shows that similar amounts of the samples were used for the Co-IP. Also, the transgenic HDAC3 proteins were clearly detected in the INPUT lysates. It seems that transgenic HDAC3 was also detected in this experiment in NCOR1 precipitates from KO HDAC3 WT and KO HDAC3 CI, although the bands are faint. Since detection of FLAG-HDAC3 did not work with the M2-FLAG antibody,

we used an alternative antibody recognizing the M2 FLAG-tag (DYKDDDDK Tag, Cell signaling).

The most surprising result is the fact, that the IgG ctrl IP of KO HDAC3 CI cells has the highest activity (**Fig. 24 B**). With 244 CPM it is as high as the activity of NCOR1 precipitated KO HDAC3 CI cell lysates, which had 219 CPM. Together with the same observation of the IgG ctrl IP of WT cells, where the deacetylase activity with 78 CPM is as high as it is in WT cells which were precipitated for NCOR1, it can be said, that IP of these samples for NCOR1 remain problematic and further optimizations are necessary. Additionally, the measurable activity in precipitated samples disappeared, when the IgG ctrl was taken in to account as background, For the NCOR1 precipitated endogenous HDAC3 this is not surprising, since activity measurement of endogenous HDAC3 was almost not possible, when it was precipitated itself in HDAC3 endogenous IP (**section 3.1.2**).

## 3.3. Transcriptome analysis of cells expressing transgenic class I HDACs and cells treated with HDAC inhibitor

Previously, our lab generated gene expression data with HAP1 cell lines which carry HDAC transgenes or are HDAC KOs and additionally with treated HAP1 WT cells (Verena Moos, in collaboration with Michael Schuster from CeMM). Briefly, HDAC KO, KO HDAC WT and KO HDAC CI cells, WT HDAC CI, and HAP1 control cells were cultivated in equal conditions and harvested for RNA-seq. Simoultanously, WT cells were subject to treatment with the HDAC inhibitors MS-275 (class I HDACi, Entinostat) and JQ12 (HDAC1/2 inhibitor, [186]) with either 1 µM or 3 µM for 24 hours [167]. A part of the rawdata was used in this master thesis and analyzed to explore the similarities and differences between the generated cell lines (with focus on HDAC KO & WT HDAC CI) and WT cells which were treated with HDAC inhibitors. For this purpose, the rawdata was processed through DEseq2 and differentially expressed genes were analysed and visualized in heatmaps. Furthermore, a limited dataset of ChIP-seq data was made available and compared to RNA-seq data. The data has been deposited to the NCBI Gene Expression Omnibus (GEO) under GSE193885:
**https://www.ncbi.nlm.nih.gov/geo/query/acc.cgi?acc=GSE193885**

### 3.3.1. Similarity analysis of RNAseq datasets of upregulated genes

Quality assessment of the RNAseq dataset was done before (Michael Schuster, [167]). Since HDAC 1, HDAC2 & HDAC3 act as gene repressors through corepressor complexes, a knockout or inhibition of HDACs leads to dysfunctionality of these complexes [47], [187]. Consequently, the direct effect of antagonistic HDAC targeting should be upregulation of genes, thus the focus of this section are upregulated genes in wildtype background and in knockouts. To compare the impact of the inactive HDAC transgenes (CI), HDAC deletion (KO) or pharmacological HDAC inactivation on the gene expression level, the similarity of gene sets with significantly upregulated genes in WT HDAC CI or HDAC KO for Class I HDACs was calculated and compared to each other and to upregulated genes in MS-275 or JQ12 treated WT cells. The comparison is visualized in form of a triangle matrix that illustrates the similarity between each gene set by the intensity of the square (binary logarithm of the odds ratio derived from fisher's exact test). The significance of the similarities is calculated by using fisher's exact test (**Fig. 25**).

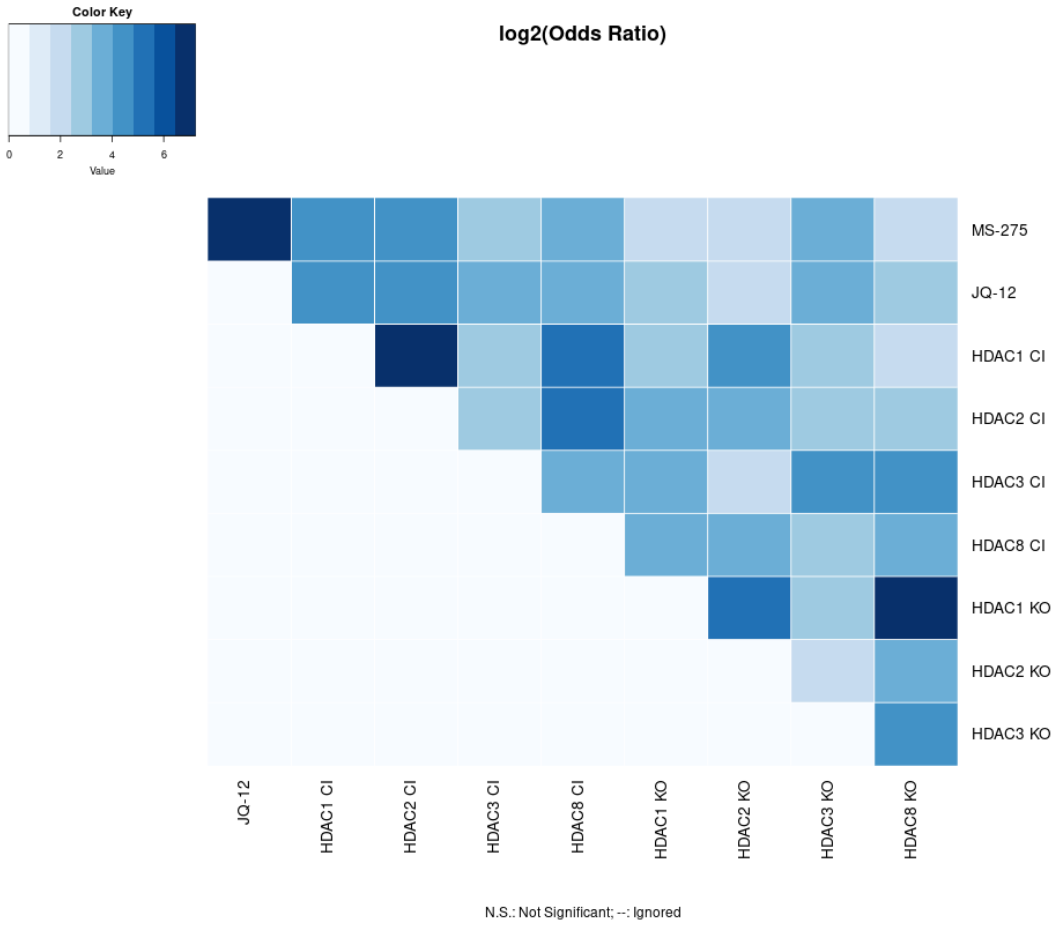


*Fig. 25:* ***Similarity analysis of upregulated genes upon introduction of mutant class I HDACs (CI = catalytically inactive) into WT cells, compared to HDAC KO cells and WT cells treated with MS-275/JQ12.*** *HDAC inhibitor treatments were done with each 1 µM concentration. Colour key values are binary logarithm of the odds ratio derived from fisher's exact test. P-values have been masked for better visibility and can be found in the supplementary material 5.2.*

At first sight it can be already seen that the cell lines into which HDAC1, HDAC2 and HDAC8 inactive transgenes were introduced possess a higher similarity to HDACi-treated cells compared to their respective HDAC1, HDAC2 and HDAC8 KO counterparts. These KOs show a relatively low similarity. A special case is HDAC3. There the KO looks slightly more similar to the inhibitor treatments than the cells with the HDAC3 CI.

A more detailed look reveals the overlap of HDAC1 mutant transgene and HDAC2 mutant transgene expressing cells to each other and to MS-275 and JQ12 treated cells which is plausible since they participate in the same HDAC complexes like NuRD, CoREST or SIN3A. Further, the very high overlap of similarity between both the HDAC1 and HDAC2 mutant transgene cell lines might be due to a high degree of overlapping functions of HDAC1 and HDAC2. It has been shown that they can partially compensate each other's loss [112].

A surprising fact is the similarity between WT HDAC1/2 CI and WT HDAC8 CI cell lines, and even more similarity between HDAC1 KO and HDAC8 KO.

### 3.3.2. Similarity of WT HDAC CI cells to HDAC KO cells

As a first step on gene expression level, we compared the upregulated genes in cells expressing the catalytic inactive HDAC variant to the genes in the respective KO cell line.

The analysis showed that for HDAC1 transgene expressing cells more than 80% of the genes which are significantly upregulated upon expressing the catalytic inactive HDAC1 transgene are at the same time not upregulated in the HDAC1 KO cells. The same analysis for HDAC2 cells with the inactive HDAC2 transgene shows that this number is at 60%, compared to HDAC2 KO cells. While, as recognized in the previous section already, HDAC3 KO gives the opposite picture: From the genes which are upregulated by expressing the inactive HDAC3 transgene, only 39% of the genes are not upregulated in the KO while the other 61% of the genes are upregulated by inactive HDAC3 transgene expression. Interestingly, in HDAC8 a similarly high number of genes as in HDAC1 can be found to be upregulated only in in the cell line with the catalytically inactive HDAC8 variant if compared to the HDAC8 KO cell line (**Table 6**).

| | WT HDAC CI upregulated | HDAC KO downregulated or unchanged | HDAC KO % down or unchanged |
|---|---|---|---|
| HDAC1 | 861 | 702 | 82% |
| HDAC2 | 1490 | 891 | 60% |
| HDAC3 | 855 | 330 | 39% |
| HDAC8 | 724 | 588 | 81% |

***Table 6: Numbers of genes which are significantly upregulated in WT HDAC CI cells and comparison of the same genes in HDAC KO cells.*** *The numbers in the column "HDAC KO % down or unchanged" show the amount of downregulated or unchanged genes compared to the total amount of deregulated genes. Model for analysis in DEseq2 takes into account WT HDAC CI, KO HDAC cells and HDACi (1 µM MS-275 or JQ12) treated WT cells with reference to gene expression levels in WT HAP1 cells. Thresholds for significance: log2fold-change > 1, adjusted p-value < 0.1*

The top 90 of upregulated genes in HAP1 cells into which either catalytically inactive HDAC1, HDAC2, HDAC3 or HDAC8 was introduced (WT HDAC CI) are depicted in heatmaps in **Fig. 26 A-D**.

The analysis of deregulated genes upon introduction of catalytically inactive HDAC into HAP1 cells and comparison to knock outs of the respective HDAC isoform show the distinct difference of which genes are upregulated depending on whether HDAC is rendered dysfunctional or is knocked out.

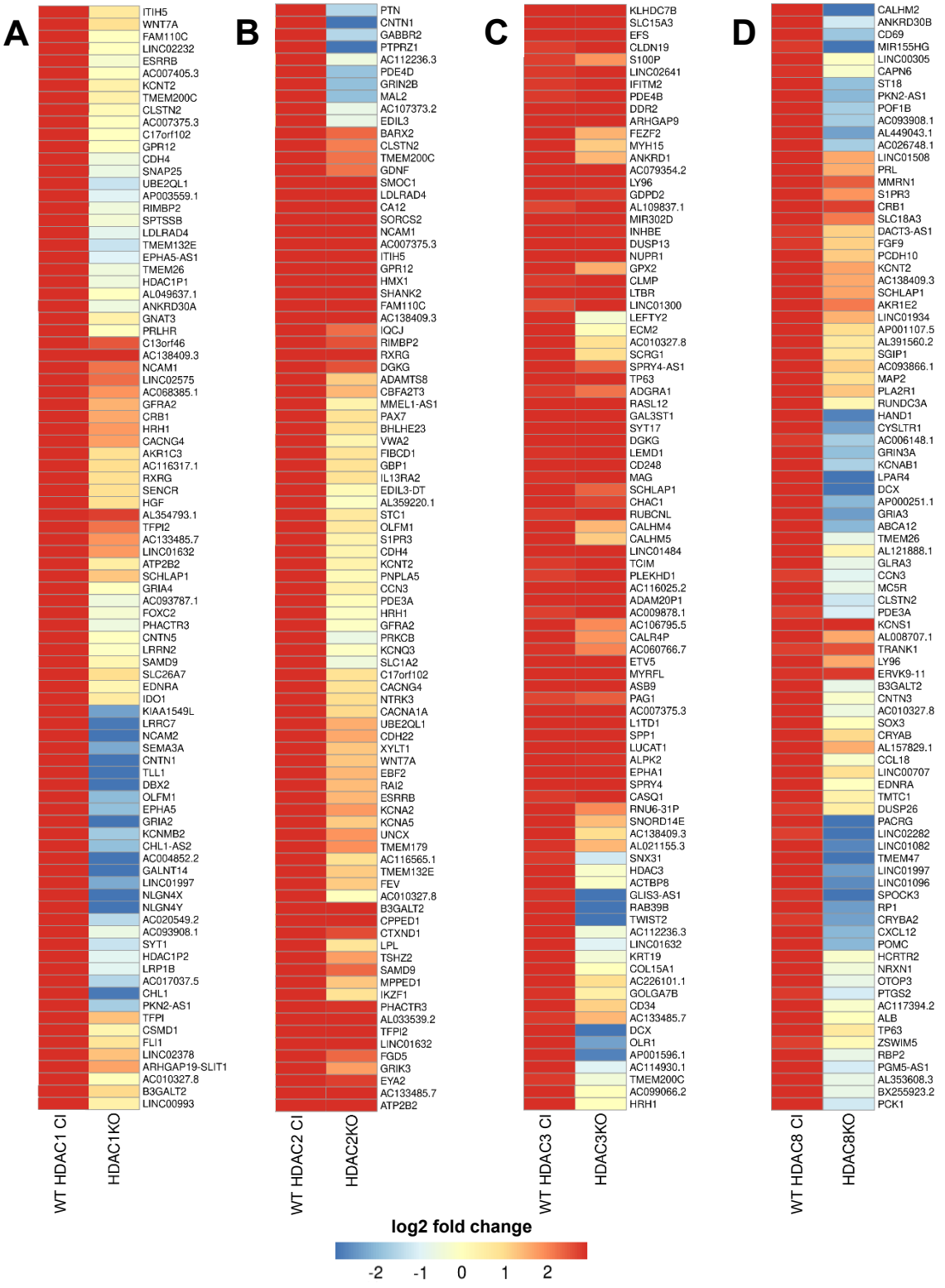


*Fig. 26:* ***Clustered heatmaps of top 90 upregulated genes for A)*** *WT HDAC1 CI,* ***B)*** *WT HDAC2 CI,* ***C)*** *WT HDAC3 CI and* ***D)*** *WT HDAC8 CI cell lines. The log2fold changes of genes from HAP1 cells carrying catalytic inactive HDAC were ranked top to bottom and visualized in a heatmap beside of gene log2 fold changes of corresponding HDAC KO cells. Red colour shows log2fold changes above 1 (upregulation). Blue colour shows log2 fold changes under -1 (downregulation). Yellow colour shows log2 fold changes between -1 and 1 (no significant change).*

### 3.3.2.1. *Common impact of catalytic inactive HDAC1 and HDAC2*

Next, we had a closer look at the genes which are only upregulated if the inactive HDAC transgene is introduced into cells but are not upregulated in the respective knock out cells. A subset of these genes could be regulated directly *via* the HDAC's catalytic activity.

HDAC1 and HDAC2 are part of common co-repressor complexes such as Sin3, CoREST and NuRD [178]. Thus, they were analysed together.

In the case of WT HDAC1 CI and WT HDAC2 CI, there are a total of 1291 genes which are upregulated only upon catalytic inactive HDAC. 702 in case of WT HDAC1 CI and 891 in case of WT HDAC2 CI. 302 genes share an upregulation in cells which express either the inactive HDAC1 variant or the inactive HDAC2 (**Fig. 27 A**). These genes are enriched for pathways regulating neuronal functions (**Fig. 27 B**). This reflects previous findings that HDAC1 and HDAC2 play a crucial role in the neuronal system [166], [167].

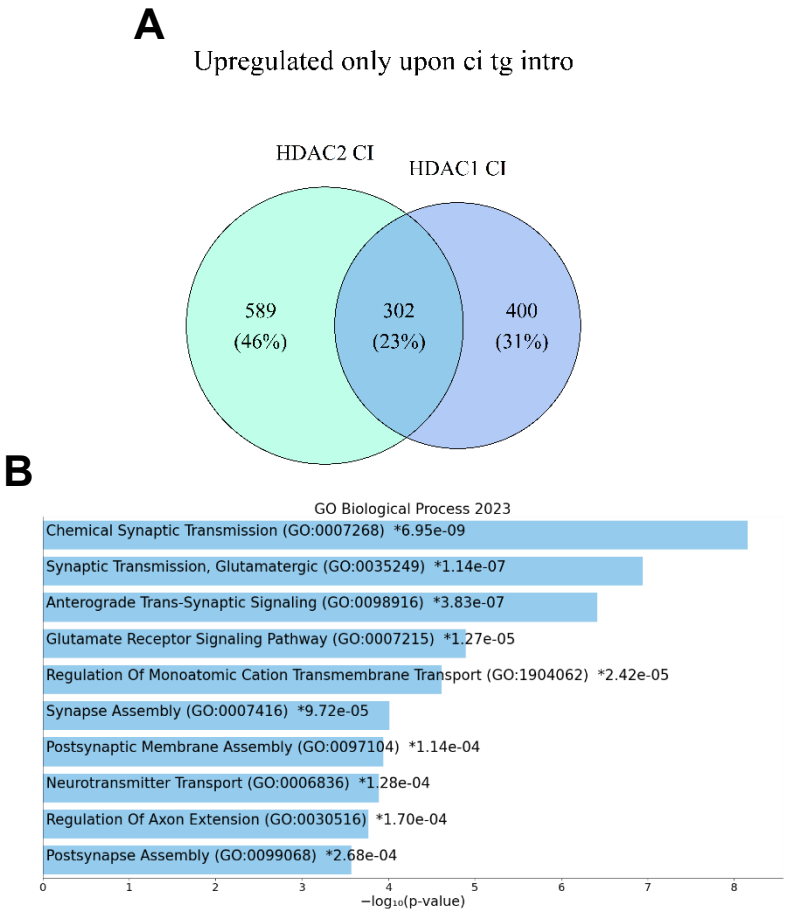


*Fig. 27:* ***Analysis of genes that show upregulation exclusively upon introduction of catalytic inactive HDAC1 or HDAC2, respectively. A)*** *702 genes are upregulated in WT HDAC1 CI cells, 891 genes are upregulated in WT HDAC1 CI cells. From these gene sets 302 common genes are upregulated due to expression of catalytic inactive HDAC1 or HDAC2.* ***B)*** *Gene ontology analysis of biological processes for enriched genes shows that especially neuronal functions are affected by catalytic inactive HDAC1 or HDAC2 (ENRICHR / GO2023).*

### 3.3.3. Effects of inactive HDAC3 transgene and HDAC3 KO

It was observed in the course of this thesis and in cell proliferation and apoptosis data from the lab of Susanna Chiocca that deletion of HDAC3 or introduction of the HDAC3 inactive transgene into HDAC3 KO cells has a higher impact on cell proliferation and viability than deletion or mutant transgene introduction of other class I HDACs [167].

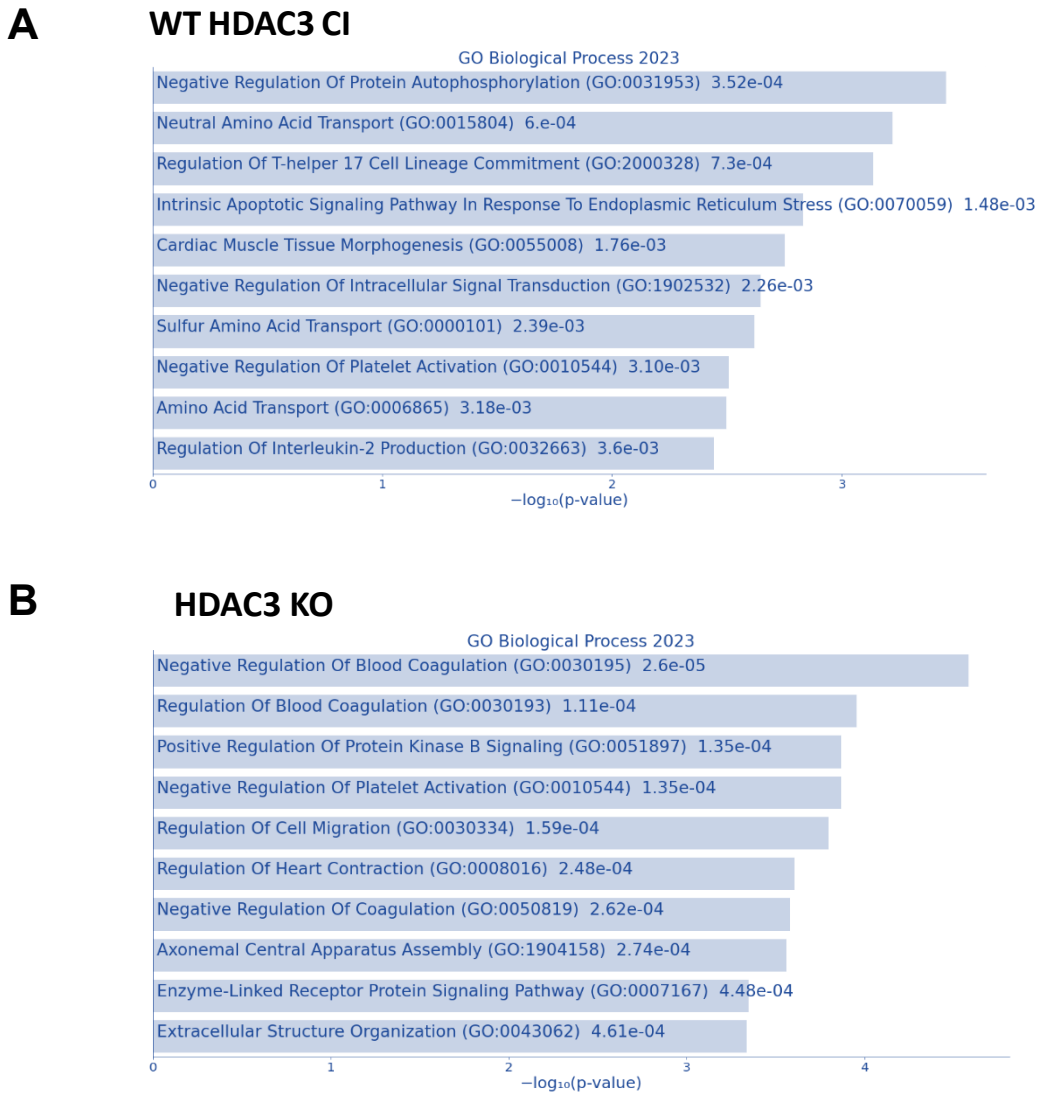


*Fig. 28:* ***Gene ontology analysis of biological processes where upregulated genes are enriched. A)*** *Upon catalytic inactive HDAC3 introduction into HAP1 WT cells* ***B)*** *Upon HDAC3 KO. p-value was used for ranking and determination of significance. (ENRICHR / GO2023).*

This was especially visible for the HDAC3 KO cells expressing the inactive HDAC3 transgene. They were growing significantly slower and had to be split only 1-2x per week, while the other cell lines had to be split 3-4x per week. The focus in this section lies in the directly derived modified HAP1 clones which are either HDAC3 KO or WT HDAC3 CI. There, gene ontology analysis of *Biological Processes* of upregulated genes in these cell

lines was of great interest to zoom into genes which are directly affected by catalytically and non-catalytically functions of HDAC3.

Analysis of upregulated genes upon HDAC3 catalytic inactive transgene expression points towards enrichment of many genes regulating processes of signal transduction especially through inhibition of phosphorylation and stress responses which can activate apoptosis (**Fig. 28 A**).

In a GO analysis of upregulated genes in WT HDAC3 CI cells the term "Negative Regulation Of Protein Autophosphorylation (GO:0031953)" shows the highest statistical enrichment with the following genes:

ERBB receptor feedback inhibitor 1 (ERRFI1) acts on MAPK and AKT signalling pathways in tumours with high EGFR levels and inhibits growth [188].

The transmembrane receptor endoglin (ENG) as important enzyme in angiogenesis and modulator of TGF-Beta plays a two-sided role in cancer which depends on the affected cell line [189].

Caveolin-1 (CAV1) is found in the cell membrane and inhibits activation of EGF and PDGF, subsequently contributing to apoptosis [190]. NACHT, LRR and PYD domains-containing protein 12 (NLRP12) can form an inflammasome as part of immune answer to certain infections. Further, it inhibits ERK and AKT in tumor tissue and was shown to prevent colon cancer [191].

CAV1 and NLRP12 are also part of the GO term “Negative Regulation Of Intracellular Signal Transduction (GO:1902532)”. Together with them, there are 7 other upregulated genes which also belong to this ontology: Dual specificity phosphatase 6, 13 & 26 (DUSP6, DUSP13, DUSP26) are regulators of the MAPK pathway members where they dephosphorylate members of the MAPK pathway and subsequently inhibit proliferation [192].

Diacylglycerol kinase gamma (DGKG) has multiple roles: While in Acute Myeloid Leukemia high expression of DGKG is associated with a more favourable prognosis [193] it promotes tumor growth of hepatocellular carcinoma [194].

Ventricular zone-expressed PH domain-containing protein homologue 1 (VEPH1) has a suppressive role in patients with gastric cancer *via* the Hippo-YAP pathway [195].

Further enriched are DNA damage-inducible transcript 3 (DDIT3) and DNA damage-inducible transcript 4 (DDIT4). DDIT3 is an important protein in the cell's stress response and regulates apoptosis pathways and cell cycle arrest [196]. DDIT4 responds also to

stress and its overexpression leads activation of apoptosis pathways. It has been shown that the diabetes drug Metformin triggers cell cycle arrest *via* DDIT4 and thus inhibits tumor growth [197].

DDIT3 is also enriched for "Intrinsic Apoptotic Signaling Pathway In Response To Endoplasmic Reticulum Stress" (GO:0070059). ChaC glutathione specific gamma-glutamylcyclotransferase 1 (CHAC1), which is part of this GO term is found downstream of DDIT3. High expression levels of CHAC1 are associated with apoptosis [198]. Recent studies found that metformin suppresses tumour growth in gastric cancer *via* CHAC1 [199].

Since gene regulation by HDAC3 seems to be influenced only to a certain degree by only the catalytic function of HDAC3 (compared to the effect in HDAC3 KO cells), we were highly interested in an analysis of the upregulated genes in HDAC3 KO cells. In the GO analysis of upregulated genes in HDAC3 KO (**Fig. 28 B**) the biological process "Negative Regulation Of Blood Coagulation" show the most significant enrichment of genes. Similar processes are in the top 10 of most significant terms.

The term "Regulation Of Cell Migration" share many genes which are enriched as well in "Regulation Of Blood Coagulation", but contains also genes which are enriched in "Enzyme-Linked Receptor Protein Signaling Pathway" and "Positive Regulation Of Protein Kinase B Signaling".

"Enzyme-Linked Receptor Protein Signaling Pathway" is enriched for the genes for Colony stimulating factor 1 receptor (CSF1R), Platelet-derived growth factor receptor beta (PDGFRB), gene rearranged during transfection (RET) & epidermal growth factor receptor (EGFR).

CSF1R is especially expressed in myeloid cells and is important for keeping up differentiation, proliferation and survival of these [200]. The receptor tyrosine kinase PDGFRB gene lies alongside of the CSF1R gene on human chromosome 5 (CIT). Both genes are proto oncogenes [201]. Deletion of the region with those both genes on chromosome 5 play a role in development of 5q- syndrome which leads to myelodysplastic syndrome (MDS). This can be treated by lenalidomide (promotes degradation of proteins through E3 ubiquitin ligase) that supresses accumulation of malignant cells with the chromosome 5q-deletion [202].

The RET gene encodes another proto-oncogene [203]. EGFR is associated with numerous cancers [204].

RET and EGFR are also part in "Positive Regulation Of Protein Kinase B Signaling". EGF itself, which is also upregulated, belongs also to this ontology. Additionally, chemokine (C-X3-C motif) ligand 1 or Fractalkine (CX3CL1) and Endoglin (ENG) are enriched for this term.

Taken together, these results suggest, that many genes which are upregulated in WT HDAC3 CI contribute to apoptosis and inhibition of proliferation. On the other hand, the effects of genes upregulated in HDAC3 KO are bivalent. Quite a number of them are known as proto-oncogenes.

### 3.3.4. Mimicking MS275 treatment with mutant class I HDACs

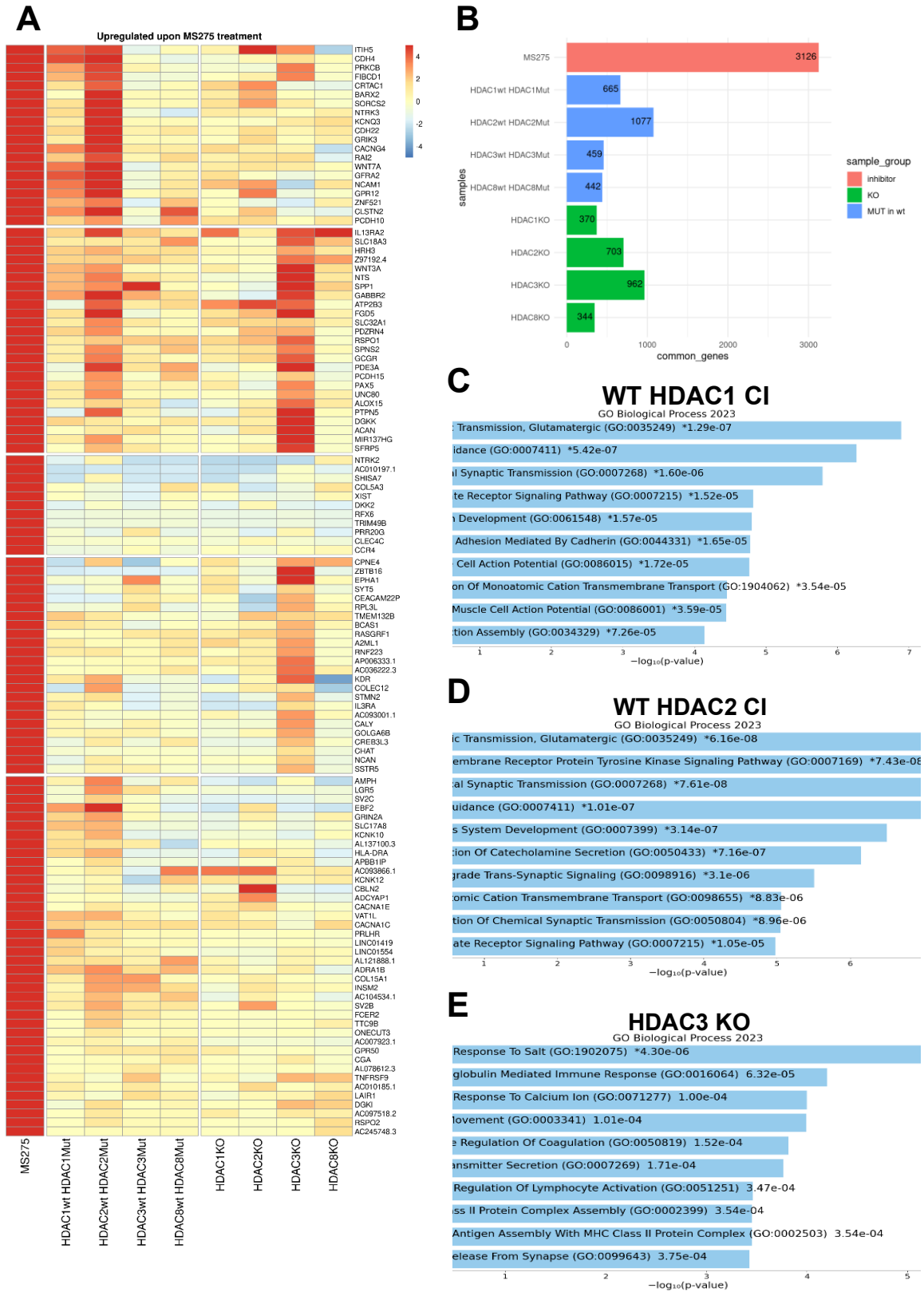


*Fig. 29:* ***Genes that are upregulated after 24h MS-275 treatment (3 µM).*** *Gene expression levels are compared to those of WT HDAC CI cells and to HDAC KO cells.* ***A)*** *Top 120 genes represented in a heatmap.* ***B)*** *Common genes of each cell line with the MS-275 treatment. C-E) GO biological processes Top enriched terms (ranked by p-value, ENRICHR / GO2023)*

The direct comparison of genes that are upregulated upon 3 µM MS-275 treatment to cells expressing class I mutant HDACs and to class I HDAC KO cell lines suggests a higher resemblance of WT HDAC1 CI and WT HDAC2 CI cell lines to the HDACi treatment than their respective knock outs HDAC1 KO & HDAC2 KO (**Fig. 29 A**). In fact, from totally 3'126 upregulated genes in the MS-275 treatment, 1077 are also upregulated in WT HDAC2 CI. 665 genes are shared with WT HDAC1 CI (**Fig. 29 B**). Analysing the genes which are upregulated through MS-275 and in WT HDAC1 CI or WT HDAC2 CI for gene ontologies (**Fig. 29 C & D**) shows high enrichment of genes for terms mainly connected to the nervous system.

For HDAC3 the upregulated genes of HDAC3 KO cells are more similar to those upregulated by MS-275, compared to cells expressing catalytically inactive HDAC3 transgene. 962 genes are upregulated in both HDAC3 KO cells and MS-275 treated cells. Gene ontology analysis for gene enrichment in biological processes reveals that the cell's response to calcium and signalling of neurons is affected (**Fig. 29 E**). Further, immunoglobulin assembly and mediated immune system responses with the very seems to be changed. The similarity of WT HDAC8 CI cells to MS-275 treated cells is less high compared to other cell lines, but still higher than of the respective HDAC8 KO to MS-275 treated.

Altogether it can be said that the introduction of catalytic inactive HDAC 1/2 (CI) into WT cells mimics the treatment with MS-275 better than the HDAC1/2 KO cells. The same is through for WT HDAC8 CI. For HDAC3 it can be said that it forms a small exception within the class I HDACs and the KO mimics MS-275 treatment better than the introduction of a catalytically inactive HDAC3.

### 3.3.5. ChIP-seq dataset

Beside of RNA-seq also ChIP-seq data were generated in our lab. At the time point of data analysis, only ChIP-seq data from class I HDAC KO cells was available, thus, in this thesis the ChIP-seq data from the KO cell lines was compared to the RNA-seq data of HDAC KO cells and the KO cell lines were also compared to MS-275 treated cells. The overlap between genes which carry the active marker H3K27ac in their regulatory region with the same genes upregulated in the RNA-seq dataset would support the feasibility of the particular experiment.

Very good similarity could be seen between the ChIP-seq and RNA-seq data sets of each HDAC KO, which is true for up- and downregulated genes (**Fig. 30**). The overlap of the ChIP-seq data from the HDAC KOs to the RNA-seq data of the inhibitor treated cells is low, similar as seen in the RNA seq experiments with HDAC KO cells in the previous section (**3.3.1**). Opposite to the RNA seq data for the HDAC3 cell line data, no overlap can be seen between H3K27ac marks of HDAC3 KO and MS-275 treated cells. Also, the RNA seq and CHIP seq data sets of MS-275 treated cells do not show consistency.

Overall, the datasets for class I HDAC KO cells are consistent, while the data of MS-275 treated cells show no significant overlap of genes with the H3K27ac mark and a corresponding deregulation of the genes.

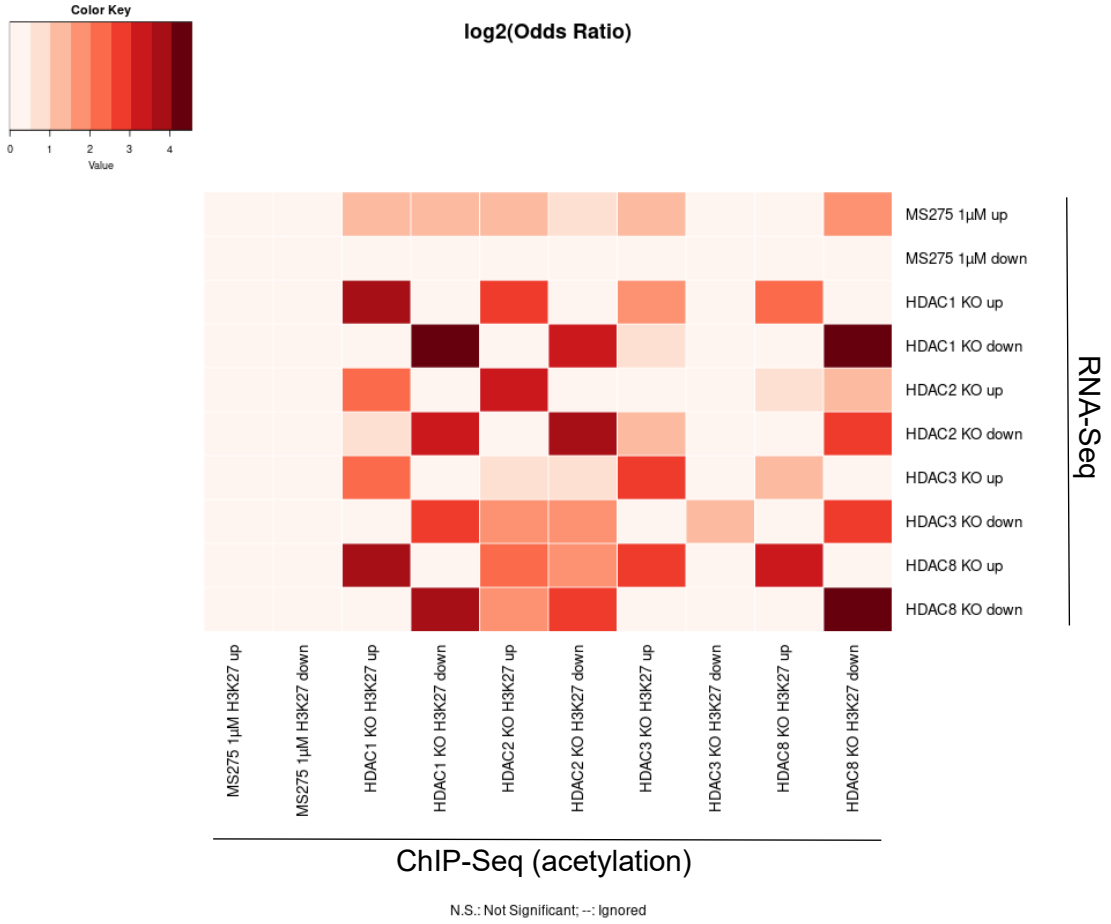


*Fig. 30:* ***Similarity analysis between RNA-seq data (right) and ChIP-seq data (bottom) of class I HDAC KO cell lines and 1 µM MS-275 treated cells.*** *Colour key values are binary logarithm of the odds ratio derived from fisher's exact test. The p-values have been masked for better visibility.*

## 3.4. Transfection of fetal liver cells harbouring mutant HDAC1 transgene with an AML oncogene

To further investigate the effects of mutated HDACs, we wanted to establish a cellular model system for acute myeloid leukemia which allows observations also *in vivo* in mice. Since fetal liver cells can be transfected with an acute myeloid leukemia oncogene (MLL-AF9) it would allow a pretesting of the cells *ex vivo*, and potential interesting effects can then be tested in follow-up experiments by injecting oncogenic fetal livers cells back into mice.

Mice carrying transgenic, mutated HDAC1 in the safe harbour locus *Rosa26*, were provided by Lena Hess (see also Master thesis and PhD thesis [169], [170]) Upstream of the HDAC1 mutant transgene a β-geo-polyA STOP cassette is integrated which can be removed upon expression of the Cre-recombinase due to flanking loxP sites (attL/attR) (**Fig. 31**). Downstream of the transgene follows an IRES-EGFP fluorochrome sequence. Importantly, upon expression of transgenic HDACs, EGFP expression is also induced. This facilitates detection of transgene expressing cells *via* fluorescence microscopy or flow cytometry.

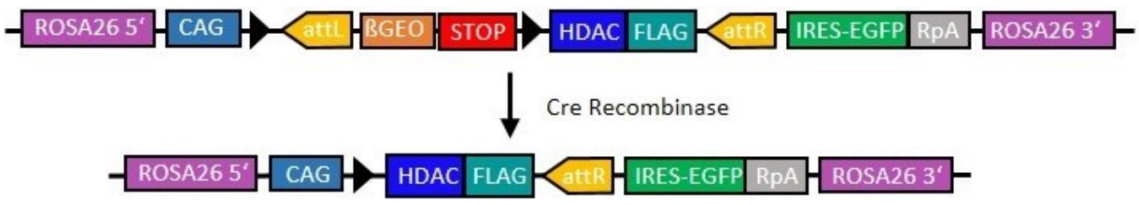


*Fig. 31:* ***Scheme of HDAC transgene in ROSA26 safe harbour locus.*** *Modified scheme provided by Lena Hess (PhD thesis, 2022).*

*Mx1-Cre+* mice were obtained from the Dagmar Stoiber-Sakaguchi lab (Sophie Edtmayer) and were crossed with our HDAC1 transgenic mice to receive mice with a *Rosa26 Hdac1 CI TG/+ Mx1 Cre+* genotype.

The plasmid MAIV (MLL-AF9-IRES-Venus) with the oncogene *MLL-AF9* was a kind gift of the Zuber lab [153]. Since the plasmid carries the VENUS fluorochrome which is detected in the same channel as the EGFP fluorochrome downstream of the HDAC transgene, the *Venus* sequence had to be replaced with another fluorochrome. We decided to substitute it with *mCherry* since it would not shine into the GFP channel [205].

### 3.4.1. Cloning

Cloning of the *mCherry* sequence into the MAIV vector was done by cutting the *mCherry* sequence out of the Rosa26_IRES_mCherry vector (obtained by Terezia Vcelkova) and cloning into MAIV vector (**Fig. 32**). No unique restriction sites shared by both vectors upstream and downstream of the desired gene sequence were existing. Especially on the Rosa26_IRES_mCherry vector many sites were found several times, which made a preliminary step of PCR necessary to add an adapter onto the *mCherry* sequence. 2 strategies were performed. Basic (standard) cloning is shown only briefly since it was not possible to clone the desired construct through this strategy (**3.4.1.1**). The strategy of TA-cloning will be shown in more detail, this strategy allowed successful cloning of mCherry into MAIV (**section 3.4.1.2**).

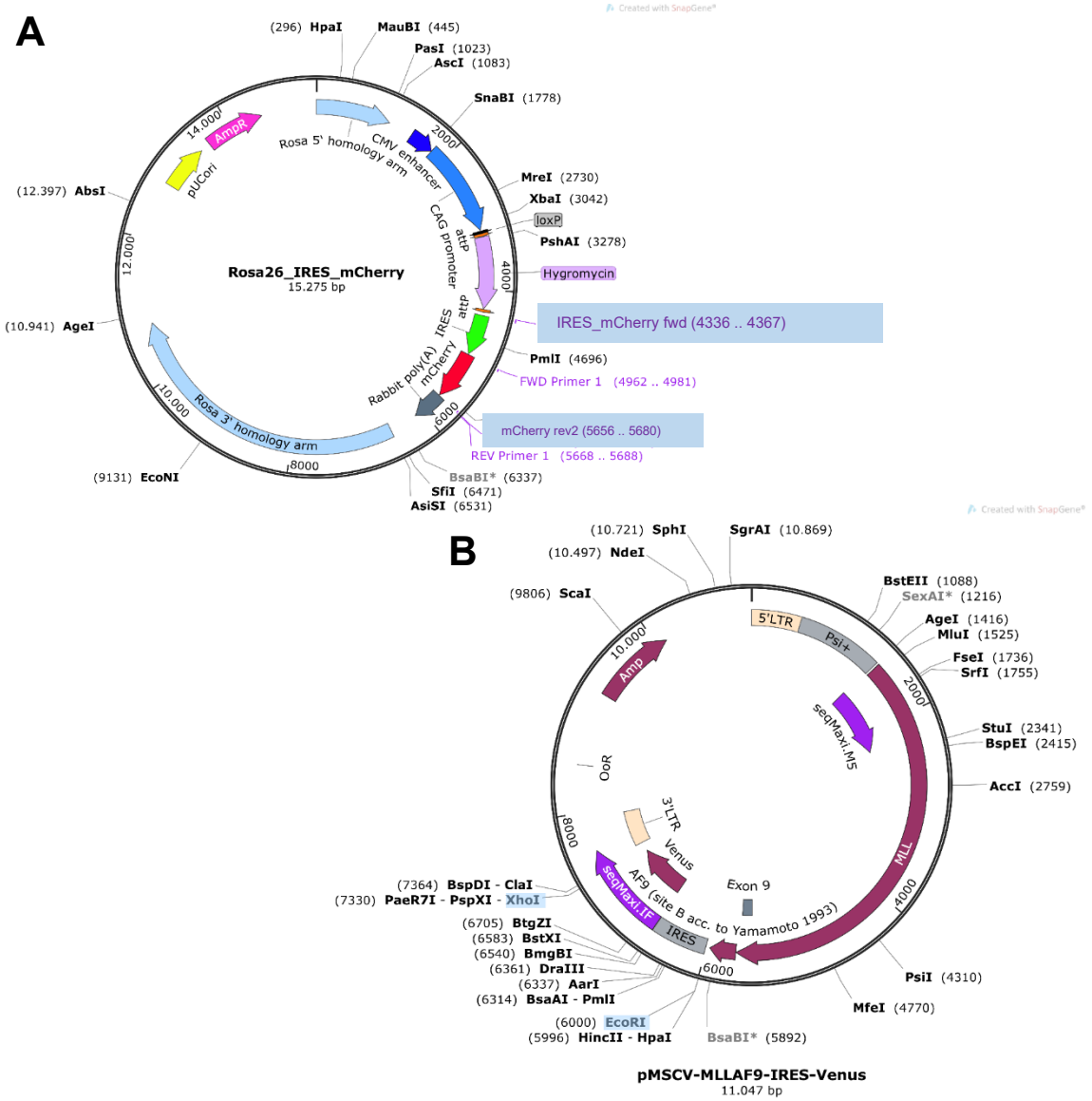


*Fig. 32:* ***Maps of plasmids used in this thesis. A)*** *Rosa26_IRES-mCherry contains the desired sequence for the mCherry fluorophore.* ***B)*** *MAIV contains the MLL-AF9 oncogene and the Venus gene. Venus has to be replaced on this vector by mCherry. EcoRI and XhoI were used as restriction enzyme cutting sites.*

### *3.4.1.1. Basic cloning*

Since MAIV carries several unique restriction enzyme (RE) target sites upstream and downstream of the *Venus* sequence (which has to be replaced), it was decided to add the sequences for these RE sites with adapters during PCR amplification to the *mCherry* sequence (The both possibilities of taking the *mCherry* sequence with or without the upstream IRES sequence were). The chosen RE sites were *EcoRI* upstream of IRES and *Venus*, *BstXI* between IRES and *Venus* (directly upstream of *Venus*) and *XhoI* downstream of *Venus*.

Two forward and two reverse primers were designed:

Concerning the design of the first forward primer, which contains parts of the IRES sequence as well as of the *mCherry* sequence (between IRES and *mCherry*), it has to be noted, that the IRES sequence and the *mCherry* sequence are separated by only 6bp, thus the *mCherry fwd primer* is overlapping with both the IRES and the *mCherry* sequence. The primer was designed in a way, that after restriction enzyme digestion with *BstXI* the ATG-codon for methionine (important for translational start) would not be disrupted and the sequence stays in frame.

The second forward primer *IRES_mCherry fwd* has the addition of the *EcoRI* RE-site towards the 5'-end as adapter to the sequence and lies upstream of IRES.

Both the reverse primers (*mCherry rev 1* and *mCherry rev 2*) contain the RE-site for *XhoI* at their 5'-end.

The primers were tested in a gradient PCR to obtain the optimal annealing temperature for amplification of the desired DNA fragment without offsite effects (**Fig. 33**).

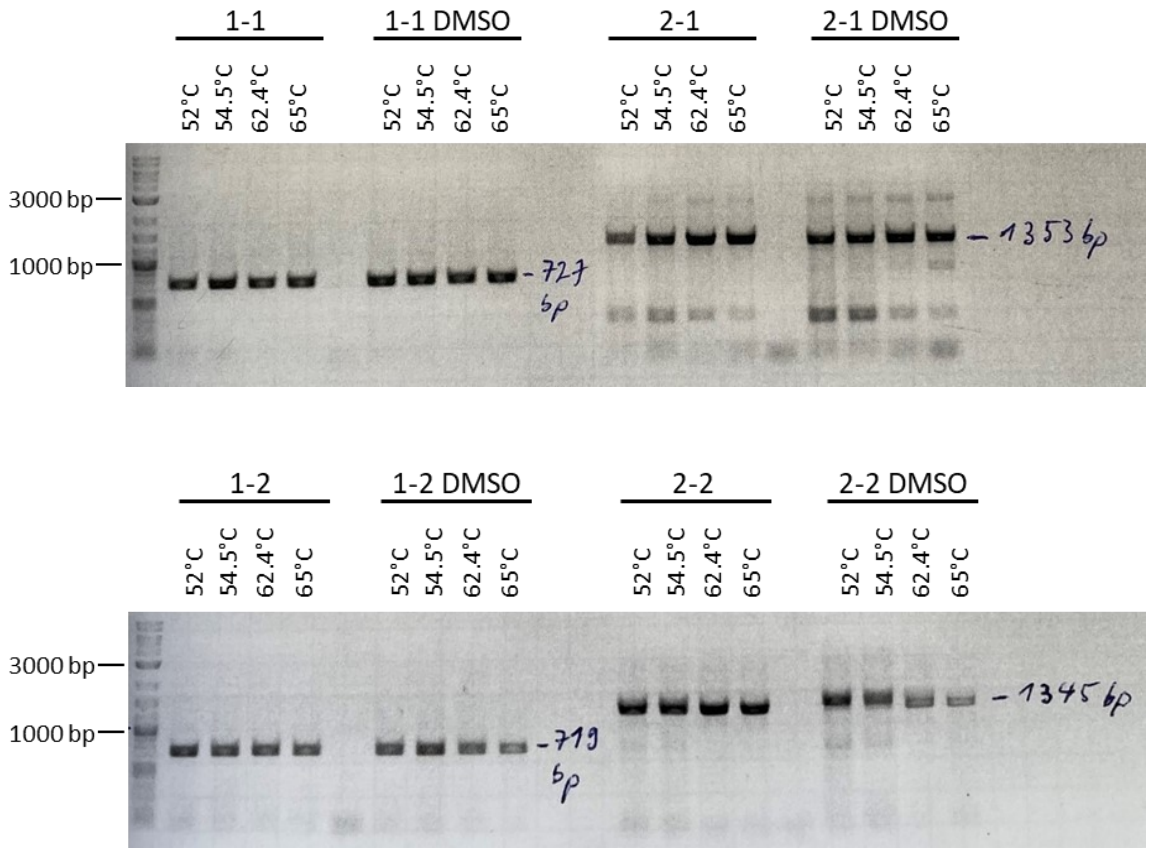


*Fig. 33: Agarose* ***DNA gel electrophoresis of temperature gradient PCR to determine the optimal annealing temperature of primer pairs used for cloning.*** *The first number depicts the forward primer 1) mCherry fwd and 2) IRES_mCherry fwd, the second number depicts the reverse primer 1) mCherry rev1 and 2) mCherry rev2. 1 kb Plus DNA Ladder (NEB) was used as gene ruler.*

All four primer combinations were tested with and without Dimethyl Sulfoxide (DMSO). DMSO is known to lower the melting temperature and hereby also serves to prevent annealing [206]. The expected fragment sizes were confirmed in all 4 combinations. *mCherry fwd* in combination with *mCherry rev1* or *mCherry rev2* were expected to have a length of 727 bp or 719 bp, respectively. The primer including the IRES sequence (*IRES_mCherry fwd*) was expected to give the longer stretches of 1353 bp in combination with *mCherry rev1* and 1345 bp in combination with *mCherry rev2*.

The combination of *IRES_mCherry fwd* and *mCherry rev2* gave the best and very clean results with an annealing temperature of 65°C. This primer combination was chosen to be used subsequently.

The PCR with the plasmid ROSA26_IRES_mCherry with the above-mentioned primer combination (*IRES_mCherry fwd* & *mCherry rev2*) was performed and the linear sequence product PCR_ROSA_IRES_mCherry was purified by gel extraction.

Both PCR_ROSA_IRES_mCherry and MAIV were then digested with *EcoRI* and *XhoI*. The digestions were gel purified after running an agarose gel (**Fig. 34**) and cutting out the bands

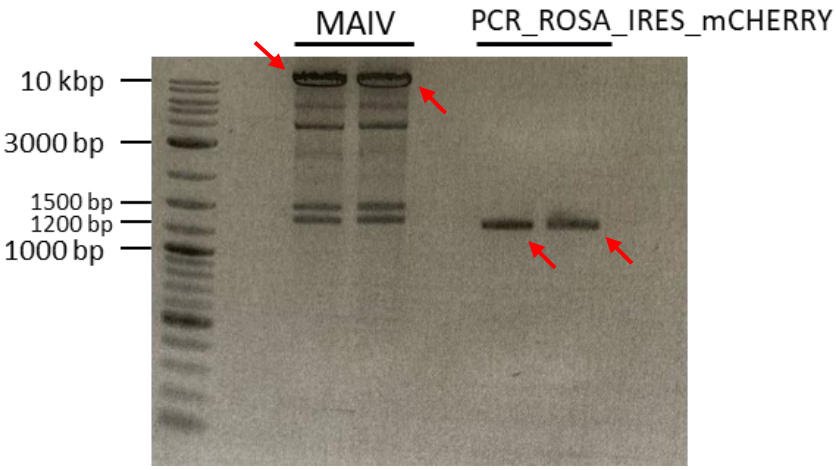


*Fig. 34: Agarose DNA gel electrophoresis blot with products from digestion with EcoRI and XhoI applied to the MAIV vector (first 2 lanes) and the mCHERRY vector with previously added restriction sites via PCR (last 2 lanes). The marked lanes were cut out and purified. 1 kb Plus DNA Ladder (NEB) was used as gene ruler.*

with the expected size (around 10 kbp for MAIV (without Venus), 1300 bp for PCR_ROSA_IRES_mCherry).

The digests were ligated with both ratios 3:1 and 4:1 (fragment:vector) and the ligated plasmid, supposably MAIM, was directly used for transformation of DH5α-F' E.coli. After colonies were obtained successfully, a colony PCR was used to check for the correct insertion of *mCherry* into the vector (**Fig. 35 B**). The first primer pair

(*MAIVmCHERRY_CPCR_fwd1* & *MAIV_CPCR_rev1*) replicated the sequence (**Fig. 35 A**) of 211 bp from the ligation product (supposably MAIM) which originated from the picked colonies. For both fragment:vector ratios 3:1 and 4:1 half of the colonies (4 out of 8) were tested positive for the ligation product with primer pair 1 (**Fig. 36 A**). Disturbing was the fact, that the sequence also replicated from the plasmid without the insert, MAIV, with this primer pair. The second primer pair did not show any replication in the colony PCR for any of the colonies.

Nevertheless, 2 colonies from each the newly cloned plasmid (MAIV_PCR_ROSA 1 & 2) and 2 colonies with the original MAIV plasmid were cultivated and purified. The obtained RNA from MAIV_PCR_ROSA colonies had a very low concentration (10.9 ng/µl and 8.9 ng/µl) while the RNA obtained from MAIV colonies yielded a concentration of 228 ng/µl and 230 ng/µl.

The product from the cloning process was checked with RE-digest using *StuI*, which should cut the desired plasmid containing *mCherry* (MAIM) into 3 fragments (with a size of 6327 bp, 4490 bp and 222 bp, **Fig. 36 B**) and the original plasmid with *Venus* (MAIV) only into 1 big, linearized fragment. The cut fragment of MAIV is visible on the gel (**Fig. 36 C**), since the band is slightly higher than the circular MAIV. But the lane which is supposed to show the MAIM plasmid harboured only a slightly visible band and around 10 kbp that was uncut, which indicates that the *mCherry* sequence was not present in this vector.

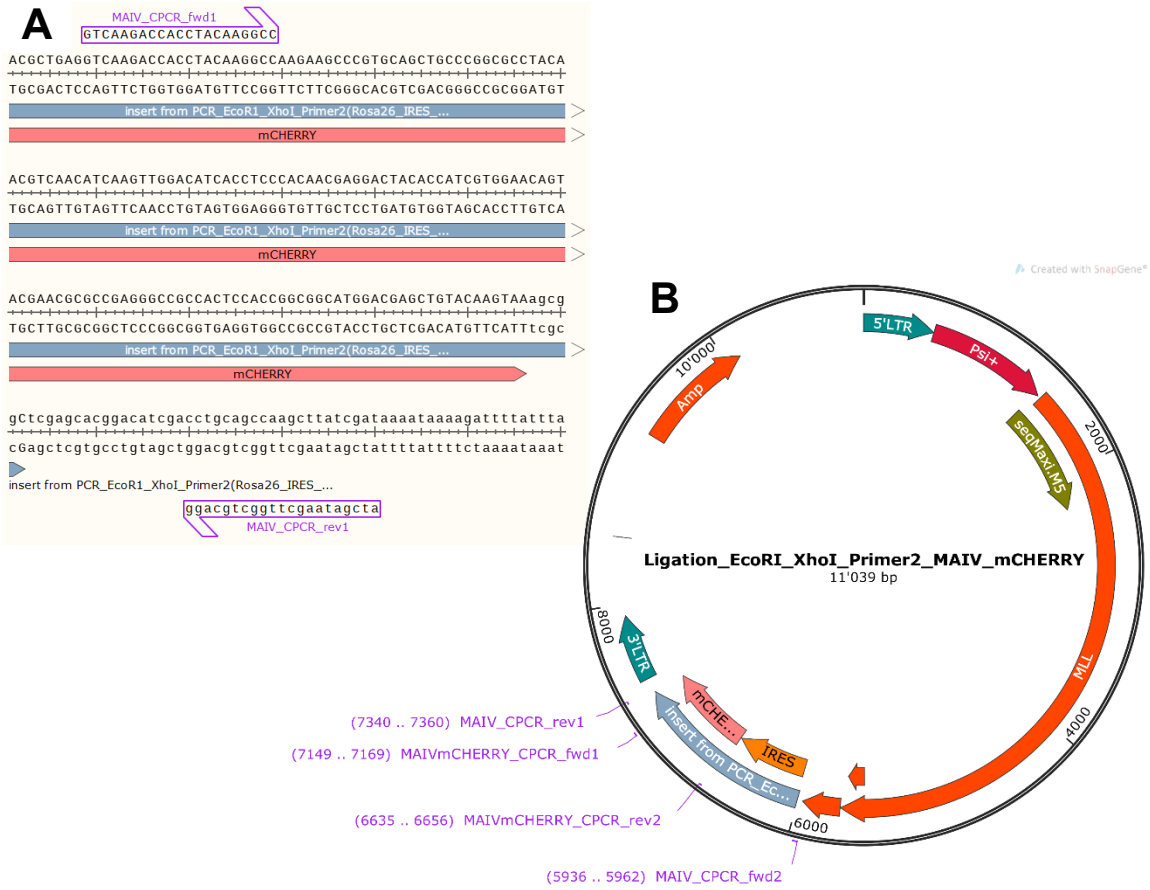


*Fig. 35:* ***Primer design for Colony PCR. A)*** *Sequence that is covered by the first Colony PCR primer pair. The second primer pair (MAIV_CPCR_fwd2 & MAIVmCHERRY_CPCR_rev2) is not shown due to lack of space.* ***B)*** *Visualization of positions of both primers (MAIVmCHERRY_CPCR_fwd1 & MAIV_CPCR_rev1) in the cloned plasmid MAIM.*

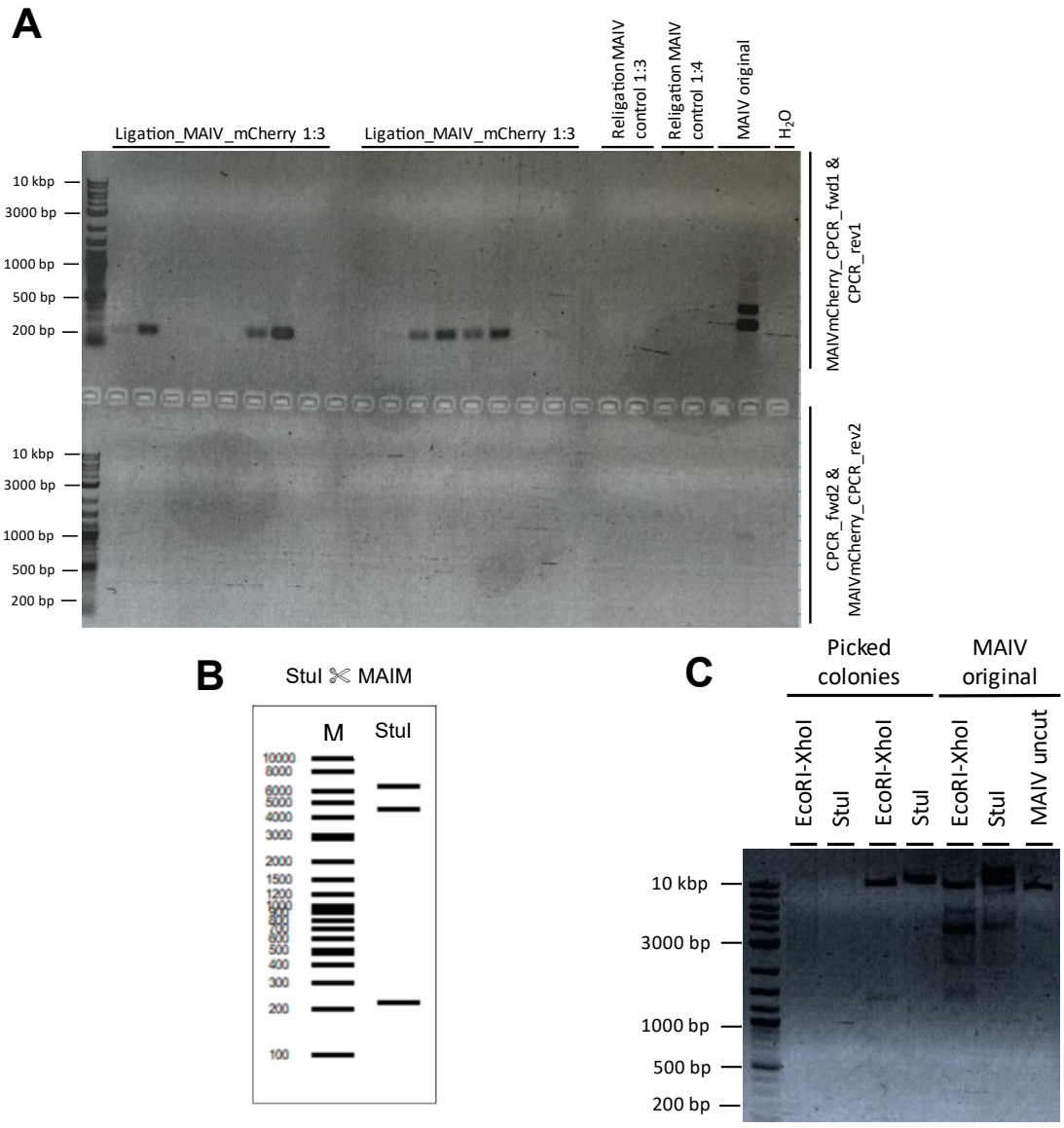


*Fig. 36:* ***DNA gel electrophoresis of A)*** *colony PCR to check successful ligation & transformation and* ***C)*** *control digest (restriction analysis) using StuI to check for presence of mCherry in plasmid.* ***B)*** *Desired outcome of restriction analysis for MAIV with mCherry insert (MAIM), StuI cuts MAIM into 3 fragments with a size of 6327 bp, 4490 bp and 222 bp. 1 kb Plus DNA Ladder (NEB) was used as gene ruler.*

We also tried the cloning strategy using *BstXI*, but no colonies were obtained after transformation.

### *3.4.1.2. TA cloning*

TA cloning uses the feature of Taq polymerase in PCR to add an adenine base at each 3'-end of the fragment which has to be cloned. The adenine overhang can easily anneal with

a 3’ thymine overhang of another strand. The linearized pCR™2.1-TOPO® vector (Invitrogen, **Fig. 37**) possesses 3’ thymine overhangs at both ends of the vector which are covalently bound by topoisomerase I. The topoisomerase I will be released and the desired DNA strand with 3’ adenine overhangs anneals into the insertion site where the full multiple cloning site (MCS) will form where several RE sites can be found upstream and downstream [207]. Also, the presence of the RE site *EcoRI* upstream of the insertion site and *XhoI* downstream of the insertion site means that the same restriction enzymes which were used in the classical cloning (**section 3.4.1.1**) can be used here.

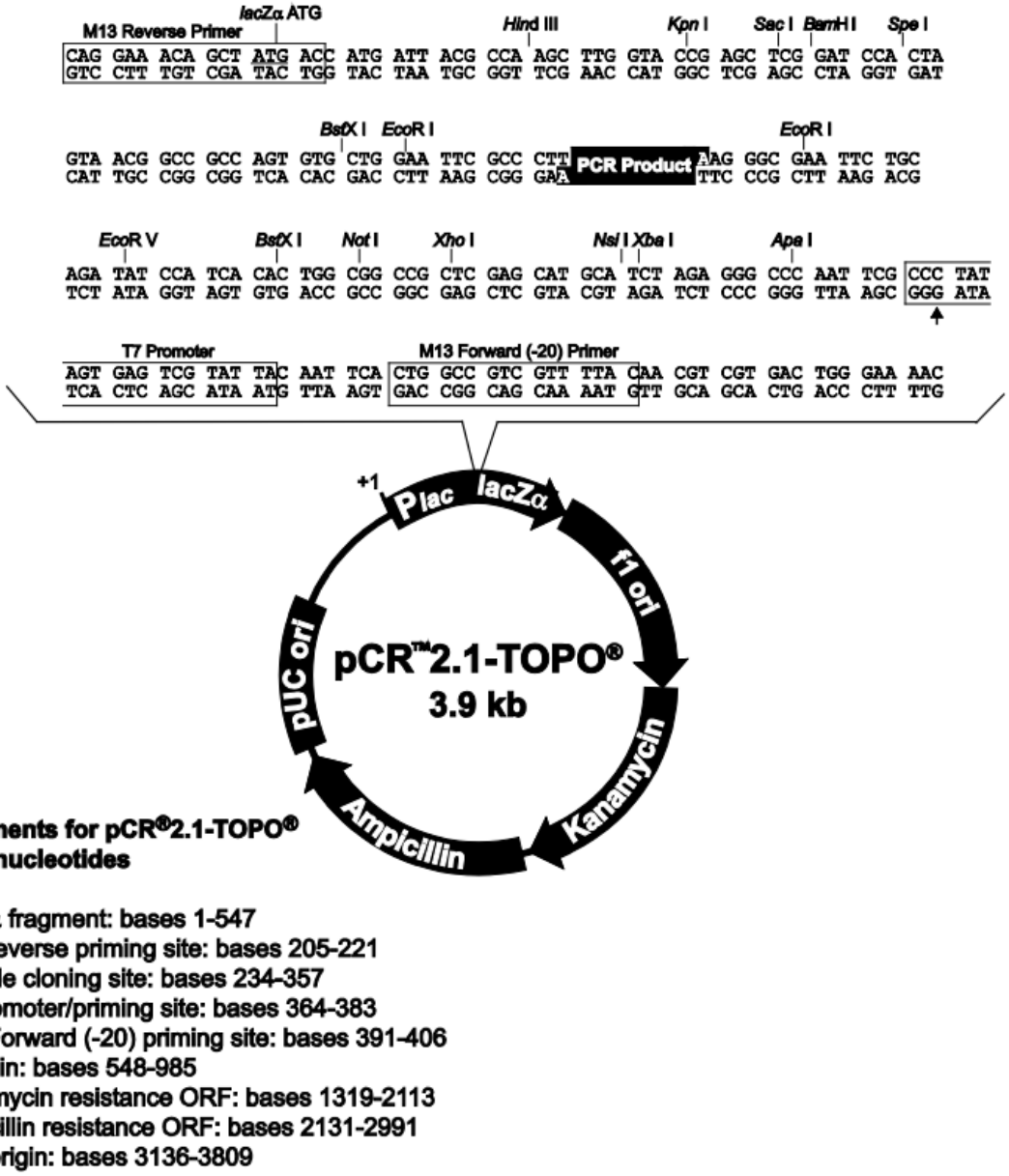


*Fig. 37: **Vector map of Plasmid pCR™2.1-TOPO® and MCS.** The figure was adapted from the TOPO® TA Cloning® kit from Invitrogen.*

IRES_mCherry was amplified with the same set of primers as in the basic cloning strategy (*IRES_mCherry fwd* and *mCherry rev 2*). The amplified product PCR_IRES_mCherry was

directly used without purification since it might interfere with the 3'-overhangs and was ligated into the pCR™2.1-TOPO® vector. Then the transformation of DH5α-F' E.coli was done with the obtained TOPOmCherry plasmid. Successfully transformed colonies were blue since a β-Galactosidase gene is present on the plasmid which can be detected by addition of X-Gal, which is converted by β-Galactosidase.

Transformation efficacy for TOPO_mCherry was low (20-30% of total colonies, not shown here), but enough (4 blue colonies, not shown here) could be obtained for a colony PCR and presence of the mCherry gene was confirmed.

After successful cloning of the *mCherry* sequence into the pCR™2.1-TOPO® vector, this vector and MAIV were both digested with *EcoRI* and *XhoI*. The resulting IRES_mCherry fragment, as well as the linearized MAIV vector (with *Venus* cut out) were gel purified and used in the subsequent ligation reaction, resulting in the MAIM vector and a control relegation of MAIV. The transformation of DH5α-F' E.coli with MAIM yielded in ~50 visible colonies after o/N incubation (**Fig. 38 A**). The transformation with the MAIV relegation yielded in only a dozen colonies (**Fig. 38 B**). Colony PCR showed a successful transformation for 8 of 10 colonies (not shown here). A control digest (**Fig. 39 A & B**) with StuI showed positive results for all 8 colonies (3 fragments expected with the lengths 6327 bp, 4490 bp and 222 bp).

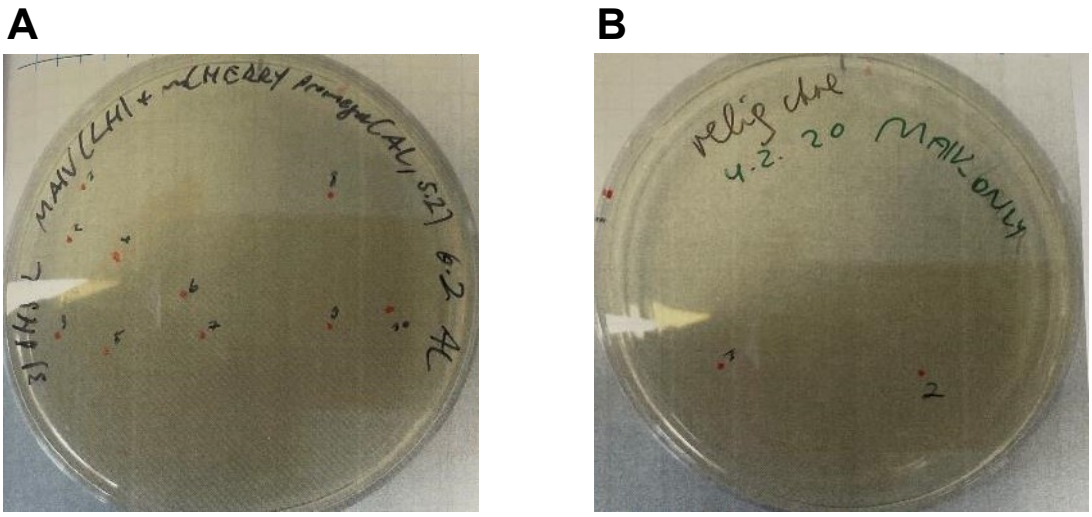


*Fig. 38:* ***Colonies of transformed DH5α-F' E.coli with ligated Plasmids. A)*** *Colonies with ligated MAIM plasmid are seen.* ***B)*** *Control (re-)ligation of the MAIV plasmid.*

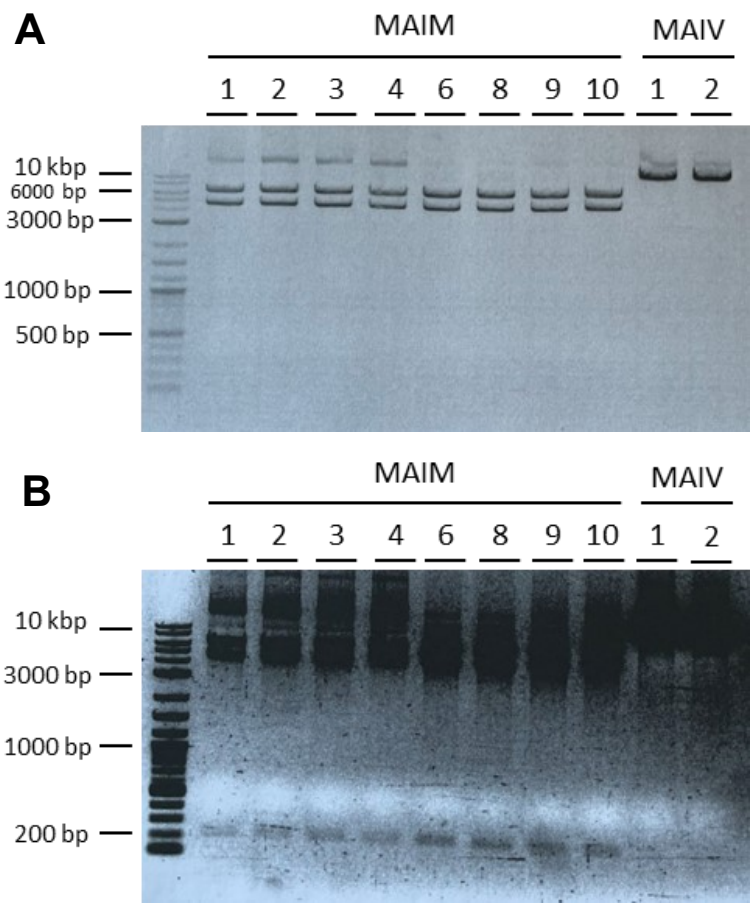


*Fig. 39:* ***Agarose DNA gel electrophoresis of digested MAIM plasmid from minipreps from 10 different clones. Digestion was done with StuI.*** *3 fragments with the lengths 6327 bp, 4490 bp and 222 bp are expected.* ***A)*** *short exposure of gel to differentiate bands in 3000 bp to 10 kbp range.* ***B)*** *long exposure with bands visible from 100 bp on. 1 kb Plus DNA Ladder (NEB) was used as gene ruler.*

4 colonies (colonies #2, #3, #6, #8) were sent to sequencing. The following primers were used: *IRES_mCherry fwd* & *MAIV_CPCR_rev1*. For 2 colonies (colony #3 and #6) a 100% match to the IRES and *mCherry* sequence was determined. The sequences of the other 2 colonies were not fully covered (low quality, insecurities about bases). For this reason, only the 2 colonies, whose sequences were fully covered, were chosen for a midiprep.

Interestingly, only the midiprep of 1 picked colony (colony #6) could be confirmed by restriction enzyme digestion with *StuI* (**Fig. 40 A**) and subsequent gel electrophoresis to provide the correct MAIM plasmid with the *mCherry* sequence downstream of the MLL-AF9 gene (**Fig. 40 B & C**).

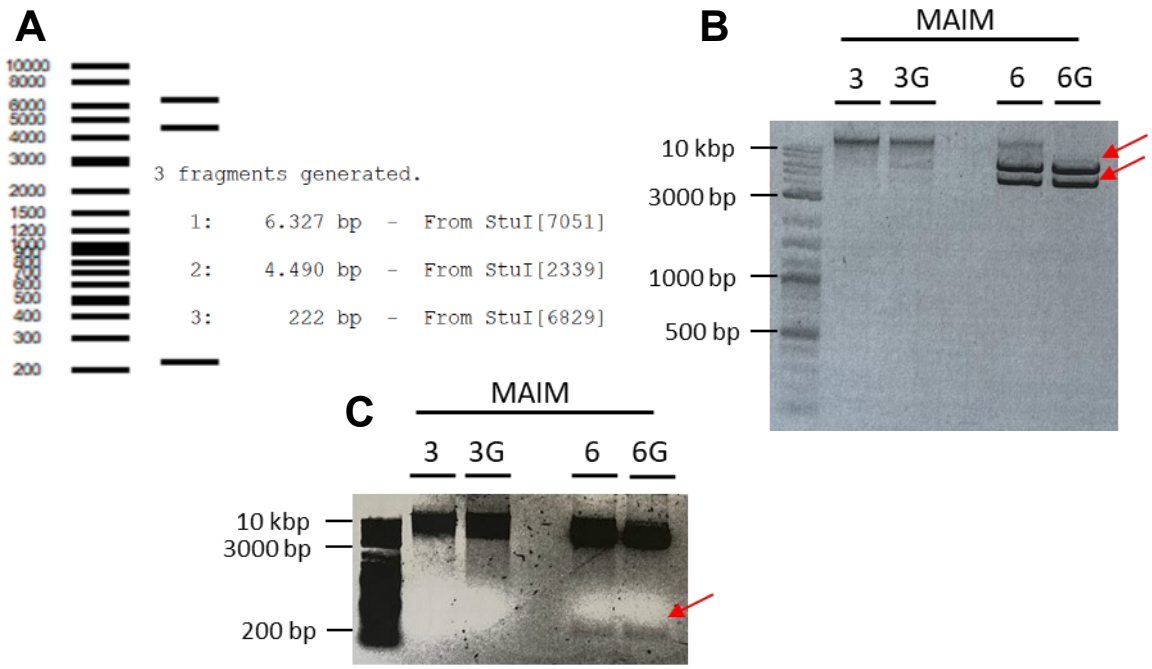


*Fig. 40:* ***Restriction analysis of MAIM plasmid of Midi-preps from clones 3 & 6 with StuI. A)*** *Expected fragments after StuI digestion of MAIM.* ***B)*** *Agarose DNA gel electrophoresis of digested Midi-preps after running the assay for 40 minutes.* ***C)*** *Same gel as in B after 20 minutes with a long exposure to make lower bands visible.*

### 3.4.2. Transfection of fetal liver cells

After successful cloning of the MAIM plasmid (**section 3.4.1.2**), we used the plasmid to transfect fetal liver cells of mice. The MAIM plasmid contains the MLL-AF9 oncogene with mCherry as reporter. Hematopoietic stem cells (HSC) make up a big part of fetal liver cells. Their transfection with the MLL-AF9 oncogene leads to development of HSCs with self-renewal capacity, reflecting features of AML [208].

In a first step, the transfection protocol was tested. Here, it was important to see whether the MAIM plasmid provides the sequence and that is is integrated successfully into the genome of the fetal liver cells. For this reason, fetal liver cells obtained from E13.5 fetuses which do either not possess the Cre recombinase gene or the HDAC1 CI transgene were transfected with the cloned MAIM plasmid (mCherry reporter) and as control with the MAIV plasmid (VENUS reporter). A homogenous population was achieved after 3 weeks with MAIM (**Fig. 41 A**). FLs transfected with MAIV show a similar development (**Fig. 41 B**).

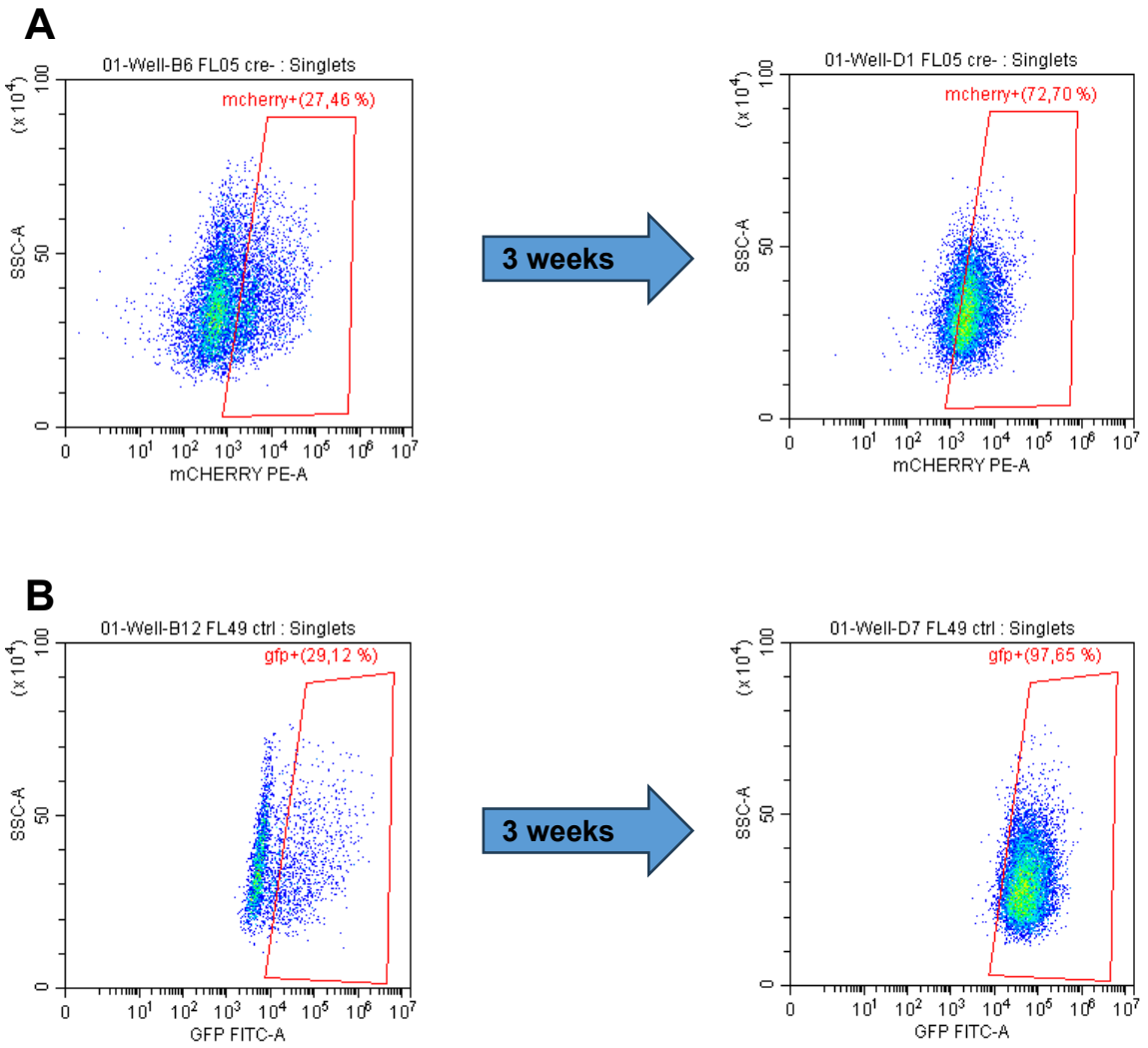


*Fig. 41:* ***Flow cytometry analysis of fetal liver cells transduced with MAIM plasmid or with MAIV plasmid, respectively.*** *FL05 and FL49 both don't express cre recombinase and can thus used as controls in future experiments. Analysis directly after transfection (week 1) and 2 weeks later (week 3) is shown* ***A)*** *FL05 was transfected with MAIM, which was cloned in this thesis. The PE channel (561 nm) is used for mCherry* ***B)*** *FL49 which was transfected with MAIV served as control whether the transfection protocol worked. The FITC channel (488 nm) is used for VENUS (GFP).*

After testing of the plasmid, the transfection was done with 3 sets of FLs from littermates from which one had the Cre recombinase and one didn't. All cells carry one copy of the catalytic inactive HDAC1 transgene. Livers were obtained from E13.5 fetuses and screened for the presence of *Hdac1* transgene and *Mx1-cre* (not shown here).

Transfection and subsequent development of population with the MLL-AF9 oncogene (mCherry positive) was monitored over the course of 5 weeks. The shift of the mCherry signal was confirmed for all samples from $10^3$ to $10^4$. The gating strategy for estimation of mCherry positive populations is depicted in **Fig. 42 A-C**. The shift is shown for FL20 and FL21 in **Fig. 42 D & E**.

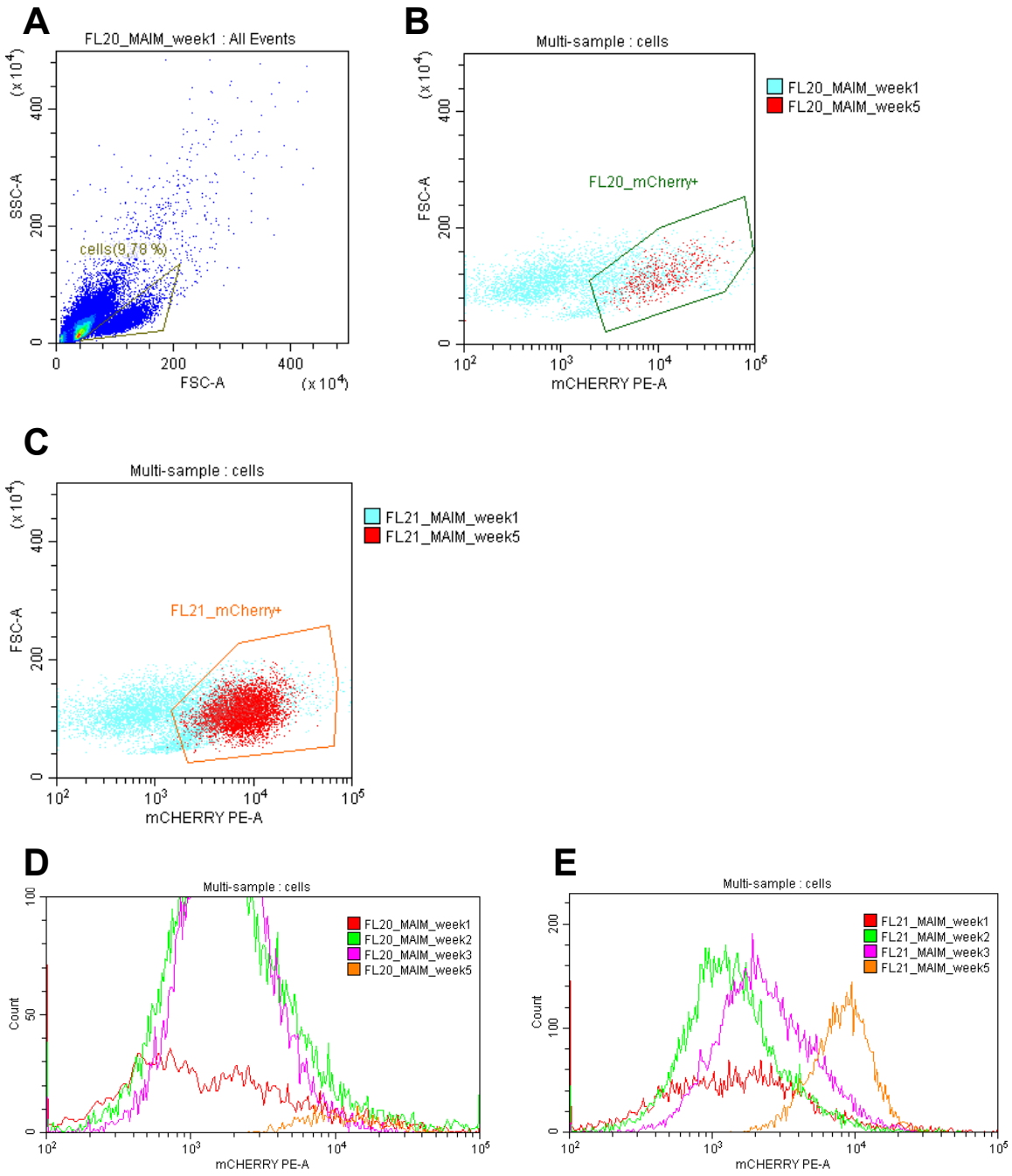


*Fig. 42:* ***Flow cytometry analysis of fetal liver cells transduced with MAIM plasmid in sample FL20 (Cre-) and FL21 (Cre+). A-C)*** *Gating strategy to determine mCherry+ cells (Expression of MLL-AF9 oncogene). The mCherry+ population is marked in the dot plot.* ***D-E)*** *Histogram overlay depicting the population shift over the weekly development of FL20 & FL21. The PE channel (561 nm) is used for mCherry.*

### 3.4.3. Induction of HDAC1 CI expression by IFN-β-inducible *Mx1-Cre*

Black 6 mice (C57BL/6) with the catalytic inactive *Hdac1* transgene were provided by my supervisor Lena Hess. *Hdac1 CI* was introduced into the safe harbor locus *Rosa26*. A STOP cassette upstream of the *Hdac1* transgene prevents its expression in absence of

the Cre recombinase. A GFP reporter downstream of *Hdac1* transgene allows confirmation of its expression.

IFN-β-inducible *Mx1-Cre* black 6 mice were a gift from Sophie Edtmayer from the Stoiber-Sakaguchi lab [174]. After mating of *Hdac1* and *Mx1-Cre* mice, fetal livers from mice at E13.5 were extracted and screened for *Hdac1* and *Mx1-cre* (not shown here).

Induction of *Mx1-Cre* with IFN-ß leads to removal of the *PolyA-stop* cassette and subsequent *Hdac1* expression.

The following fetal livers (FL) cells were subjected in tests of inducibility of *Mx1-Cre* and subsequent confirmation of HDAC1 CI expression *via* flow cytometry (**Table 7**).

| | ***Hdac1 CI*** | ***Mx1-Cre*** |
|---|---|---|
| **FL 5** | tg/+ | - |
| **FL 4** | tg/+ | + |
| **FL 18** | tg/+ | - |
| **FL 19** | tg/+ | + |
| **FL 20** | tg/+ | - |
| **FL 21** | tg/+ | + |

*Table 7:* ***Hdac1 CI Transgenes in fetal livers (FL) and presence of Mx1-Cre.***

After passaging the FLs 4 weeks after transfection with the *MLL-AF9* oncogene, the inducibility of the *Hdac1 CI* transgene in *Mx1-Cre*+ cells, by IFN-ß, was tested. In previous flow cytometry analysis, we realized that FL19, which is *Hdac1 CI TG/+ Mx1-Cre*+, showed an autoinduction of the *Hdac1 CI* transgene even without IFN-β. For this reason, the test was done mainly with the cell lines FL20 and FL21.

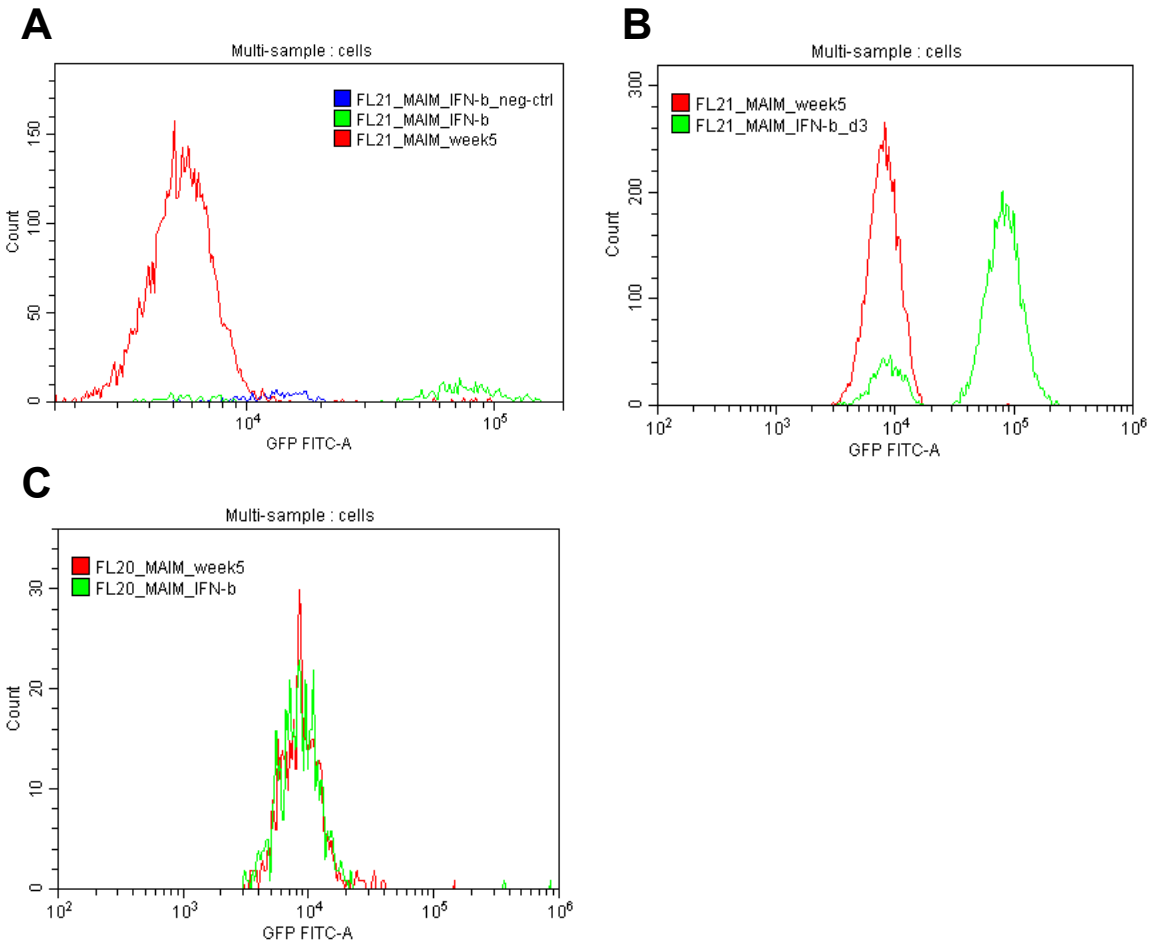


*Fig. 43:* ***Flow cytometry analysis of fetal liver cells that have been treated with IFN-ß to induce Hdac1 CI transgene expression.*** Fetal liver cells were incubated with 1000U IFN-β for 24 hours to activate expression of *Mx1-Cre. FL21 is Mx1-Cre+,* FL20 is *Mx1-C*re- and serves as negative ctrl ***A)*** *Analysis 24 h after treatment.* ***B)*** *Repeated analysis of treated cells and untreated 3 days post treatment. &* ***C)*** *Same analysis 24 h after treatment with Mx1-Cre- FLs as negative control. GFP was measured in the FITC channel.*

By flow cytometry analysis (**Fig. 43**) we determined that IFN-β led to a significant shift (10-fold) of GFP expression in the *Mx1-Cre+* FL21, while no GFP expression was detectable in the *Mx1-Cre* negative FL20. Not all cells were induced after the 24 h treatment with 1000U of IFN-β and the population was rather mixed. Moreover, the available number of cells for flow cytometry was limited. For this reason, the induced cells were measured again after 3 days, which showed a shift from $10^4$ to $10^5$ for the induced population, thus positive for expression of the *Hdac1* transgene. Overall, this data shows that the induction of the mutant HDAC1 construct in the *Rosa26* locus is possible in fetal liver cells which were retrovirally infected with the *MLL-AF9* oncogene with help of the MAIM plasmid.

### 3.4.4. Detection of HDAC1 protein expression levels and measurement of total cellular HDAC activity

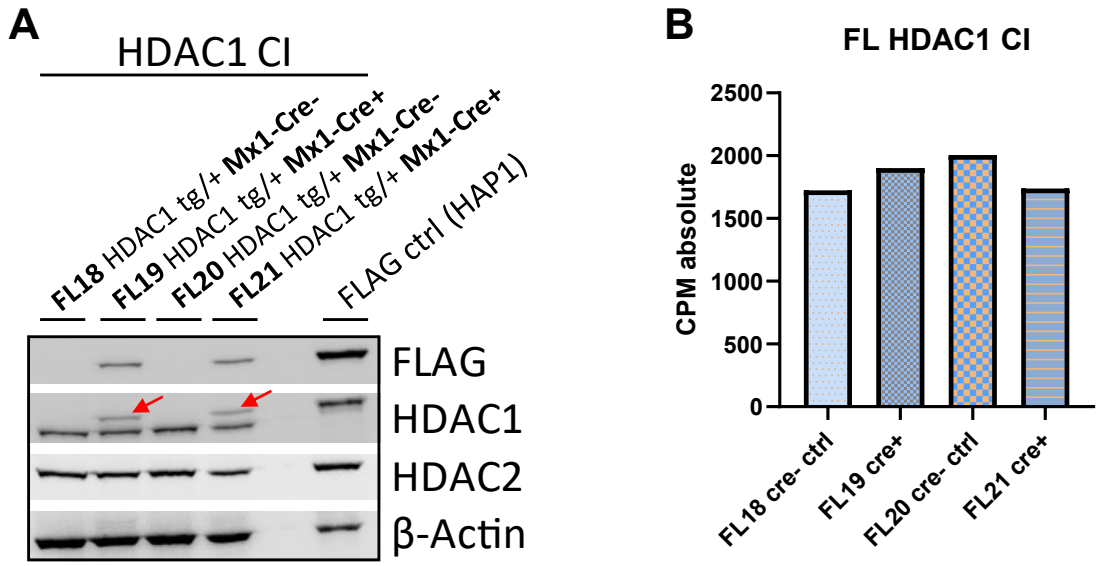


*Fig. 44:* ***WB analysis and Activity Assay of fetal livers infected with MLL-AF9 and expressing catalytic inactive HDAC1 from the safe harbor locus Rosa26****. A) 10µg of lysate was loaded on a 10% SDS-PAGE gel per sample. Detection was done with M2 FLAG, HDAC1and HDAC2. Loading of similar amounts was confirmed with β-Actin.Transgenic HDAC1 bands which are visible above of the endogenous HDAC1 bands are marked with arrows.* ***B)*** *Bar chart showing HDAC activity of total protein extracts. Fetal livers lysed in Hunt buffer were incubated 1 h for HDAC activity assay.* n=1

The expression of the *Hdac1 CI* transgene, following IFN-ß induction of *Mx1-Cre*, was also observed in WB analysis and the total histone deacetylation activity was measured with HDAC activity assay. Therefore, an aliquot of FL cells was harvested and lysed.

Expression of transgenic HDAC1 CI could be clearly seen in FL21 and FL19 (**Fig. 44 A**). The antibody used for HDAC1 detection (SAT208) can recognize both the transgenic and endogenic protein. The band of transgenic HDAC1 (larger in size with the attached FLAG-tag) is visible above of the band of endogenous HDAC1. The expression levels of endogenous HDAC1 and HDAC2 were not affected. Also, the activity of the samples does not differ significantly (**Fig. 44 B**).

### 3.4.5. Detection of HDAC2 levels and activity assay

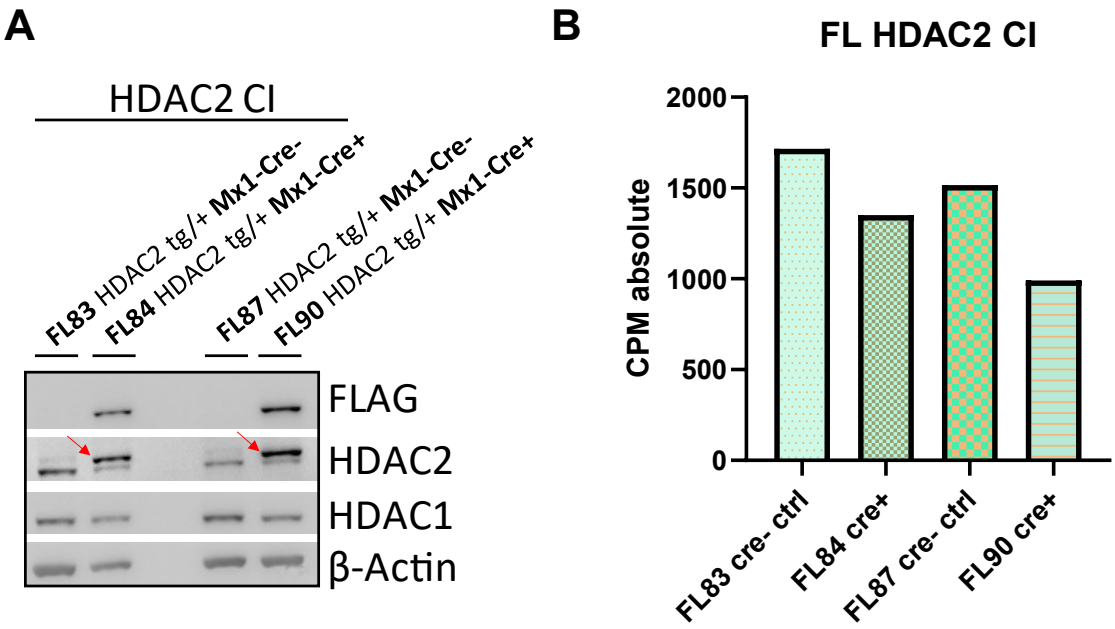


*Fig. 45:* ***WB analysis and Activity Assay of fetal livers infected with MLL-AF9 and expressing catalytic inactive HDAC2 from the safe harbor locus Rosa26****. A) 9 µg of lysate was loaded on a 10% SDS-PAGE gel per sample. Detection was done with M2 FLAG, HDAC1 and HDAC2. Loading of similar amounts was confirmed with β-Actin A5316. Transgenic HDAC2 bands which are visible above of the endogenous HDAC2 bands are marked with arrows.* ***B)*** *Bar chart showing HDAC activity of total protein extracts. Fetal livers lysed in Hunt buffer were incubated 90 min for HDAC activity assay.* n=1

FLs from mice whose *Hdac2 CI* transgene expression is inducible with IFN-ß, were also retrovirally transduced with the *MLL-AF9* oncogene by Lena Hess and *Mx1-Cre* induced with IFN-ß (PhD thesis Lena Hess, 2022). Similar to FLs expressing *Hdac1 CI* transgene, it was observed that cells spontaneously autoinduced *Hdac2 CI* transgene expression without IFN-ß treatment.

After confirmation of GFP expression by flow cytometry an aliquot of these cells was also taken to extract proteins, to determine expression of transgenic HDAC2 CI and to further estimate the amount of endogenous HDAC1 and HDAC2. The total histone deacetylation activity of the lysates was also measured by activity assay. Therefore, an aliquot of FL cells was harvested and lysed.

In contrast to the Western Blot analysis of HDAC1 (**section 3.4.4**) the transgenic HDAC2 has a much higher expression and seems to slightly lower the expression of endogenous HDAC2 (**Fig. 45 A**). HDAC1 expression looks to be same for all samples.

Concerning deacetylation activity (**Fig. 45 B**), a slight disruptive trend of HDAC2 CI in the total deacetylation activity is visible (FL83 + FL84 and FL87 + FL90) which was not observed in the analysis of the cells with HDAC1 CI expression (**section 3.4.4**).

# 4. Summary and Discussion

## 4.1. Novel model system in HAP1 cells for consistent study of class I HDACs

A systematic study of all class I HDACs in a single model system has not been done so far. Comparison of results from different studies can be challenging especially when models differ. Therefore, our lab established a consistent model in HAP1 cells which increases reliability and allows for a straightforward review and comparison of different class I HDAC conditions [167].

The primary goal was to explore the differences between knockout and catalytic inactivation of class I HDACs and compare them to HDAC inhibitor (HDACi) treatment. Complete deletion of HDAC1 or HDAC2 leads to the absence of the protein which is usually found in corepressor complexes such as CoREST, SIN3A and NURD as homo- or heterodimers. It was observed, that HDAC1 & HDAC2 can compensate each other in the absence of one of the HDACs in corepressor complexes [112], [160]. However, catalytically inactivated HDACs are present in the complex, therefore the loss of function cannot be compensated. For instance, heterozygous catalytic inactivation of HDAC2 causes a more severe phenotype, such as brain dysfunction leading to perinatal lethality, compared to complete ablation of HDAC2 in C57BL/6 mice [166]. This was therefore called dominant negative effect. The circumstance that inactive HDACs have this dominant negative effect in *in vivo* models led to the hypothesis that the effects of pharmacological HDAC inhibition could be rather studied in models with catalytically inactive (CI) HDACs in contrast to KO models used in other studies [166].

The HAP1 cells used for the class I HDAC models are derived from the near haploid leukemia cell line KBM7. Through CRISPR/Cas9 targeted deletion of the remaining diploid genes, the HAP1 cell line was created which is almost perfectly haploid [168]. Thus, further engineering, to create knockout or knock-in cell lines is relatively straightforward and was done in collaboration with the company Horizon genomics. For this process, CRISPR/Cas9 targeting technology was greatly beneficial [209].

HDAC knockout cell lines were generated by CRISPR/Cas9 targeting of respective sequences and introduction of an indel. Catalytically inactive HDACs were introduced into both wildtype HAP1 cell lines as well as into the corresponding HDAC knockout cell lines, as illustrated in **Fig. 6** [167].

Catalytically inactive class I HDACs which carry a point mutation in the catalytic center (HDAC1 H141A, HDAC2 H142A, HDAC3 H135A, HDAC8 H143A) were introduced each into HAP1 cells. Additionally, a FLAG-tag was inserted C-terminally of each HDAC transgene to allow for enrichment through immunoprecipitation (**Fig. 6B**). The ability of inactive and FLAG-tagged HDACs to be still incorporated into co-repressor complexes was checked and confirmed by Western blot analysis and activity assays [166], [167].

The measurement of HDAC activity by using [$^3$H]-acetate-labelled histones as substrate in these different cell lines is a crucial tool for characterization regarding deacetylation. The [$^3$H]-acetate is removed in the presence of active deacetylases and the radioactive signal is measured with a scintillation counter [210]. The usage of this method has the disadvantage that slightly radioactive material that emits low range β particles must be handled with caution [211] and the incubation time spans about 4-6 hours to reach the necessary sensitivity. Further, the separation of the generated acetyl group from the substrate is also time consuming [212]. Nevertheless, this established process was the method of choice, since it is still cost effective and specificity bias in class I HDACs was thought to be not all too significant due to the high similarity. Class I HDACs share a very high similarity in their catalytic domain and thus it would be expected that the activity can be measured with the [$^3$H]-acetate-labeled histone HDAC activity assay. [117].

In most experiments, 2 µl of [$^3$H]-acetate-labeled chicken erythrocyte histone substrate were used while in previous studies in the lab 4 µl of histone substrate were used. This explains the lower HDAC activity measurement values.

## 4.2. Measurement of endogenous HDACs in HAP1 cells

One of the tasks in this thesis was to optimize IP and activity measurements for class I HDACs.

Regarding the optimization process it must be said that the obtained activity levels for equal amounts of precipitated class I HDACs vary. HDAC1 and HDAC2 are on a similar level. After a first IP which led to measured results between 800 to 900 counts per minute (CPM) we tested a fresh aliquot of antibodies, which were previously produced in collaboration with the Ogris lab. This optimized the signal well over 1100 to 1300 CPM.

Under optimal conditions HDAC3 returns just 1/3 to half of the activity measured in HDAC1 & HDAC2, which impedes already a distinct analysis of HDAC3 activity data. In case of endogenous HDAC3 the relative activity signal from wildtype cells compared to the signal

from HDAC3 KO cells could only be increased by a combination of using higher amounts of protein for immunoprecipitation (IP), more primary antibody and the change of lysis buffer composition (switch to Karin buffer). IP3(1,4,5) – Inositol 1,4,5-trisphosphate – which seems to have a stabilizing effect on HDAC complexes according to studies, was also tested [137], [180]. Potentially, the interaction between HDAC3 and NCOR1/2 could be stabilized by providing IP3(1,4,5). But no change of activity measurement could be observed in this thesis after addition of IP3(1,4,5) into the buffer for lysis and IP. This could be because the IP3 was already present in the lysate in a concentration high enough were no further increase of HDAC3 binding to NCOR could be achieved. Stabilizing effects have been observed in literature also with less salt in the lysis buffer [180]. There was also no influence of the activity found in this thesis when salt content was reduced to half the amount (50 mM instead of 100 mM). The opposite was the case, since the switch to Karin buffer led to a success in better distinction of wildtype cells and HDAC3 KO cells. Its salt content is slightly higher with 138 mM in comparison to the 100 mM in the Hunt buffer. The slightly higher salt content provides a better solubility of proteins. EDTA as a chelating agent is 10x higher in Karin buffer which should support enzyme activity. The same is supposed to be done by glycerol. Last but not least, the double amount of NP-40 makes the Karin buffer harsher than the Hunt buffer. All in all, this could lead to a more efficient extraction of proteins and allows the HDAC3 3G6 antibody to better discriminate and provide a cleaner pull down which is analysed in HDAC activity assay.

Another important, yet surprising observation was that HDAC3 expression is returning very early in HDAC3 KO cells in passages as low as p14. This renders some experiments misleading since this circumstance was not known in the early stage of the experiment for this thesis. The passage numbers are mentioned in **section 3.1.2** about endogenous HDAC3 optimization for comparison. In the beginning of the section, a Western blot visualizes the progression of the HDAC3 return from passage to passage.It should be pointed out that the company Horizon Genomics (former Haplogen) created a number of clones from which only one could be obtained with loss of HDAC3 protein. In fact, most clones analysed by indel sequencing showed in frame indels suggesting a vital function of HDAC3 in HAP1 cells. Even though it is recommended that in future projects more clones should be generated and kept as a backup for such cases.

The signal strength from the HDAC activity assay was high enough for HDAC1, HDAC2 & HDAC3, but it was not possible to measure activities above background level for HDAC8. This unexpected result could come mainly from structural deviations which are present only in HDAC8, but not in the other class I HDACs. This might allow for a higher specificity even without interaction partners, unlike in HDAC1, HDAC2 & HDAC3 [213]. Furthermore

this specificity allows HDAC8 to targetnon-histone targets such as p53 rather than histones [214]. This was also shown by Deardorff et al. where deacetylation of SMC3 by HDAC8 is an important factor for dissociation of the cohesin complex at the end of mitosis for renewal (so it can be localized chromatin in the next cell cycle). The loss of HDAC8 was in this case linked to Cornelia de Lange syndrome [215]. Data from the acetylome retrieved by our lab lately has also shown the preference of HDAC8 to recognize mostly other targets than histones [167]. The need for a specific substrate for HDAC8 was perceived and we tried an HDAC8 kit from Sigma that is based on a peptide substrate which is [R-H-K(Ac)-K(Ac)-] but the activity levels of HDAC8 were also not sufficient with this kit. Even worse, the activities of HDAC1, HDAC2 & HDAC3 were obtained on a high level with the HDAC8 kit. Tests with the HDAC3 kit from Sigma which harbors the peptide sequence [R-H-K(Ac)-] as substrate showed the same results. Due to a lack of means to measure HDAC8 activity with a consistent method as it was done with the other class I HDACs, HDAC8 was excluded from future analysis in this thesis. The development of activity assays with more specific substrates for HDAC isoforms would be very helpful and broaden the way to better understanding changes in the cell upon deacetylation.

## 4.3. Comparison of HDAC WT and HDAC CI transgenes in HAP1 cells

The established system of HDAC transgenes in HAP1 cells in our lab allows for systematic comparison of class I HDACs. Each cell line (**Table 5**) expresses another HDAC1-8 isoform either in active (WT) or catalytically inactive (CI) form. The comparison of cells with catalytically active versus cells with catalytically inactive HDACs let us directly observe consequences regarding histone deacetylase activity of HDACs as well as of corepressor complexes. The protein complexes could easily be pulled down with one antibody against the FLAG sequence attached to each transgene and ensure similar precipitation efficacy. Additionally, catalytically inactive HDAC1-8 was also introduced into wildtype HAP1 cells which enable observation *in vitro* of the dominant negative effect in a wildtype background setting.

To start comparisons, the amount had to be determined of how much of each of the different whole cell lysates (WCL) from HAP1 cells has to be applied in assays and FLAG immunoprecipitation (IP) to obtain a comparable amount of enzyme to be analysed. From KO HDAC3 WT WCL the amount to be applied was 10-fold higher than for other WCL such as KO HDAC1 WT. In most cases, 1000 µg of WCL were used for the IP of KO

HDAC3 WT. This has displayed as an obstacle to deal with, since pull downs from HDAC3 IPs came regularly with a high background where even ß-Actin or VINCULIN could be detected on the blot. Independent of this issue, a HAP1 WT control IP with the same amount of applied WCL as for KO HDAC3 WT was included to subtract the high background and eliminate the contribution of other deacetylases, nonetheless it is not ideal.

It has been shown that co-repressor enzymes such as SIN3A, COREST and NURD are co-precipitated with transgenic HDAC1 & HDAC2, and during this thesis it was tried to show that NCOR1/2 co-precipitates with transgenic HDAC3. NCOR1/2 could not be shown successfully on the Western Blot but in retrospective maybe the usage of Karin buffer could be a way to make NCOR1 or NCOR2 visible, since traces of the band appeared to be present on the blot. Another possibility to prove binding of transgenic HDAC3 to NCOR would be mass spectrometry of enriched NCOR1 or NCOR2.

Also, reversed co-IPs were conducted and were successful for transgenic HDAC1 & HDAC2 which co-precipitated in SIN3A, COREST and MTA2 (for NURD) IPs. Again, this has proven difficult with NCOR1/2 for HDAC3. After a few tries and under optimized conditions with Karin buffer and lysis through sonication, a trace or trend towards a visible band on Western blot was achieved (see **Fig. 24**). The application of a light chain antibody as secondary antibody for detection on Western Blot was another helpful tool which allowed for usage of detection antibodies that were produced in the same species as the antibody that was used for the NCOR IP (Rabbit in this case). Further optimizations are necessary to mediate the possibility of proofing co-precipitation of transgenic HDAC3 with NCOR1 or NCOR2.

## 4.4. Transcriptome analysis of cells expressing transgenic class I HDACs and cells treated with HDAC inhibitor

The biochemical characterization of generated HAP1 cell lines that express transgenic class I HDACs in catalytically active and inactive form was already informative. To receive a deeper insight into the regulatory mechnisms, the transcriptome was analysed. Our lab generated gene expression data with HAP1 cell lines which carry HDAC transgenes or are HDAC KOs. Additionally, HAP1 WT cells were sequenced after HDACi treatment (Verena Moos, in collaboration with Michael Schuster, CeMM Vienna). Briefly, HDAC KO, KO HDAC WT, KO HDAC CI cells, WT HDAC CI, and HAP1 control cells were cultivated in equal conditions and harvested for RNA-seq. Simoultanously, WT cells were subject to

treatment with the HDAC inhibitors MS-275 (class I HDACi, Entinostat) and JQ12 (HDAC1/2 inhibitor, [186]) with either 1 µM or 3 µM for 24 hours [167]. A part of the data was used in this Master thesis and analyzed to explore the similarities and differences between the generated cell lines (with focus on HDAC KO & WT HDAC CI) and WT cells which were treated with HDAC inhibitors.

For this purpose a series of R scripts were written. The code was made available on Github in the following repository:

**https://github.com/laubera14/HDAC_HAP_RNAseq/tree/main**

The analysis has focused on upregulated genes since a loss of deacetylation capability would mainly result in higher gene activity as direct effect. The analysis of transcription factors which are affected and their indirect effects on gene regulation and non-histone effects would have gone beyond the scope of this thesis and were therefore not analysed.

The data was available as gene counts for each sample. This was used as input for DEseq2, which normalizes the gene counts and allow comparison of differential expression of genes. The reference for changes of gene expression was always HAP1 WT. A similarity analysis (see **Fig. 25**) of each data set was performed, and it already underlined the strong similarity of cell lines with catalytically inactive (CI) HDAC1, HDAC2 and HDAC8 to HDAC inhibitor treatment (MS-275 and JQ12). Catalytically inactive HDAC3 obtained less similarity but therefore there was a strong similarity of HDAC3 KO cells to MS-275 and JQ12 treatment. Also, HDAC1 CI and HDAC2 CI cell lines resembled each other in their data sets which is also true for the knockout forms of HDAC1 and HDAC2. That makes perfectly sense, since they participate in the same HDAC complexes like NuRD, CoREST or SIN3A and knocking out the gene for HDAC1/2 or introducing a mutant transgene affects functions which overlap to a high degree. It was a big surprise though, that the HDAC8 KO cell line has a strong similarity to the HDAC1 KO. It was proposed recently, that both HDAC1 and HDAC8 can interact with p53 as a highly important regulator in the cell and as tumor suppressor one of the most important key players in cancers [216]. However, to date the interaction between these two HDACs has not been proven in our lab and could be subject to further investigation. Last but not least, HDAC8 CI has also a resemblance to HDAC1 CI and HDAC2 CI which would be also interesting to investigate.

The similarity analysis gave an important overview and confirmed the assumption that HDACi treatment can be mimicked by introduction of catalytically inactive HDACs rather than by HDAC knockout. Further, the comparison of differentially expressed genes from WT HDAC CI cells to HDAC KO cells showed clear differences. In HDAC1 82% of the

genes that are upregulated due to HDAC1 CI transgene introduction are unchanged or even downregulated in HDAC1 KO. For HDAC2 this number is 60%. This means, that there is a distinct effect on the transcriptome upon HDAC1 CI or HDAC2 CI introduction and it affects different genes, gene sets and pathways than the knockout of HDAC1 or HDAC2 does. Further, this could support the observation of the dominant negative effect which has been described in our lab previously in-vivo and is explained by the disruption of Co-repressor complexes by one mutant HDAC rather than the knockout of one HDAC since HDAC1 and HDAC2 can compensate each other if one isoform is missing in the cell (discussed in **section 4.1**). Finally, the fact that a big partition of genes which are caused to be upregulated in WT HDAC CI cells are not upregulated in KO cells points towards the importance of catalytic function of HDAC1 & HDAC2 in Co-repressor complexes and that the KO is surely distinct from catalytical inactive HDAC introduction. HDAC3 shows the opposite picture where 61% of the genes respond in the same way no matter whether HDAC3 is knocked out or is replaced by the catalytically inactive transgene. Finally, HDAC8 has a similarly high number of genes (81%) which are not upregulated in HDAC8 KO while they are upregulated in WT HDAC8 CI as in HDAC1 CI. The high portion of genes that are upregulated in WT HDAC1 CI and WT HDAC8 CI but not in HDAC1 KO and HDAC8 KO could give a hint to an interesting overlap of functions or relationship between HDAC1 and HDAC8 which could be subject to further investigation.

The distinct effect of the introduction of a catalytical inactive HDAC1, 2 or 8 isoform versus the knockout of the same HDAC1, 2 or 8 isoform has been visualized with help of a clustered heatmap of the top 90 upregulated genes upon respective transgene introduction in **Fig. 26**. The heatmap clearly reflect the numbers of **Table 6** which show that HDAC1 and HDAC8 have the highest number of genes (80%) that are upregulated due to introduction of a catalytically inactive isoform but are not upregulated in the knockout cell lines of HDAC1 and HDAC8. HDAC2, which has only 60% of genes upregulated exclusively in the WT HDAC2 CI, shares 31 genes of the top 90 upregulated genes with WT HDAC1 CI. WT HDAC8 CI shares still 12 genes of the top 90 upregulated genes with WT HDAC1 CI. This is the second highest number of genes from the top 90 upregulated genes which overlap between two WT HDAC CI lines and underlines again certain similarities of HDAC1, HDAC2 and HDAC8 in terms of the catalytic function. While there are some similarities with gene upregulation between WT HDAC1 CI, WT HDAC2 CI and WT HDAC8 CI, an introduction of inactive HDAC3 shows no relevant similarities to them.

The investigation of common upregulated genes of WT HDAC1 CI and WT HDAC2 CI leaves mostly gene ontologies (GOs) for biological processes which are neurological or are part of the neuronal system (**Fig. 27**). The importance of HDAC1 and HDAC2 for the

neuronal system, especially in ontogenesis has been shown before in our lab [161], [166], [167].

GO analysis of WT HDAC3 CI clustered many genes in significant biological processes that are known to suppress cell growth and are inhibitory for cancer progression. The clusters from HDAC3 KO analysis harbor genes which are proto-oncogenes but also genes that inhibit cancer growth (**Fig. 28**). First, the importance of distinguishing between knockout and introduction of catalytically inactive HDAC is illustrated. Second, the data suggests that a catalytic inhibition of HDAC3 would be the better therapy than a HDAC3 knockout. Interestingly, the data from cell viability analysis, performed by the lab of Susann Chiocca, shows that contrariwise, growth of HDAC3 KO cells is slowed down significantly, while growth of WT HDAC3 CI cells is nearly unaffected, compared to HAP1 wildtype cells. This discrepancy could be explained by the fact that HDAC3 KO cells are normally not viable and the ability to grow is an adapted feature of our HAP1 cells, which are dependent on HDAC3 to be viable [167]. Further, HDAC3 has been shown to be essential for DNA repair and a deletion therefore leads to accumulation of DNA damage and chromatin structure loss which consequently can contribute to cancer development as shown for instance in hepatocytes [217].

The analysis of upregulated genes due to HDAC inhibitor treatment, MS-275, compared to WT HDAC CI and HDAC KO cells, showed that the WT HDAC2 CI cells have the highest similarity to MS-275 treatment (**Fig. 29**). In general, it was observed that from the genes which are upregulated in MS-275 treated cells the number of genes which are also upregulated in the cell lines for HDAC1, HDAC2 and HDAC8 is higher in the wildtype cells with the catalytically inactive HDAC than in plain knockouts of these cell lines. As already mentioned in this section, HDAC3 states an exception, and its knockout has a higher number of genes upregulated which it shares with the MS-275 treatment than the WT HDAC3 CI cells. It can be discussed whether this effect could have its seed in a lower expressed amount of catalytically inactive HDAC3 which would then not be sufficient to displace endogenous HDAC3 in the co-repressor complex. Nevertheless, it's the second highest number of common upregulated genes with MS-275 in this analysis. The outstanding role of HDAC3 might be due to its (almost) sole importance for the NCOR1 and NCOR2 co-repressor complexes.

Taken together, the role of HDACs in cancer needs to be still elucidated and the mechanisms of how exactly HDACs influence development of the neuronal system, synaptic transmission and memory have to be still clarified more detailed in the future.

Model systems as developed in our lab with catalytically inactive HDAC isomers are beneficial because of their greater resemblance to HDAC inhibitor treatment.

There was also ChIP-seq data available which was generated by Verena Moos in collaboration with Michael Schuster from CEMM. One chosen target was H3K27ac which is a marker for active transcription [218]. At the time of writing this thesis, the data for WT HDAC CI cells from ChIP-seq was not available, thus only the data from HDAC KO cells was taken. The data sets of up- and downregulated genes in these knockout cells were compared (**Fig. 30**). A significant overlap could be shown for all HDAC KO isomers. As an example, it was observed, that in HDAC1 KO cell the genes which carry an upregulated H3K27ac mark (compared to HAP1 wildtype control) are indeed upregulated according to RNA-seq data. An overlap was also shown between different HDAC knockouts. For instance, there is a strong overlap of genes from HDAC 8 KO cells which have the H3K27ac mark downregulated and genes from HDAC1 KO cells which are downregulated. Interestingly, the ChIP-seq data from cells treated with MS-275 do not share an overlap with the same cell in the RNA-seq data. Also, there is only little overlap between MS-275 treated cells and different HDAC KO cells. The reason for that is not fully understood, but with the knowledge that HDACi treatment mimics rather catalytically inactive HDAC introduction and not KO, this could be explained in general. Further, up- or downregulation of genes in MS-275 treated cells could be caused by several indirect effects, independently of gene/chromatin acetylation and for this reason is probably not reflected in ChiP-seq data.

## 4.5. Fetal liver model for study of catalytic inactive HDACs in AML

To further investigate the effects of mutated HDACs, we wanted to establish a cellular model system for acute myeloid leukemia which allows observations also *in vivo* in mice. Since fetal liver cells can be transfected with an acute myeloid leukemia oncogene (MLL-AF9) it would allow a pretesting of the cells *ex vivo*, and potential interesting effects can then be tested in follow-up experiments by injecting oncogenic fetal livers cells back into mice.

The plasmid MAIV (MLL-AF9-IRES-Venus) with the oncogene *MLL-AF9* was a kind gift of the Zuber lab [153]. Since the plasmid carries the Venus fluorochrome which is detected in the same channel as the EGFP fluorochrome downstream of the *Hdac* transgene, the

*Venus* sequence had to be replaced with another fluorochrome. We decided to substitute it with mCherry since it would not shine into the GFP channel [205].

The first attempt of cloning failed at the ligation stage of the linearized MAIV vector with the cut fragment which contained the *mCherry* fluorophore gene sequence. It was not possible to obtain bacteria colonies which contain the ligated plasmid.

In a second attempt a “helper plasmid”, the linearized pCR™2.1-TOPO® vector from Invitrogen was used and the *mCherry* sequence was ligated into the pCR™2.1-TOPO® vector. A digestion of this vector and MAIV with *EcoRI* and *XhoI* brought the desired result. Colonies carrying the newly generated MAIM vector were obtained and the plasmid stored after purifying *via* Midi-prep until further usage for transduction. The picked clones were a match in the restriction enzyme analysis (with *StuI*, **Fig. 40**) and a 100% match in sequencing analysis compared to the predicted sequence (**Fig. 35**). The sequencing was done to eliminate last doubts about the presence and right insertion of the sequence, since the reason for the failure of the first cloning attempt was unknown and could be also had happened caused by inaccuracies of the provided plasmid sequence initially.

In the beginning, the flow cytometry analysis of transduced fetal livers cells (mostly hematopoietic stem cells, HSC) was quite promising. As expected, a heterogenous population for the *MLL-AF9* oncogene was observed [174]. About a quarter of the cells were carrying the oncogene according to mCherry signals. These were the cells which would be able to replicate and maintain the primary cell culture. In general, there was a homogenous population in the FLOW analysis with cells carrying the *MLL-AF9* oncogene after 5 weeks, while the shift of the signal was mostly already visible after 3 weeks.

While the FLOW analysis of the GFP reporter showed, that the induction with IFN-ß works and hence the *Hdac1* transgene expression is induced, the problem with many of the immortalized fetal liver cells was the autoinduction of the *Mx1-Cre* promoter (see **3.4.3 and** Hess, 2022**)**. The most obvious explanation for triggering the promoter would be the spontaneous production of IFN-ß of the cells. Attempts of my supervisor, Lena Hess, of re-cloning the plasmid and repeated transduction of fetal liver cells led to the same result. So, contamination could be excluded. Another source which was thought of is the viral transduction process [170]. The murine stem cell virus, MSCV, which is produced by Platinum-E cells, was used for transduction of the fetal liver cells so they produce the *MLL-AF9* oncogene. MSCV possesses two single stranded RNAs (ssRNA) [219]. This ssRNA can be detected by toll-like receptors (TLRs) such as TLR7 [220]. Interestingly, TLR7 is widely expressed on HSCs and in Acute Myeloid Leukemia (AML) cells [221]. In this case the remaining virus in cell culture after the transduction process could have had activated

IFN-ß *via* one of its major pathways, TLR7 [220]. Spontaneous induction of the *Mx1-Cre* system in HSCs has been observed already *in vivo* if mice were subject to undesired inflammatory processes [222]. The use of the *Mx1-Cre* promoter system displays a disadvantage in HSCs. Ideally, it should be exchanged with another system for conditional transgene expression. To date an alternative is not existing and would have to be yet developed.

In fetal livers with induced transgene expression of HDAC1 CI or HDAC2 CI the expression levels of HDAC1 and HDAC2 (transgene and wildtype) were estimated on western blot and a quantification of the total histone deacetylation activity was made. Regarding expression levels, the introduction of HDAC2 CI had obviously a higher effect than of the HDAC1 CI. In HDAC2 CI fetal liver cells there is a trend towards lower deacetylation activity. This could not be observed in HDAC1 CI fetal liver cells. That makes sense in light of the previous results which showed, that HDAC2 CI has the highest disruptive effect.

# 5. Supplementary Material

## 5.1. Immunoprecipitation of class I WT HDAC and HDAC KO cells

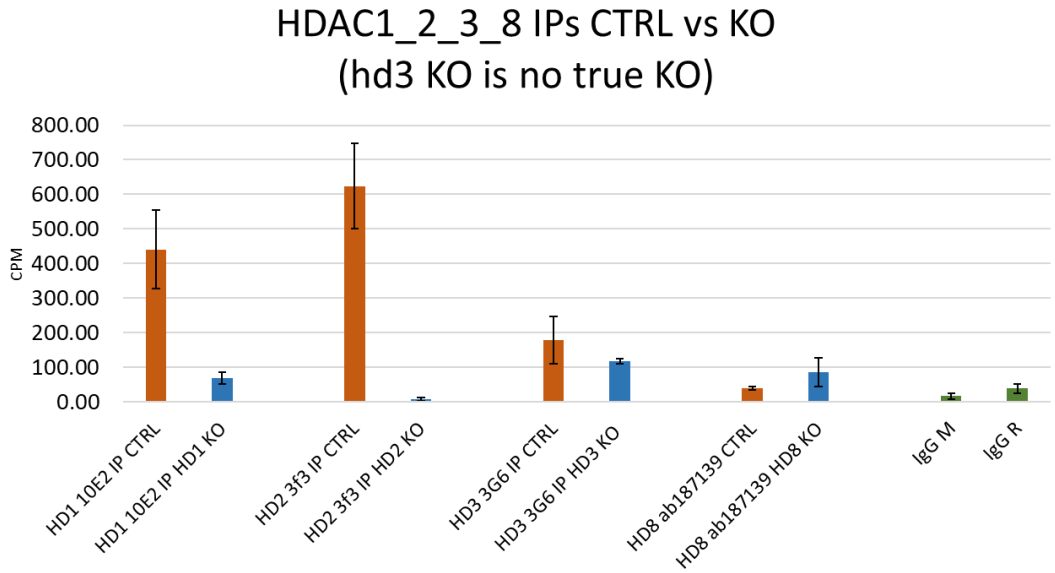


***Preliminary experiment with my supvervisor, Lena Hess for activity measurement of precipitated endogenous HDACs**. Endogenous HDAC1, HDAC2, HDAC3 and HDAC8 enzymes were precipitated from wildtype HAP1 cells. KO cell lines were included in the experiment as background controls. As additional negative control sample, mouse and rabbit IgG antibody were used for IP, together with wildtype HAP1 cellular extract. 700 µg of each whole cell lysate were used for each IP. Bar charts showing absolute deacetylase activity of precipitated HDACs towards histones in CPM (counts per minute).*

## 5.2. Gene set overlap matrix with p-values

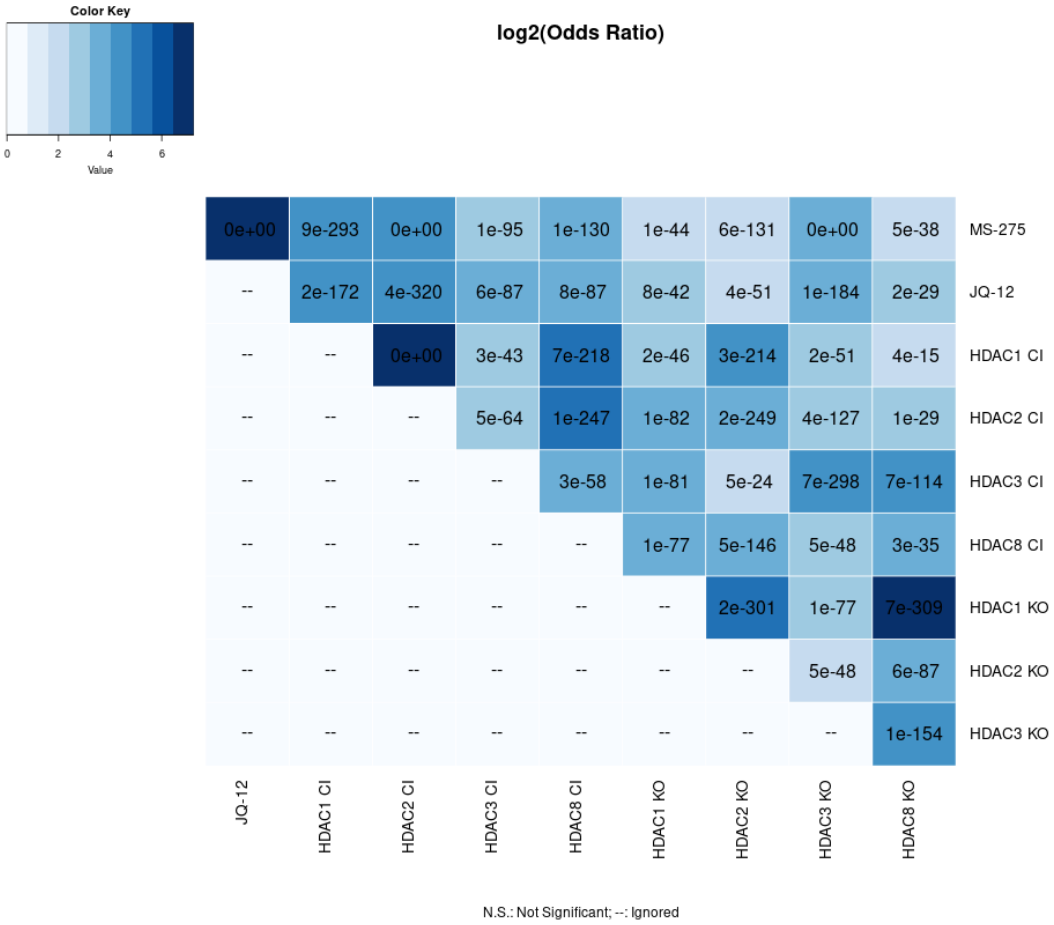


***Similarity analysis of upregulated genes upon introduction of mutant class I HDACs (CI = catalytically inactive) into WT cells, compared to HDAC KO cells and WT cells treated with MS-275/JQ12.*** *HDAC inhibitor treatments were done with each 1 μM concentration. Colour key values are binary logarithm of the odds ratio derived from fisher's exact test. This is the same figure as Fig. 25, but with p-values in each square which indicate the significance of the odds ratio between two gene sets.*

# 6. References


[1] C. H. Waddington, “The Epigenotype,” *Int. J. Epidemiol.*, vol. 41, no. 1, pp. 10–13, Feb. 2012.

[2] R. E. Franklin and R. G. Gosling, “The structure of sodium thymonucleate fibres. I. The influence of water content,” *Acta Crystallogr.*, vol. 6, no. 8, pp. 673–677, Sep. 1953.

[3] J. D. Watson and F. H. C. Crick, “Molecular Structure of Nucleic Acids: A Structure for Deoxyribose Nucleic Acid,” *Nat. 1953 1714356*, vol. 171, no. 4356, pp. 737–738, Apr. 1953.

[4] C. H. Waddington, “CANALIZATION OF DEVELOPMENT AND THE INHERITANCE OF ACQUIRED CHARACTERS,” *Nat. 1942 1503811*, vol. 150, no. 3811, pp. 563–565, 1942.

[5] C. H. Waddington, *The strategy of the genes: A discussion of some aspects of theoretical biology*. London: George Allen & Unwin, Ltd., 1957.

[6] C. Li and J. Wang, “Quantifying Waddington landscapes and paths of non-adiabatic cell fate decisions for differentiation, reprogramming and transdifferentiation,” *J. R. Soc. Interface*, vol. 10, no. 89, Dec. 2013.

[7] L. Xu, K. Zhang, and J. Wang, “Exploring the Mechanisms of Differentiation, Dedifferentiation, Reprogramming and Transdifferentiation,” *PLoS One*, vol. 9, no. 8, p. e105216, Aug. 2014.

[8] S. L. Berger, T. Kouzarides, R. Shiekhattar, and A. Shilatifard, “An operational definition of epigenetics,” *Genes Dev.*, vol. 23, no. 7, pp. 781–783, Apr. 2009.

[9] W. Flemming, *Zellsubstanz, Kern und Zelltheilung /*. 1882.

[10] T. Boveri, “Ergebnisse über die Konstitution der chromatischen Substanz des Zellkerns.,” *Verlag von Gustav Fischer Jena*, 1904.

[11] A. T. Sumner, H. J. Evans, and R. A. Buckland, “New Technique for Distinguishing between Human Chromosomes,” *Nat. New Biol. 1971 23227*, vol. 232, no. 27, pp. 31–32, Jul. 1971.

[12] S. Ohno, “Sex chromosomes and sex-linked genes. (Monographs on endocrinology, Vol. 1.).,” *Sex Chromosom. sex-linked genes. (Monographs Endocrinol. Vol. 1.).*, 1967.

[13] M. F. Lyon, “Gene action in the X-chromosome of the mouse (mus musculus L.),” *Nature*, vol. 190, no. 4773, pp. 372–373, 1961.

[14] A. L. Olins and D. E. Olins, “Spheroid Chromatin Units (v Bodies),” *Science (80-. ).*, vol. 183, no. 4122, pp. 330–332, Jan. 1974.

[15] P. Oudet, M. Gross-Bellard, and P. Chambon, “Electron microscopic and biochemical evidence that chromatin structure is a repeating unit,” *Cell*, vol. 4, no. 4, pp. 281–300, Apr. 1975.

[16] D. R. Hewish and L. A. Burgoyne, “Chromatin sub-structure. The digestion of chromatin DNA at regularly spaced sites by a nuclear deoxyribonuclease,” *Biochem. Biophys. Res. Commun.*, vol. 52, no. 2, pp. 504–510, May 1973.

[17] R. D. Kornberg and J. O. Thomas, “Chromatin structure: Oligomers of the histones,” *Science (80-. ).*, vol. 184, no. 4139, pp. 865–868, May 1974.

[18] R. J. DeLange, J. A. Hooper, and E. L. Smith, “Histone III,” *J. Biol. Chem.*, vol. 248, no. 9, pp. 3261–3274, May 1973.

[19] L. Patthy, E. L. Smith, and J. Johnson, “Histone III: V. THE AMINO ACID SEQUENCE OF PEA EMBRYO HISTONE III,” *J. Biol. Chem.*, vol. 248, no. 19, pp. 6834–6840, Oct. 1973.

[20] Y. V. Ilyin, A. Y. Varshavsky, U. N. Mickelsaar, and G. P. Georgiev, “Studies on Deoxyribonucleoprotein Structure,” *Eur. J. Biochem.*, vol. 22, no. 2, pp. 235–245, Sep. 1971.

[21] P. Oudet, J. E. Germond, M. Sures, D. Gallwitz, M. Bellard, and P. Chambon, “Nucleosome Structure I: All Four Histones, H2A, H2B, H3, and H4, Are Required to Form a Nucleosome, but an H3–H4 Subnucleosomal Particle Is Formed with H3–H4 Alone,” *Cold Spring Harb. Symp. Quant. Biol.*, vol. 42, no. 1, pp. 287–300, Jan. 1978.

[22] J. C. Hansen and A. P. Wolffe, “Influence of Chromatin Folding on Transcription Initiation and Elongation by RNA Polymerase III,” *Biochemistry*, vol. 31, no. 34, pp. 7977–7988, 1992.

[23] M. Shogren-Knaak, H. Ishii, J. M. Sun, M. J. Pazin, J. R. Davie, and C. L. Peterson, “Histone H4-K16 acetylation controls chromatin structure and protein interactions,” *Science (80-. ).*, vol. 311, no. 5762, pp. 844–847, Feb. 2006.

[24] B. R. Shaw, T. M. Herman, R. T. Kovacic, G. S. Beaudreau, and K. E. Van Holde,

"Analysis of subunit organization in chicken erythrocyte chromatin.," *Proc. Natl. Acad. Sci.*, vol. 73, no. 2, pp. 505–509, Feb. 1976.

[25] K. Luger, A. W. Mäder, R. K. Richmond, D. F. Sargent, and T. J. Richmond, "Crystal structure of the nucleosome core particle at 2.8 Å resolution," *Nat. 1997 3896648*, vol. 389, no. 6648, pp. 251–260, 1997.

[26] C. A. Davey, D. F. Sargent, K. Luger, A. W. Maeder, and T. J. Richmond, "Solvent Mediated Interactions in the Structure of the Nucleosome Core Particle at 1.9 Å Resolution," *J. Mol. Biol.*, vol. 319, no. 5, pp. 1097–1113, Jun. 2002.

[27] G. Arents and E. N. Moudrianakis, "Topography of the histone octamer surface: repeating structural motifs utilized in the docking of nucleosomal DNA.," *Proc. Natl. Acad. Sci.*, vol. 90, no. 22, pp. 10489–10493, Nov. 1993.

[28] D. L. Bates and J. O. Thomas, "Histories H1 and H5: one or two molecules per nucleosome?," *Nucleic Acids Res.*, vol. 9, no. 22, pp. 5883–5894, Nov. 1981.

[29] F. Thoma, T. Koller, and A. Klug, "Involvement of histone H1 in the organization of the nucleosome and of the salt-dependent superstructures of chromatin," *J. Cell Biol.*, vol. 83, no. 2 I, pp. 403–427, 1979.

[30] V. I. Risca, S. K. Denny, A. F. Straight, and W. J. Greenleaf, "Variable chromatin structure revealed by in situ spatially correlated DNA cleavage mapping," *Nature*, vol. 541, no. 7636, pp. 237–241, 2017.

[31] W. Ma *et al.*, "Mixed secondary chromatin structure revealed by modeling radiation-induced DNA fragment length distribution," *Sci. China Life Sci.*, vol. 63, no. 6, pp. 825–834, 2020.

[32] F. Song *et al.*, "Cryo-EM study of the chromatin fiber reveals a double helix twisted by tetranucleosomal units," *Science (80-. ).*, vol. 344, no. 6182, pp. 376–380, Apr. 2014.

[33] D. P. Ryan and T. Owen-Hughes, "Snf2-family proteins: chromatin remodellers for any occasion," *Curr. Opin. Chem. Biol.*, vol. 15, no. 5, p. 649, Oct. 2011.

[34] J. A. Eisen, K. S. Sweder, and P. C. Hanawalt, "Evolution of the SNF2 family of proteins: subfamilies with distinct sequences and functions," *Nucleic Acids Res.*, vol. 23, no. 14, pp. 2715–2723, Jul. 1995.

[35] B. John, "The biology of heterochromatin," in *Heterochromatin molecular and structural aspects.*, 1988, p. 147.

[36] Y. Ma, K. Kanakousaki, and L. Buttitta, “How the cell cycle impacts chromatin architecture and influences cell fate,” *Frontiers in Genetics*, vol. 5, no. FEB. 2015.

[37] L. J. Benson *et al.*, “Modifications of H3 and H4 during chromatin replication, nucleosome assembly, and histone exchange,” *J. Biol. Chem.*, vol. 281, no. 14, pp. 9287–9296, Apr. 2006.

[38] H. Tagami, D. Ray-Gallet, G. Almouzni, and Y. Nakatani, “Histone H3.1 and H3.3 Complexes Mediate Nucleosome Assembly Pathways Dependent or Independent of DNA Synthesis,” *Cell*, vol. 116, no. 1, pp. 51–61, Jan. 2004.

[39] R. E. Sobel, R. G. Cook, C. A. Perry, A. T. Annunziato, and C. D. Allis, “Conservation of deposition-related acetylation sites in newly synthesized histones H3 and H4.,” *Proc. Natl. Acad. Sci.*, vol. 92, no. 4, pp. 1237–1241, Feb. 1995.

[40] E. Heitz, “Das Heterochromatin der Moose.,” *Jahrbücher für Wissenschaftliche Bot.*, vol. 69, pp. 762–818, 1928.

[41] C. Jin *et al.*, “H3.3/H2A.Z double variant-containing nucleosomes mark ‘nucleosome-free regions’ of active promoters and other regulatory regions,” *Nat. Genet. Vol.*, vol. 41, no. 8, 2009.

[42] M. D. Meneghini, M. Wu, and H. D. Madhani, “Conserved histone variant H2A.Z protects euchromatin from the ectopic spread of silent heterochromatin,” *Cell*, vol. 112, no. 5, pp. 725–736, Mar. 2003.

[43] G. Felsenfeld, J. Boyes, J. Chung, D. Clark, and V. Studitsky, “Chromatin structure and gene expression.,” *Proc. Natl. Acad. Sci.*, vol. 93, no. 18, pp. 9384–9388, Sep. 1996.

[44] D. S. Gross and W. T. Garrard, “Nuclease hypersensitive sites in chromatin,” *Annual Review of Biochemistry*, vol. 57. Annual Reviews 4139 El Camino Way, P.O. Box 10139, Palo Alto, CA 94303-0139, USA, pp. 159–197, 28-Nov-1988.

[45] H. Kwon, A. N. Lmbalzanot, P. A. Khavarit, R. E. Kingstont, M. R. Green, and T. Howard, “Nucleosome disruption and enhancement of activator binding by a human SW1/SNF complex,” 1994.

[46] T. Tsukiyama and C. Wu, “Purification and properties of an ATP-dependent nucleosome remodeling factor,” *Cell*, vol. 83, no. 6, pp. 1011–1020, Dec. 1995.

[47] J. R. Davie and M. J. Hendzel, “Multiple functions of dynamic histone acetylation,” *J. Cell. Biochem.*, vol. 55, no. 1, pp. 98–105, 1994.

[48] K. S. Weiler and B. T. Wakimoto, “Heterochromatin and gene expression in Drosophila,” *Annual Review of Genetics*, vol. 29. pp. 577–605, 1995.

[49] S. W. Brown, “Heterochromatin,” *Science (80-. ).*, vol. 151, no. 3709, pp. 417–425, Jan. 1966.

[50] P. Trojer and D. Reinberg, “Facultative Heterochromatin: Is There a Distinctive Molecular Signature?,” *Mol. Cell*, vol. 28, no. 1, pp. 1–13, Oct. 2007.

[51] J. H. A. Martens *et al.*, “The profile of repeat-associated histone lysine methylation states in the mouse epigenome,” *EMBO J.*, vol. 24, no. 4, pp. 800–812, Feb. 2005.

[52] D. K. Palmer, K. O’Day, H. L. E. Trong, H. Charbonneau, and R. L. Margolis, “Purification of the centromere-specific protein CENP-A and demonstration that it is a distinctive histone.,” *Proc. Natl. Acad. Sci.*, vol. 88, no. 9, pp. 3734–3738, May 1991.

[53] P. E. Warburton *et al.*, “Immunolocalization of CENP-A suggests a distinct nucleosome structure at the inner kinetochore plate of active centromeres,” *Curr. Biol.*, vol. 7, no. 11, pp. 901–904, Nov. 1997.

[54] J. P. Cooper, E. R. Nimmo, R. C. Allshire, and T. R. Cech, “Regulation of telomere length and function by a Myb-domain protein in fission yeast,” *Nature*, vol. 385, no. 6618, pp. 744–747, 1997.

[55] N. Saksouk, E. Simboeck, and J. Déjardin, “Constitutive heterochromatin formation and transcription in mammals,” *Epigenetics and Chromatin*, vol. 8, no. 1, pp. 1–17, Jan. 2015.

[56] L. Aagaard *et al.*, “Functional mammalian homologues of the Drosophila PEV-modifier Su(var)3-9 encode centromere-associated proteins which complex with the heterochromatin component M31,” *EMBO J.*, vol. 18, no. 7, pp. 1923–1938, Apr. 1999.

[57] R. Eils *et al.*, “Three-dimensional reconstruction of painted human interphase chromosomes: Active and inactive X chromosome territories have similar volumes but differ in shape and surface structure,” *J. Cell Biol.*, vol. 135, no. 6, pp. 1427–1440, 1996.

[58] A. Kohlmaier, F. Savarese, M. Lachner, J. Martens, T. Jenuwein, and A. Wutz, “A Chromosomal Memory Triggered by Xist Regulates Histone Methylation in X Inactivation,” *PLOS Biol.*, vol. 2, no. 7, p. e171, 2004.

[59] R. Srivastava, U. M. Singh, and N. K. Dubey, “Histone Modifications by different histone modifiers,” *J. Biol. Sci. Med.*, vol. 2, no. 1, pp. 45–54, 2016.

[60] I. O. Torres and D. G. Fujimori, “Functional coupling between writers, erasers and readers of histone and DNA methylation,” *Current Opinion in Structural Biology*, vol. 35. pp. 68–75, 2015.

[61] T. Jenuwein and C. D. Allis, “Translating the histone code,” *Science (80-. ).*, vol. 293, no. 5532, pp. 1074–1080, Aug. 2001.

[62] B. D. Strahl and C. D. Allis, “The language of covalent histone modifications,” *Nature*, vol. 403, no. 6765. pp. 41–45, 2000.

[63] M. Lachner, D. O’Carroll, S. Rea, K. Mechtler, and T. Jenuwein, “Methylation of histone H3 lysine 9 creates a binding site for HP1 proteins,” *Nature*, vol. 410, no. 6824, pp. 116–120, Mar. 2001.

[64] V. G. Allfrey, R. Faulkner, and A. E. Mirsky, “ACETYLATION AND METHYLATION OF HISTONES AND THEIR POSSIBLE ROLE IN THE,” *Proc. Natl. Acad. Sci. United States*, vol. 51, pp. 786–794, 1964.

[65] B. G. Pogo, V. G. Allfrey, and A. E. Mirsky, “RNA synthesis and histone acetylation during the course of gene activation in lymphocytes.,” *Proc. Natl. Acad. Sci. U. S. A.*, vol. 55, no. 4, pp. 805–812, 1966.

[66] L. Hong, G. P. Schroth, H. R. Matthews, P. Yau, and E. M. Bradbury, “Studies of the DNA binding properties of histone H4 amino terminus. Thermal denaturation studies reveal that acetylation markedly reduces the binding constant of the H4 ‘tail’ to DNA,” *J. Biol. Chem.*, vol. 268, no. 1, pp. 305–314, 1993.

[67] D. Y. Lee, J. J. Hayes, D. Pruss, and A. P. Wolffe, “A positive role for histone acetylation in transcription factor access to nucleosomal DNA,” *Cell*, vol. 72, no. 1, pp. 73–84, Jan. 1993.

[68] G. D. Bowman, M. G. Poirier, and T. C. Jenkins, “Post-Translational Modifications of Histones That Influence Nucleosome Dynamics,” 2014.

[69] S. Kleff, E. D. Andrulis, C. W. Anderson, and R. Sternglanz, “Identification of a gene encoding a yeast histone H4 acetyltransferase,” *J. Biol. Chem.*, vol. 270, no. 42, pp. 24674–24677, Oct. 1995.

[70] M. R. Parthun, J. Widom, and D. E. Gottschling, “The Major Cytoplasmic Histone Acetyltransferase in Yeast: Links to Chromatin Replication and Histone

Metabolism," *Cell*, vol. 87, no. 1, pp. 85–94, Oct. 1996.

[71] C. E. McCullough and R. Marmorstein, "Molecular Basis for Histone Acetyltransferase Regulation by Binding Partners, Associated Domains, and Autoacetylation," *ACS Chem. Biol.*, vol. 11, no. 3, pp. 632–642, Mar. 2016.

[72] L. Shi and B. P. Tu, "Acetyl-CoA and the regulation of metabolism: mechanisms and consequences," *Curr. Opin. Cell Biol.*, vol. 33, pp. 125–131, Apr. 2015.

[73] E. Korzus *et al.*, "Transcription factor-specific requirements for coactivators and their acetyltransferase functions," *Science (80-. ).*, vol. 279, no. 5351, pp. 703–707, Jan. 1998.

[74] R. Marmorstein and M. M. Zhou, "Writers and Readers of Histone Acetylation: Structure, Mechanism, and Inhibition," *Cold Spring Harb. Perspect. Biol.*, vol. 6, no. 7, p. a018762, Jul. 2014.

[75] T. Umehara, Y. Nakamura, M. Wakamori, K. Ozato, S. Yokoyama, and B. Padmanabhan, "Structural implications for K5/K12-di-acetylated histone H4 recognition by the second bromodomain of BRD2," *FEBS Lett.*, vol. 584, no. 18, pp. 3901–3908, Sep. 2010.

[76] J. Peng, W. Dong, L. Chen, T. Zou, Y. Qi, and Y. Liu, "Brd2 is a TBP-associated protein and recruits TBP into E2F-1 transcriptional complex in response to serum stimulation," *Mol. Cell. Biochem.*, vol. 294, no. 1–2, pp. 45–54, Jan. 2007.

[77] D. Zhao, Y. Li, X. Xiong, Z. Chen, and H. Li, "YEATS Domain-A Histone Acylation Reader in Health and Disease," 2017.

[78] G. E. Zentner and S. Henikoff, "Regulation of nucleosome dynamics by histone modifications," *Nat. Struct. Mol. Biol. 2013 203*, vol. 20, no. 3, pp. 259–266, Mar. 2013.

[79] S. Zhao, X. Zhang, and H. Li, "Beyond histone acetylation-writing and erasing histone acylations," *Curr. Opin. Struct. Biol.*, vol. 53, pp. 169–177, 2018.

[80] B. R. Sabari *et al.*, "Intracellular Crotonyl-CoA Stimulates Transcription through p300-Catalyzed Histone Crotonylation," *Mol. Cell*, vol. 58, no. 2, pp. 203–215, Apr. 2015.

[81] Z. Kaczmarska *et al.*, "Structure of p300 in complex with acyl-CoA variants," *Nat. Publ. Gr.*, 2017.

[82] W. Wei *et al.*, "Class I histone deacetylases are major histone decrotonylases:

evidence for critical and broad function of histone crotonylation in transcription," *Cell Res.*, vol. 27, pp. 898–915, 2017.

[83] K. Murray, "The Occurrence of ϵ-N-Methyl Lysine in Histones," *Biochemistry*, vol. 3, no. 1, pp. 10–15, Jan. 1964.

[84] A. Di Lorenzo and M. T. Bedford, "Histone arginine methylation," *FEBS Lett.*, vol. 585, no. 13, pp. 2024–2031, Jul. 2011.

[85] B. Rao, Y. Shibata, B. D. Strahl, and J. D. Lieb, "Dimethylation of Histone H3 at Lysine 36 DemarcatesRegulatory and Nonregulatory ChromatinGenome-Wide," *Mol. Cell. Biol.*, vol. 25, no. 21, pp. 9447–9459, Nov. 2005.

[86] H. Wang *et al.*, "Purification and functional characterization of a histone H3-lysine 4-specific methyltransferase," *Mol. Cell*, vol. 8, no. 6, pp. 1207–1217, Dec. 2001.

[87] M. Vermeulen *et al.*, "Quantitative Interaction Proteomics and Genome-wide Profiling of Epigenetic Histone Marks and Their Readers," *Cell*, vol. 142, no. 6, pp. 967–980, Sep. 2010.

[88] A. Laugesen, J. W. Højfeldt, and K. Helin, "Role of the Polycomb Repressive Complex 2 (PRC2) in Transcriptional Regulation and Cancer," *Cold Spring Harb. Perspect. Med.*, vol. 6, no. 9, Sep. 2016.

[89] A. J. Bannister *et al.*, "Selective recognition of methylated lysine 9 on histone H3 by the HP1 chromo domain," *Nat. 2001 4106824*, vol. 410, no. 6824, pp. 120–124, Mar. 2001.

[90] J. Suso Platero, T. Hartnett, and J. C. Eissenberg, "Functional analysis of the chromo domain of HP1.," *EMBO J.*, vol. 14, no. 16, pp. 3977–3986, Aug. 1995.

[91] Y. Shi *et al.*, "Histone demethylation mediated by the nuclear amine oxidase homolog LSD1," *Cell*, vol. 119, no. 7, pp. 941–953, Dec. 2004.

[92] N. Mosammaparast *et al.*, "The histone demethylase LSD1/KDM1A promotes the DNA damage response," *J. Cell Biol.*, vol. 203, no. 3, pp. 457–470, Nov. 2013.

[93] Y. Wang *et al.*, "LSD1 Is a Subunit of the NuRD Complex and Targets the Metastasis Programs in Breast Cancer," *Cell*, vol. 138, no. 4, pp. 660–672, Aug. 2009.

[94] T. Banerjee and D. Chakravarti, "A Peek into the Complex Realm of Histone Phosphorylation," *Mol. Cell. Biol.*, vol. 31, no. 24, pp. 4858–4873, Dec. 2011.

[95] F. Mattiroli and L. Penengo, “Histone Ubiquitination: An Integrative Signaling Platform in Genome Stability,” *Trends Genet.*, vol. 37, no. 6, pp. 566–581, Jun. 2021.

[96] H.-Y. Ryu and M. Hochstrasser, “SURVEY AND SUMMARY Histone sumoylation and chromatin dynamics,” *Nucleic Acids Res.*, vol. 49, no. 11, pp. 6043–6052, 2021.

[97] R. D. Hotchkiss, “THE QUANTITATIVE SEPARATION OF PURINES, PYRIMIDINES, AND NUCLEOSIDES BY PAPER CHROMATOGRAPHY,” *J. Biol. Chem.*, vol. 175, no. 1, pp. 315–332, Aug. 1948.

[98] J. Doskočil and F. Šorm, “Distribution of 5-methylcytosine in pyrimidine sequences of deoxyribonucleic acids,” *Biochim. Biophys. Acta - Spec. Sect. Nucleic Acids Relat. Subj.*, vol. 55, no. 6, pp. 953–959, Jun. 1962.

[99] S. J. Compere and R. D. Palmiter, “DNA methylation controls the inducibility of the mouse metallothionein-I gene in lymphoid cells,” *Cell*, vol. 25, no. 1, pp. 233–240, Jul. 1981.

[100] M. Okano, D. W. Bell, D. A. Haber, and E. Li, “DNA methyltransferases Dnmt3a and Dnmt3b are essential for de novo methylation and mammalian development,” *Cell*, vol. 99, no. 3, pp. 247–257, Oct. 1999.

[101] M. Monk, M. Boubelik, and S. Lehnert, “Temporal and regional changes in DNA methylation in the embryonic, extraembryonic and germ cell lineages during mouse embryo development,” *Development*, vol. 99, no. 3, pp. 371–382, Mar. 1987.

[102] R. Stein, Y. Gruenbaum, Y. Pollack, A. Razin, and H. Cedar, “Clonal inheritance of the pattern of DNA methylation in mouse cells,” *Proc. Natl. Acad. Sci. U. S. A.*, vol. 79, no. 1, pp. 61–65, 1982.

[103] J. A. Yoder, N. S. Soman, G. L. Verdine, and T. H. Bestor, “DNA (cytosine-5)-methyltransferases in mouse cells and tissues. studies with a mechanism-based probe,” *J. Mol. Biol.*, vol. 270, no. 3, pp. 385–395, Jul. 1997.

[104] H. Leonhardt, A. W. Page, H. U. Weier, and T. H. Bestor, “A targeting sequence directs DNA methyltransferase to sites of DNA replication in mammalian nuclei,” *Cell*, vol. 71, no. 5, pp. 865–873, Nov. 1992.

[105] F. Watt and P. L. Molloy, “Cytosine methylation prevents binding to DNA of a HeLa cell transcription factor required for optimal expression of the adenovirus major late promoter.,” *Genes Dev.*, vol. 2, no. 9, pp. 1136–1143, Sep. 1988.

[106] P. L. Jones *et al.*, “Methylated DNA and MeCP2 recruit histone deacetylase to repress transcription,” *Nat. Genet. 1998 192*, vol. 19, no. 2, pp. 187–191, 1998.

[107] M. Gardiner-Garden and M. Frommer, “CpG Islands in vertebrate genomes,” *J. Mol. Biol.*, vol. 196, no. 2, pp. 261–282, Jul. 1987.

[108] A. Inoue and D. Fujimoto, “Enzymatic deacetylation of histone,” *Biochem. Biophys. Res. Commun.*, vol. 36, no. 1, pp. 146–150, 1969.

[109] S. Spange, T. Wagner, T. Heinzel, and O. H. Krämer, “Acetylation of non-histone proteins modulates cellular signalling at multiple levels,” *International Journal of Biochemistry and Cell Biology*, vol. 41, no. 1. pp. 185–198, 2009.

[110] I. V Gregoretti, Y. M. Lee, and H. V Goodson, “Molecular evolution of the histone deacetylase family: Functional implications of phylogenetic analysis,” *J. Mol. Biol.*, vol. 338, no. 1, pp. 17–31, 2004.

[111] O. Witt, H. E. Deubzer, T. Milde, and I. Oehme, “HDAC family: What are the cancer relevant targets?,” *Cancer Lett.*, vol. 277, no. 1, pp. 8–21, May 2009.

[112] M. A. Moser, A. Hagelkruys, and C. Seiser, “Transcription and beyond: The role of mammalian class I lysine deacetylases,” *Chromosoma*, vol. 123, no. 1–2. pp. 67–78, 2014.

[113] G. Milazzo *et al.*, “Histone Deacetylases (HDACs): Evolution, Specificity, Role in Transcriptional Complexes, and Pharmacological Actionability,” *Genes (Basel).*, vol. 11, no. 5, p. 556, May 2020.

[114] J. Taplick, V. Kurtev, K. Kroboth, M. Posch, T. Lechner, and C. Seiser, “Homo-Oligomerisation and Nuclear Localisation of Mouse Histone Deacetylase 1,” 2000.

[115] W. Fischle *et al.*, “Enzymatic activity associated with class II HDACs is dependent on a multiprotein complex containing HDAC3 and SMRT/N-CoR,” *Mol. Cell*, vol. 9, no. 1, pp. 45–57, 2002.

[116] M. S. Finnin *et al.*, “Structures of a histone deacetylase homologue bound to the TSA and SAHA inhibitors,” *Nat. 1999 4016749*, vol. 401, no. 6749, pp. 188–193, Sep. 1999.

[117] J. R. Somoza *et al.*, “Structural snapshots of human HDAC8 provide insights into the class I histone deacetylases,” *Structure*, vol. 12, no. 7, pp. 1325–1334, 2004.

[118] C. J. Millard *et al.*, “Class I HDACs share a common mechanism of regulation by inositol phosphates,” *Mol. Cell*, vol. 51, no. 1, pp. 57–67, 2013.

[119] M. Bantscheff *et al.*, “Chemoproteomics profiling of HDAC inhibitors reveals selective targeting of HDAC complexes,” *Nat. Biotechnol. 2011 293*, vol. 29, no. 3, pp. 255–265, Jan. 2011.

[120] E. Seto and M. Yoshida, “Erasers of Histone Acetylation: The Histone Deacetylase Enzymes,” *Cold Spring Harb. Perspect. Biol.*, vol. 6, no. 4, p. a018713, Apr. 2014.

[121] G. E. Adams, A. Chandru, and S. M. Cowley, “Co-repressor, co-activator and general transcription factor: the many faces of the Sin3 histone deacetylase (HDAC) complex,” *Biochem. J.*, vol. 475, no. 24, pp. 3921–3932, Dec. 2018.

[122] C. D. Laherty, W. M. Yang, S. Jian-Min, J. R. Davie, E. Seto, and R. N. Eisenman, “Histone deacetylases associated with the mSin3 corepressor mediate Mad transcriptional repression,” *Cell*, vol. 89, no. 3, pp. 349–356, May 1997.

[123] C. Yao *et al.*, “Sin3a regulates epithelial progenitor cell fate during lung development,” *Dev.*, vol. 144, no. 14, pp. 2618–2628, Jul. 2017.

[124] B. Lakowski, I. Roelens, and S. Jacob, “CoREST-like complexes regulate chromatin modification and neuronal gene expression,” *J. Mol. Neurosci.*, vol. 29, no. 3, pp. 227–239, Jan. 2006.

[125] Y. Huang, S. J. Myers, and R. Dingledine, “Transcriptional repression by REST: recruitment of Sin3A and histone deacetylase to neuronal genes,” *Nat. Neurosci. 1999 210*, vol. 2, no. 10, pp. 867–872, Oct. 1999.

[126] S. M. Kooistra and K. Helin, “Molecular mechanisms and potential functions of histone demethylases,” *Nat. Rev. Mol. Cell Biol. 2012 135*, vol. 13, no. 5, pp. 297–311, Apr. 2012.

[127] M. G. J. M. van Bergen and B. A. van der Reijden, “Targeting the GFI1/1B—CoREST Complex in Acute Myeloid Leukemia,” *Front. Oncol.*, vol. 9, p. 479718, Oct. 2019.

[128] M. P. Torchy, A. Hamiche, and B. P. Klaholz, “Structure and function insights into the NuRD chromatin remodeling complex,” *Cellular and Molecular Life Sciences*, vol. 72, no. 13. pp. 2491–2507, 2015.

[129] A. Brero *et al.*, “Methyl CpG-binding proteins induce large-scale chromatin reorganization during terminal differentiation,” *J. Cell Biol.*, vol. 169, no. 5, pp. 733–743, 2005.

[130] M. Luo *et al.*, “NuRD Blocks Reprogramming of Mouse Somatic Cells into

Pluripotent Stem Cells," *Stem Cells*, vol. 31, no. 7, pp. 1278–1286, Jul. 2013.

[131] S. Shao *et al.*, "CHD4/NuRD complex regulates complement gene expression and correlates with CD8 T cell infiltration in human hepatocellular carcinoma," *Clin. Epigenetics*, vol. 12, no. 1, pp. 1–13, Feb. 2020.

[132] K. Lee, S. D. Whedon, Z. A. Wang, P. A. Cole, and Y. J. Zhang, "Distinct biochemical properties of the class I histone deacetylase complexes," *Curr. Opin. Chem. Biol.*, vol. 2022, p. 102179, 2022.

[133] M. G. Guenther, O. R. R. Barak, and M. A. Lazar, "The SMRT and N-CoR Corepressors Are Activating Cofactors for Histone Deacetylase 3," vol. 21, no. 18, pp. 6091–6101, 2001.

[134] P. Ordentlich, M. Downes, W. Xie, A. Genin, N. B. Spinner, and R. M. Evans, "Unique forms of human and mouse nuclear receptor corepressor SMRT," *Proc. Natl. Acad. Sci. U. S. A.*, vol. 96, no. 6, pp. 2639–2644, 1999.

[135] A. Soufi, G. Donahue, and K. S. Zaret, "Facilitators and Impediments of the Pluripotency Reprogramming Factors' Initial Engagement with the Genome," *Cell*, vol. 151, no. 5, pp. 994–1004, Nov. 2012.

[136] M. M. Wong, C. Guo, and J. Zhang, "Nuclear receptor corepressor complexes in cancer: mechanism, function and regulation," *Am. J. Clin. Exp. Urol.*, vol. 2, no. 3, p. 169, 2014.

[137] S. en Wu *et al.*, "Microbiota-derived metabolite promotes HDAC3 activity in the gut," *Nature*, vol. 586, no. 7827, pp. 108–112, 2020.

[138] M. R. Heideman *et al.*, "Dosage-dependent tumor suppression by histone deacetylases 1 and 2 through regulation of c-Myc collaborating genes and p53 function," *Blood*, vol. 121, no. 11, pp. 2038–2050, Mar. 2013.

[139] P. Matthias, "Too much or too little, how much HDAC activity is good for you?," *Blood*, vol. 121, no. 11, pp. 1930–1931, Mar. 2013.

[140] P. Atadja, "Development of the pan-DAC inhibitor panobinostat (LBH589): Successes and challenges," *Cancer Letters*, vol. 280, no. 2. pp. 233–241, 2009.

[141] P. Garrido Castro *et al.*, "The HDAC inhibitor panobinostat (LBH589) exerts in vivo anti-leukaemic activity against MLL-rearranged acute lymphoblastic leukaemia and involves the RNF20/RNF40/WAC-H2B ubiquitination axis," *Leuk. 2018 322*, vol. 32, no. 2, pp. 323–331, Jul. 2017.

[142] E. T. Roussos Torres *et al.*, “Phase I study of entinostat and nivolumab with or without ipilimumab in advanced solid tumors (ETCTN-9844),” *Clin. Cancer Res.*, vol. 27, no. 21, pp. 5828–5837, Nov. 2021.

[143] M. D. Minden, J. E. Till, and E. A. McCulloch, “Proliferative state of blast cell progenitors in acute myeloblastic leukemia (AML),” *Blood*, vol. 52, no. 3, pp. 592–600, Sep. 1978.

[144] N. J. Short, M. E. Rytting, and J. E. Cortes, “Acute myeloid leukaemia,” *The Lancet*, vol. 392, no. 10147. pp. 593–606, 2018.

[145] E. Papaemmanuil *et al.*, “Genomic Classification and Prognosis in Acute Myeloid Leukemia,” *N. Engl. J. Med.*, vol. 374, no. 23, pp. 2209–2221, Jun. 2016.

[146] D. Shafer and S. Grant, “Update on rational targeted therapy in AML,” *Blood Rev.*, vol. 30, no. 4, pp. 275–283, Jul. 2016.

[147] J. P. Bewersdorf, R. Shallis, M. Stahl, and A. M. Zeidan, “Epigenetic therapy combinations in acute myeloid leukemia: what are the options?,” *Ther. Adv. Hematol.*, vol. 10, pp. 1–19, Jan. 2019.

[148] H. Döhner *et al.*, “Diagnosis and management of AML in adults: 2017 ELN recommendations from an international expert panel,” *Blood*, vol. 129, no. 4, pp. 424–447, Jan. 2017.

[149] U. Creutzig *et al.*, “Diagnosis and management of acute myeloid leukemia in children and adolescents: recommendations from an international expert panel,” *Blood*, vol. 120, no. 16, pp. 3187–3205, Oct. 2012.

[150] A. V. Krivtsov and S. A. Armstrong, “MLL translocations, histone modifications and leukaemia stem-cell development,” *Nat. Rev. Cancer 2007 711*, vol. 7, no. 11, pp. 823–833, Nov. 2007.

[151] T. C. P. Somervaille and M. L. Cleary, “Identification and characterization of leukemia stem cells in murine MLL-AF9 acute myeloid leukemia,” *Cancer Cell*, vol. 10, no. 4, pp. 257–268, 2006.

[152] N. Zhu *et al.*, “MLL-AF9-and HOXA9-mediated acute myeloid leukemia stem cell self-renewal requires JMJD1C,” *J. Clin. Invest.*, vol. 126, no. 3, pp. 997–1011, Mar. 2016.

[153] J. Zuber *et al.*, “An integrated approach to dissecting oncogene addiction implicates a Myb-coordinated self-renewal program as essential for leukemia maintenance,”

*Genes Dev.*, vol. 25, no. 15, pp. 1628–1640, 2011.

[154] I. B. Weinstein, “Cancer: Addiction to oncogenes - The Achilles heal of cancer,” *Science*, vol. 297, no. 5578. American Association for the Advancement of Science, pp. 63–64, 05-Jul-2002.

[155] R. Pagliarini, W. Shao, and W. R. Sellers, “Oncogene addiction: pathways of therapeutic response, resistance, and road maps toward a cure,” *EMBO Rep.*, vol. 16, no. 3, pp. 280–296, Mar. 2015.

[156] G. Lagger *et al.*, “Essential function of histone deacetylase 1 in proliferation control and CDK inhibitor repression,” *EMBO J.*, vol. 21, no. 11, pp. 2672–2681, Jun. 2002.

[157] S. Lagger *et al.*, “Crucial function of histone deacetylase 1 for differentiation of teratomas in mice and humans,” *EMBO J.*, vol. 29, no. 23, pp. 3992–4007, Dec. 2010.

[158] R. L. Montgomery *et al.*, “Histone deacetylases 1 and 2 redundantly regulate cardiac morphogenesis, growth, and contractility,” *Genes Dev.*, vol. 21, no. 14, pp. 1790–1802, Jul. 2007.

[159] C. M. Trivedi *et al.*, “Hdac2 regulates the cardiac hypertrophic response by modulating Gsk3β activity,” *Nat. Med. 2007 133*, vol. 13, no. 3, pp. 324–331, Feb. 2007.

[160] M. Winter *et al.*, “Divergent roles of HDAC1 and HDAC2 in the regulation of epidermal development and tumorigenesis,” *EMBO J.*, vol. 32, no. 24, pp. 3176–3191, Dec. 2013.

[161] A. Hagelkruys *et al.*, “A single allele of Hdac2 but not Hdac1 is sufficient for normal mouse brain development in the absence of its paralog,” *Development*, vol. 141, no. 3, pp. 604–616, Feb. 2014.

[162] J. Schwaller, “Learning from mouse models of MLL fusion gene-driven acute leukemia,” *Biochim. Biophys. Acta - Gene Regul. Mech.*, vol. 1863, no. 8, 2020.

[163] V. Stavropoulou, S. Kaspar, L. Brault, P. J. M. Valk, and A. H. F. M. Peters, “MLL-AF9 Expression in Hematopoietic Stem Cells Drives a Highly Invasive AML Expressing EMT-Related Genes Linked to Poor Outcome,” *Cancer Cell*, vol. 30, pp. 43–58, 2016.

[164] S. Jamaladdin *et al.*, “Histone deacetylase (HDAC) 1 and 2 are essential for accurate cell division and the pluripotency of embryonic stem cells,” *Proc. Natl.*

*Acad. Sci. U. S. A.*, vol. 111, no. 27, pp. 9840–9845, Jul. 2014.

[165] O. M. Dovey, C. T. Foster, and S. M. Cowley, “Histone deacetylase 1 (HDAC1), but not HDAC2, controls embryonic stem cell differentiation,” *Proc. Natl. Acad. Sci. U. S. A.*, vol. 107, no. 18, pp. 8242–8247, May 2010.

[166] A. Hagelkruys *et al.*, “Essential Nonredundant Function of the Catalytic Activity of Histone Deacetylase 2 in Mouse Development,” *Mol. Cell. Biol.*, vol. 36, no. 3, pp. 462–474, 2016.

[167] L. Hess *et al.*, “A toolbox for class I HDACs reveals isoform specific roles in gene regulation and protein acetylation,” *PLOS Genet.*, vol. 18, no. 8, p. e1010376, Aug. 2022.

[168] J. E. Carette *et al.*, “Ebola virus entry requires the cholesterol transporter Niemann-Pick C1,” *Nature*, vol. 477, no. 7364, pp. 340–343, 2011.

[169] L. Hess, “Dissection of catalytic and non-catalytic functions of HDAC1 and HDAC2,” Universität Wien, 2017.

[170] L. Hess, “Mimicking isoform-specific histone deacetylase inhibition in vitro and in vivo,” Medizinische Universität Wien, 2022.

[171] R. Kühn, F. Schwenk, M. Aguet, and K. Rajewsky, “Inducible Gene Targeting in Mice,” *Science (80-. ).*, vol. 269, no. 5229, pp. 1427–1429, Sep. 1995.

[172] P. Wang, Z. Wang, and J. Liu, “Role of HDACs in normal and malignant hematopoiesis,” *Mol. Cancer 2020 191*, vol. 19, no. 1, pp. 1–21, Jan. 2020.

[173] S. Leiter, “MASTERARBEIT / MASTER ’ S THESIS „Set-up of an expression system for class I HDACs in human tumor cells“,” 2017.

[174] S. R. Edtmayer, “MASTER ’ S THESIS „The role of alternatively spliced STAT3 isoforms in acute myeloid leukemia“,” 2020.

[175] M. V. Kuleshov *et al.*, “Enrichr: a comprehensive gene set enrichment analysis web server 2016 update,” *Nucleic Acids Res.*, vol. 44, no. 1, pp. W90–W97, Jul. 2016.

[176] Z. Xie *et al.*, “Gene Set Knowledge Discovery with Enrichr,” *Curr. Protoc.*, vol. 1, no. 3, p. e90, Mar. 2021.

[177] S. A. Aleksander *et al.*, “The Gene Ontology knowledgebase in 2023,” *Genetics*, vol. 224, no. 1, May 2023.

[178] R. D. W. Kelly and S. M. Cowley, “The physiological roles of histone deacetylase

(HDAC) 1 and 2: Complex co-stars with multiple leading parts," in *Biochemical Society Transactions*, 2013, vol. 41, no. 3, pp. 741–749.

[179] C. J. Millard, P. J. Watson, L. Fairall, and J. W. R. Schwabe, "Targeting Class I Histone Deacetylases in a 'Complex' Environment," *Trends in Pharmacological Sciences*, vol. 38, no. 4. Elsevier Ltd, pp. 363–377, 01-Apr-2017.

[180] P. J. Watson, L. Fairall, G. M. Santos, and J. W. R. Schwabe, "Structure of HDAC3 bound to co-repressor and inositol tetraphosphate," *Nature*, vol. 481, no. 7381, pp. 335–340, 2012.

[181] V. Moos, "Catalytic and non-catalytic functions of histone deacetylases HDAC1 and HDAC2 - Universität Wien," University Vienna, 2016.

[182] A. Riegler, "Regulation of HDAC1 expression and activity in haploid human tumor cells," Medical University Vienna, 2020.

[183] P. Lapšanská, "Expression and characterization of catalytically inactive class I HDACs in HAP1 cells," Wien, 2018.

[184] A. Vannini *et al.*, "Substrate binding to histone deacetylases as shown by the crystal structure of the HDAC8-substrate complex," *EMBO Rep.*, vol. 8, no. 9, pp. 879–884, 2007.

[185] W. M. Yang, S. C. Tsai, Y. Der Wen, G. Fejé, and E. Seto, "Functional domains of histone deacetylase-3," *J. Biol. Chem.*, vol. 277, no. 11, pp. 9447–9454, 2002.

[186] P. Siliphaivanh *et al.*, "Design of novel histone deacetylase inhibitors," *Bioorg. Med. Chem. Lett.*, vol. 17, no. 16, pp. 4619–4624, Aug. 2007.

[187] J. I. Nakayama and T. Hayakawa, "Physiological roles of class i HDAC complex and histone demethylase," *J. Biomed. Biotechnol.*, vol. 2011, 2011.

[188] J. Cairns, B. L. Fridley, G. D. Jenkins, Y. Zhuang, J. Yu, and L. Wang, "Differential roles of ERRFI1 in EGFR and AKT pathway regulation affect cancer proliferation," *EMBO Rep.*, vol. 19, no. 3, p. e44767, Mar. 2018.

[189] T. G. Muñoz, A. T. Amaral, P. Puerto-Camacho, H. Peinado, and E. de Álava, "Endoglin in the Spotlight to Treat Cancer," *Int. J. Mol. Sci. 2021, Vol. 22, Page 3186*, vol. 22, no. 6, p. 3186, Mar. 2021.

[190] H. N. Fridolfsson, D. M. Roth, P. A. Insel, and H. H. Patel, "Regulation of intracellular signaling and function by caveolin," *FASEB J.*, vol. 28, no. 9, p. 3823, Sep. 2014.

[191] I. C. Allen *et al.*, “Article NLRP12 Suppresses Colon Inflammation and Tumorigenesis through the Negative Regulation of Noncanonical NF-kB Signaling,” *Immunity*, vol. 36, pp. 742–754, 2012.

[192] H. B. Low and Y. Zhang, “Regulatory Roles of MAPK Phosphatases in Cancer,” *Immune Netw.*, vol. 16, no. 2, pp. 85–98, Apr. 2016.

[193] T. Gravina *et al.*, “Role of Diacylglycerol Kinases in Acute Myeloid Leukemia,” *Biomedicines*, vol. 11, no. 7, p. 1877, Jul. 2023.

[194] L. Zhang *et al.*, “Endothelial DGKG promotes tumor angiogenesis and immune evasion in hepatocellular carcinoma,” *J. Hepatol.*, vol. 80, no. 1, pp. 82–98, Jan. 2024.

[195] X. Nie *et al.*, “VEPH1 suppresses the progression of gastric cancer by regulating the Hippo-YAP signalling pathway,” *Dig. Liver Dis.*, vol. 56, no. 1, pp. 187–197, Jan. 2024.

[196] A. Jauhiainen *et al.*, “Distinct Cytoplasmic and Nuclear Functions of the Stress Induced Protein DDIT3/CHOP/GADD153,” *PLoS One*, vol. 7, no. 4, p. e33208, Apr. 2012.

[197] I. Ben Sahra *et al.*, “Metformin, independent of AMPK, induces mTOR inhibition and cell-cycle arrest through REDD1,” *Cancer Res.*, vol. 71, no. 13, pp. 4366–4372, Jul. 2011.

[198] I. N. Mungrue, J. Pagnon, O. Kohannim, P. S. Gargalovic, and A. J. Lusis, “CHAC1/MGC4504 Is a Novel Proapoptotic Component of the Unfolded Protein Response, Downstream of the ATF4-ATF3-CHOP Cascade,” *J. Immunol.*, vol. 182, no. 1, pp. 466–476, Jan. 2009.

[199] H. H. Tseng *et al.*, “Metformin inhibits gastric cancer cell proliferation by regulation of a novel Loc100506691-CHAC1 axis,” *Mol. Ther. Oncolytics*, vol. 22, pp. 180–194, Sep. 2021.

[200] E. R. Stanley and V. Chitu, “CSF-1 Receptor Signaling in Myeloid Cells,” *Cold Spring Harb. Perspect. Biol.*, vol. 6, no. 6, 2014.

[201] E. Guérit, F. Arts, G. Dachy, B. Boulouadnine, and J. B. Demoulin, “PDGF receptor mutations in human diseases,” *Cell. Mol. Life Sci. 2021 788*, vol. 78, no. 8, pp. 3867–3881, Jan. 2021.

[202] S. D. Nimer, “Myelodysplastic syndromes,” *Blood*, vol. 111, no. 10, pp. 4841–4851,

May 2008.

[203] C. Eng, “RET proto-oncogene in the development of human cancer,” *J. Clin. Oncol.*, vol. 17, no. 1, pp. 380–393, Sep. 1999.

[204] S. Sigismund, D. Avanzato, and L. Lanzetti, “Emerging functions of the EGFR in cancer,” *Mol. Oncol.*, vol. 12, no. 1, pp. 3–20, Jan. 2018.

[205] N. C. Shaner, R. E. Campbell, P. A. Steinbach, B. N. G. Giepmans, A. E. Palmer, and R. Y. Tsien, “Improved monomeric red, orange and yellow fluorescent proteins derived from Discosoma sp. red fluorescent protein,” *Nat. Biotechnol. 2004 2212*, vol. 22, no. 12, pp. 1567–1572, Nov. 2004.

[206] N. Chester and D. R. Marshak, “Dimethyl Sulfoxide-Mediated Primer Tm Reduction: A Method for Analyzing the Role of Renaturation Temperature in the Polymerase Chain Reaction,” *Anal. Biochem.*, vol. 209, no. 2, pp. 284–290, Mar. 1993.

[207] M. Y. Zhou and C. E. Gomez-Sanchez, “Universal TA cloning.,” *Current issues in molecular biology*, vol. 2, no. 1. pp. 1–7, 2000.

[208] K. Reckzeh *et al.*, “Molecular and cellular effects of oncogene cooperation in a genetically accurate AML mouse model,” *Leuk. 2012 267*, vol. 26, no. 7, pp. 1527–1536, Feb. 2012.

[209] M. Jinek, K. Chylinski, I. Fonfara, M. Hauer, J. A. Doudna, and E. Charpentier, “A programmable dual-RNA-guided DNA endonuclease in adaptive bacterial immunity,” *Science (80-. ).*, vol. 337, no. 6096, pp. 816–821, Aug. 2012.

[210] A. Leopoldi, “In vivo and in vitro analysis of biotin-tagged histone deacetylase 1 and 2,” Wien, 2014.

[211] I. Fairlie, “The hazards of tritium – revisited,” *Med. Confl. Surviv.*, vol. 24, no. 4, pp. 306–319, Oct. 2008.

[212] D. Wegener, C. Hildmann, and A. Schwienhorst, “Recent progress in the development of assays suited for histone deacetylase inhibitor screening,” *Mol. Genet. Metab.*, vol. 80, no. 1–2, pp. 138–147, Sep. 2003.

[213] D. Wegener, C. Hildmann, D. Riester, and A. Schwienhorst, “Improved fluorogenic histone deacetylase assay for high-throughput-screening applications,” *Anal. Biochem.*, vol. 321, no. 2, pp. 202–208, Oct. 2003.

[214] N. A. Wolfson, C. Ann Pitcairn, and C. A. Fierke, “HDAC8 substrates: Histones and beyond,” *Biopolymers*, vol. 99, no. 2, pp. 112–126, Feb. 2013.

[215] M. A. Deardorff *et al.*, “HDAC8 mutations in Cornelia de Lange syndrome affect the cohesin acetylation cycle,” *Nat. 2012 4897415*, vol. 489, no. 7415, pp. 313–317, Aug. 2012.

[216] X. Yu *et al.*, “Involvement of p53 Acetylation in Growth Suppression of Cutaneous T-Cell Lymphomas Induced by HDAC Inhibition,” *J. Invest. Dermatol.*, vol. 140, no. 10, pp. 2009-2022.e4, 2020.

[217] S. Bhaskara *et al.*, “Hdac3 is essential for the maintenance of chromatin structure and genome stability,” *Cancer Cell*, vol. 18, no. 5, pp. 436–447, Nov. 2010.

[218] M. P. Creyghton *et al.*, “Histone H3K27ac separates active from poised enhancers and predicts developmental state,” *Proc. Natl. Acad. Sci. U. S. A.*, vol. 107, no. 50, pp. 21931–21936, Dec. 2010.

[219] W. Volkwein *et al.*, “Detection and differentiation of murine leukemia virus (MLV) and murine stem cell virus (MSCV) and therefrom derived nucleic acids,” *J. Virol. Methods*, vol. 299, p. 114316, Jan. 2022.

[220] C. Asselin-Paturel and G. Trinchieri, “Production of type I interferons: Plasmacytoid dendritic cells and beyond,” *Journal of Experimental Medicine*, vol. 202, no. 4. pp. 461–465, Aug-2005.

[221] A. K. Brenner and Ø. Bruserud, “Functional Toll-Like Receptors (TLRs) Are Expressed by a Majority of Primary Human Acute Myeloid Leukemia Cells and Inducibility of the TLR Signaling Pathway Is Associated with a More Favorable Phenotype,” *Cancers 2019, Vol. 11, Page 973*, vol. 11, no. 7, p. 973, Jul. 2019.

[222] T. Velasco-Hernandez, P. Säwén, D. Bryder, and J. Cammenga, “Potential Pitfalls of the Mx1-Cre System: Implications for Experimental Modeling of Normal and Malignant Hematopoiesis,” *Stem Cell Reports*, vol. 7, no. 1, pp. 11–18, Jul. 2016.